# Amorphous silicon thin film solar cells with engineered nanoparticles

*A thesis submitted for the degree of*

*Doctor of Philosophy*

by

**Boyuan Cai**

Principal Supervisor: Associate Professor Baohua Jia

Coordinating Supervisor: Professor Min Gu

Centre for Micro-Photonics

Faculty of Science Engineering and Technology

Swinburne University of Technology

Melbourne, Australia

2015

# Abstract

Silicon thin film solar cells with thicknesses in the range of few hundreds of nanometers to few micrometers are regarded to be good substitutes for traditional wafer based solar cells due to their low cost and easily scaling-up fabrication technology. However, the efficiencies of such thin film silicon solar cells are much lower than their wafer-based counterparts, which mainly arise from the large mismatch between the minority-carrier diffusion length and the absorption depth in the active materials. In addition, the initial efficiency of the amorphous silicon (a-Si) thin film solar cells normally decreases by around 20% (known as the light induced degradation) and then maintains stable during the long-term solar illumination. To address this issue, effective light trapping strategies need to be applied into the solar cells to reduce the a-Si thickness without compromising the optical properties of solar cells. The conventional texture approach is not applicable any more when the silicon thickness is less than the wavelength of the incident light. In this case, subwavelength nanoparticles and nanostructures have been proven to be effective in manipulating the incident light in a nanoscale to increase the light path in the solar cells. By carefully designing the geometry of the nanoparticles in the solar cell environment, light can be coupled into specific modes inside the active materials. As a result, macroscale properties such as reflection, transmission, and absorption can be manipulated.

In this thesis, we first explore the scattering effect of large metallic nanoparticles (Ag and Al) and $SiO_2$ dielectric nanoparticles on the absorbance in the standard n-i-p a-Si solar cells through numerical modelling in the literature review. By optimising the sizes and surface coverage densities of the metallic nanoparticles on top of the solar cells, overall absorption enhancements of 10% and 11.6% are obtained for Al nanoparticles and Ag nanoparticles, respectively. The enhancements are lower than what has been achieved (14.5%) by using the closely-packed $SiO_2$ nanoparticles under the optimised condition.

In the first part of this thesis, we investigate the use of small metallic nanoparticles for enhancing the absorbance and the efficiency of a-Si thin film solar cells. The near-field light concentration from plasmonic nanostructures has been predicted to be able to significantly improve the solar cell conversion efficiency since the inception of plasmonic solar cells. We propose and demonstrate ultra-small (a few nanometers) metallic nanoparticles integrated in a-Si solar cells between the front electrode and the photoactive layer. Significant enhancements in both the photocurrent (14.1%) and the fill factor (12.3%) are achieved due to the strong plasmonic near-field concentration and the reduced contact resistance, respectively.

The second part of this thesis depicts a new solar cell geometry with the experimental integration of closely-packed $SiO_2$ nanoparticles half embedded into the a-Si solar cells from the top surface. It is demonstrated that the designed solar cell structures can result in an approximate 30%-50% significant photocurrent enhancement over the flat solar cells with a thickness of approximate 150 nm. We also develop a simulation model using the finite difference time domain (FDTD) method to accurately calculate the absorption of the a-Si in these novel solar cell structures and investigate the mechanisms of the absorption enhancement.

In the last Chapter, through the comparison of the influence of small and large metallic nanoparticles and the dielectric $SiO_2$ nanoparticles on the absorbance in the a-Si solar cell geometries discussed previously, we propose a new nanoparticle model. A nanoparticle consists of closely packed $SiO_2$ nanospheres as the core and ultra-small metallic nanoparticles on the surface, which we name as the hetero-structured lumpy nanoparticles. By imprinting the lumpy nanoparticles partially into the top surface of the solar cells, an even higher absorption enhancement in solar cells is achieved in the entire solar spectrum. Through comparing the quantum efficiency (QE) response from the solar cells with the $SiO_2$ nanoparticles and the lumpy nanoparticles to the reference flat solar cell, a higher QE response is obtained for the solar cells integrated with the lumpy nanoparticles compared to those integrated with only the $SiO_2$ nanoparticles. A relative short circuit current density ($J_{SC}$) enhancement of 37.5% compared to the flat reference solar cell is obtained for solar cells with the $SiO_2$ nanoparticles; while a relative $J_{SC}$ enhancement of 62.5% can be achieved for the lumpy nanoparticles integrated solar cell. From the numerical modelling, further potential of this solar cell structure is investigated. It has been found through integrating the hetero-structured nanoparticles, a 20 nm thick a-Si conformal layer can achieve a comparative absorption to a 300 nm thick standard a-Si solar cell with the conventional anti-reflection coating. This exciting finding demonstrates that nanoparticles approaches hold great promise in solving the key bottle-neck challenge of low conversion efficiency of ultrathin silicon thin film solar cells.

# Acknowledgements

During the past four years studying as a PhD candidate in the Centre for Micro-Photonics (CMP) of Swinburne University of Technology, there are so many people who I would like to thank for making this journey possible. First, I would like to truly thank my supervisor Prof. Min Gu for providing me the opportunity to join the exciting research project in the plasmonic solar cell field over the past four years. Prof. Min Gu is a great scientist with full of enthusiasm, patient, and inspiration, who I have learnt a lot from. One of the most valuable lessons I learn from Min is the research vision, which always guides my research project in a right direction when I feel confused and I believe this lesson will continue to help me in my future career. I quite appreciate the many discussions we had regarding to my research project which inspire me with many good ideas, besides I also appreciate many resources and facilities that Min has provided. I also would like to express my deep gratitude to the previous CEO of Suntech Power Holdings Co. Pty, Dr. Zhengrong Shi, who recruited me from Nankai University and approved me to work in the R&D department of thin film silicon solar cells for one year in the company. Many thanks go to Suntech Power for providing me the scholarship to join the Victoria-Suntech Advanced Solar Facility (VSASF) project which was founded by Victoria government, Swinburne University and Suntech Power.

I also would like to give my sincere thanks to my supervisor A. Prof. Baohua Jia, who helps me a lot both in the aspects of life and research. During her supervising period, she has taught me a lot with her experiments skills and experiments experience. These useful experiences help me very much to grow up from a master student to a PhD candidate and help me to get adapted to the life in Australia. I really appreciate all the detailed discussions we had regarding to my research project, which are the inspiration of trigger for me. One important lesson she has taught me is how to motivate myself especially when I face kinds of difficulties during the research period, which makes me stronger. Many thanks go to her for constructive comments and kindness help during the past four years.

I would like to thank the research staff from the VSASF group, starting with Dr. Xi Chen who trained me about the synthesis of nanoparticles and Dr. Zi Ouyang who helped us maintain most of our equipment and gave training to me regarding to the characterisation of solar cells. I would like to especially thank Dr. Nicholas Stokes for his contribution on developing the simulation model for thin film solar cells in the very beginning time. In addition, many thanks go to all the members from the CMP for the discussion and the help during my PhD studying period. Many thanks go to Dr. Yaoyu Cao and Dr. Zongsong Gan for the discussion about the plasmonic nanoparticles and quantum dots. Many thanks go to Ms. Pierrette Michaux for her help in my training of the physical vapour deposition systems, electron beam lithography, and nano-imprinting systems. Many thanks go to Mr. Yinan Zhang and Ms. Shouyi Xie for the discussion of the solar cells. I would like to thank Dr. James Wang from the Centre for Atom Optics and Ultrafast Spectroscopy in Swinburne University of Technology for his training of scanning electron microscopy.

I would express my deep gratitude to Dr. Yongqian Wang from Suntech Power for training me about the thin film solar cell fabrication and characterisation when I was doing experiments in the R&D department in Suntech Power. I also would like to thank Prof. Xiaodan Zhang and Mr. Jia Fang from Nankai University for discussion and the help regarding to the solar cell fabrication based on the nanovoid structures solar cell geometry.

I would like to thank administrative staff members in the CMP Ms. Johanna Cooper, Ms. Barbara Gillespie, Ms. Lou Jia and Ms. Kerrie Lawrence for their help with student paper work during my study.

At last but not the least, I would like to thank my parents for encouraging and supporting me during the past four years and I would like to express my greatest gratitude to my wife, Dongdong, who has always been supportive and considerate to my project even though she is not together with me at Melbourne.

Boyuan Cai

Melbourne Australia, April, 2015

# Declaration

I, Boyuan Cai, declare that this thesis entitled:

**“Amorphous silicon thin film solar cells with engineered nanoparticles”**

is my own work and has not been submitted previously, in whole or in part, in respect of any other academic award.

Boyuan Cai

Centre for Micro-Photonics

Faculty of Science, Engineering and Technology

Swinburne University of Technology

Australia

Dated this day, 2nd April 2015

# Contents

## 5. Hetero-structured lumpy nanoparticle for high absorbance of ultrathin film amorphous silicon solar cells ................................................................. 105

## 6. Conclusion and future work ..................................................................... 131

# List of Figures

# List of Tables

# List of Abbreviations

PV: photovoltaic

TW: terawatts

CdTe: cadmium telluride

CIGS: copper indium gallium selenide

a-Si: amorphous silicon

nc-Si: nano-crystalline silicon

μ-Si: microcrystalline silicon

PECVD: plasma enhanced chemical vapour deposition

TCO: transparent conductive oxide

EQE: external quantum efficiency

I-V: current density-voltage

FF: fill factor

$J_{SC}$: short circuit current density

$V_{OC}$: open circuit voltage

LSP: localised surface plasmon

SPP: surface plasmon polariton

WGM: whispering gallery modes
NP: nanoparticle
PMMA: Poly(methyl methacrylate)
PS: polystyrene
ARC: anti-reflective coating
IRL: intermediate reflector layer
NIR: near infrared
UV: ultra-violet
SEM: scanning electron microscope
AZO: ZnO:Al
ITO tin-oxide doped indium-oxide
SC: surface coverage
FDTD: Finite-difference time-domain
FP: Fabry-Perot
3D three-dimensional
EBL: electron beam lithography
PC: photonic crystal

# Chapter 1

## Introduction

High-speed economic development in a modern society requires enormous energy consumption, in which electricity plays an important role. In the year 2012, the global electric consumption was over 19,000 billion kilowatt-hours [1], mostly produced by burning the fossil fuels, which generates carbon dioxide ($CO_2$) contributing detrimentally to climate change through the greenhouse effect [2]. In addition, with the quick depletion of the fossil fuels, sustainability becomes another major issue for the energy. Solutions for the grant energy challenge need to have a high conversion efficiency, long-term sustainability, low environmental impact, and scalability for meeting the human energy demands, especially for countries with high economy growth speed. One of the most promising solutions is to utilise the solar photovoltaics, which comes from the sun. The annual solar energy on earth is $1.76\times10^5$ terawatts (TW) and the current world usage is estimated to be only 15 TW [3] which means the photovoltaic (PV) power has the potential to meet all the energy needs for the entire world.

Currently the PV industry is dominated by crystalline silicon solar cells [4-6], the most developed solar PV devices, which are composed of mono-crystalline or multi-crystalline silicon [7-10]. However, the cost of this kind of solar cells is high due to the involved complicated production process and the expensive material. To make the PV energy competitive with the traditional energy solutions, it is imperative to investigate low cost PV devices, for example the thin film solar cells, which are the promising candidates for reducing the cost. Thin film solar cells with thicknesses of hundreds of nanometers have been developed during the last thirty years with lower production costs. The main commercial thin film solar cell technologies are cadmium telluride (CdTe) from First Solar with the highest laboratory efficiency 17.3% [11-12]; copper indium gallium selenide (CIGS) from Zentrum fuer Sonnenenergie and Wasserstoff-Forschung, Baden-Wuerttemberg (ZSW) with an efficiency around 20% [13]; and amorphous Si (a-Si) thin film solar cells from Oerlikon with a stable efficiency 10.1% for single junction [14] and 12.2% for double junction configurations [15]. Among the commercial thin film solar cell technologies, both CIGS and CdTe cells utilise scarce and toxic elements such as In and Te, which are harmful to the environment. In addition, the achieved high efficiencies are not scalable to meet the ever-increasing energy demand. Amorphous Si thin film solar cells have the longest commercial history, because of its low-cost and comparatively simple fabrication procedure and the non-toxic material involved [16-22]. Therefore in this thesis, we mainly focus on the a-Si thin film solar cells.

## 1.1Amorphous Si thin film solar cells

In 1976, Carlson and Wronski from RCA Laboratories reported the first hydrogenated amorphous silicon (a-Si) based solar cell [16], with a conversion efficiency of 2.4%. In 1990s, with the development of silicon wafer based solar cells, thin-film silicon solar cells also achieved important enhancements. Yamamoto from Kaneka Company [18], Guha from United Solar Ovonic [20], and Meier from University of Neuchatel presented various designs of tandem and triple junction solar cells based on a-Si, microcrystalline silicon (μ-Si), and amorphous silicon-germanium (a-SiGe). Amorphous Si has always been one of the most commonly used semiconductor materials applied as the active layer in silicon based thin film solar cells due to its high absorption coefficient shown in Fig. 1.1.

Fig. 1.1 shows the absorption coefficients α of a-Si and some other amorphous alloys in the spectrum range between 1 eV and 3 eV. We can clearly see that the absorption coefficient of a-Si is higher than the reference crystalline silicon (c-Si). Such a high absorption coefficient allows one to make a much thinner solar cell without compromising the efficiency. For example, in the visible wavelength range, an ideal single junction solar cell with a 1 μm thick a-Si layer would convert up to 87% of the usable energy with a broad-band anti-reflective coating and a perfect back reflector. While in the same wavelength range, a 1 μm solar cell using the c-Si absorber layer would only convert 61% of the total available energy.

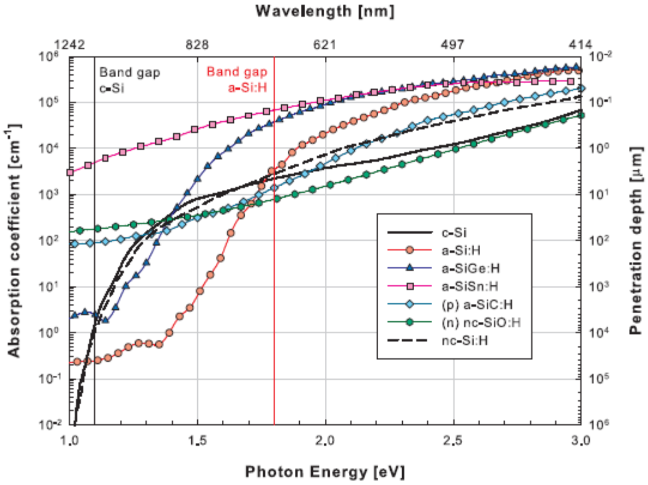

Fig. 1.1 Absorption coefficients of a-Si, μ-Si and c-Si [23].

However, in the early days a-Si could not be used as a photovoltaic material as it contains many dangling bonds which will act as recombination centres. It was until Chittick *et. al.* added hydrogen atoms in the material to passivate the bonds, a-Si became a more stable material that could be seriously used as a photovoltaic material [21]. Another advantage of a-Si is that it can be easily doped to either n-type or p-type by adding phosphine or diborane, respectively, to the gas mixture in the plasma enhanced chemical vapour deposition (PECVD) system for depositing a-Si thin film solar cells. In the next Section, we will introduce some typical structures of a-Si solar cells which are different from the c-Si based solar cells.

### 1.1.1 Amorphous silicon solar cell structure

Different from the traditional wafer based c-Si p-n junction solar cell structure, a-Si cannot be functional with the same structure due to the smaller carrier diffusion length than that of the c-Si. So a modified structure of either p-i-n or n-i-p [24-25] is utilised, as shown in Fig. 1.2, where the ‘n’ and ‘p’ stand for n-type and p-type doped layers while ‘i’ stands for the intrinsic layer. The collection of electron-hole pairs is mainly dependent on the built in electric field across the whole junction derived from the difference between the Femi levels of the n-layer and the p-layer. To absorb light sufficiently and extract the electron-hole pairs generated effectively, the thickness of the i-layer has to be optimised for the best solar cell performance.

The standard structure of a-Si solar cells generally consists of four different types of materials. In the sequence of deposition on the glass substrate, a p-i-n geometry contains the following layers: (i) front transparent conductive oxide (TCO) acting as the top electrode layer (from 0.6 μm to 2 μm) to collect holes, (ii) p-type, intrinsic, and n-type a-Si layers forming the p-i-n junction, (iii) back TCO acting as a protection layer from the metal back electrode (around 100 nm), and (iv) metal layer acting as the back reflector and electrode to collect electrons. The thickness of the doped layers is usually around 20 nm while the intrinsic layer is adjusted from 300-350 nm. In such a p-i-n geometry, the short wavelength range light is mainly absorbed in the front side of the junction within one single pass and the longer wavelength light can be absorbed sufficiently by several times internal bounces due to the total internal reflection. Because the hole diffusion length is smaller than that of the electron, the deposition of the p-layer always comes first in the formation of the junction so that the holes travel a shorter distance to the top electrode. At the rear side, the combination of the back TCO and the metal operates as the standard back reflector increasing the path length of longer wavelength light.

On the other hand, it is also possible to fabricate a-Si solar cells on flexible substrates, such as stainless steel [27], due to the low deposition temperature of the a-Si layers (usually around 200°C). In this case, an inverted deposition sequence is used to make the p-type layer still at the front side, as show in Fig. 1.2 (b). This type of solar cells is referred as the n-i-p structure. The n-type layer is deposited first on the back reflector followed by the other layers. Random textures are usually applied at the front TCO/p-layer interface for the p-i-n structure or at the back TCO/Ag interface for the n-i-p structure for light trapping.

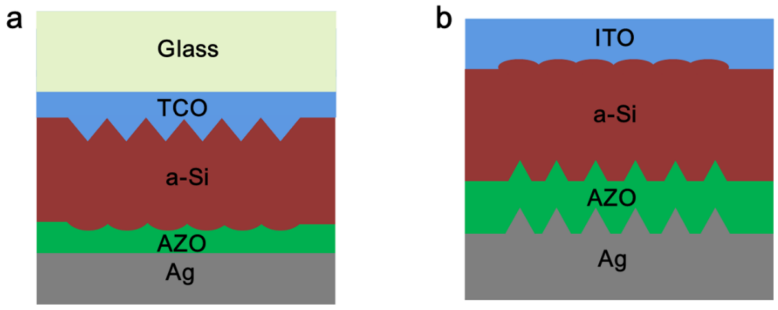

Fig. 1.2 Geometry of the a-Si solar cell in p-i-n configuration (a) or n-i-p configuration (b).

There are several challenges that remain in single junction a-Si solar cells to further increase the efficiency. One challenge is the light induced degradation known as the Staebler Wronki effect [28], which is related to the i-layer thickness. There is approximately a 15-25% efficiency loss with a long-term sunlight exposure for a-Si solar cells with a normal thickness (300 nm). The efficiency loss can be partially reversed by a high temperature annealing process at around 200°C. The degradation is dependent on the i-layer thickness, and can be reduced by using a thinner i-layer. However improved light trapping strategies are required in this case to maintain high solar cell efficiencies [29]. The other challenge is the low efficiency of single junction solar cell due to the bandgap of a-Si. The a-Si usually has a bandgap of around 1.75 eV, which only allows the a-Si solar cell to absorb the light less than 800 nm. To decrease the light induced degradation and improve the cell efficiency, the concept of multi-junction solar cells has been developed. Multi-junction solar cells can absorb sun light in much longer wavelength ranges [30-33]. The common tandem solar cell structure is the micromorph solar cell [17, 30] in which the bottom cell is a low bandgap material μ-Si (1.1 eV) and the top cell is a higher bandgap a-Si (1.75 eV) as shown in Fig. 1.3. Tandem solar cells can also be made of two or more subcells connected together from the top to the bottom. For commercial applications, two or three connected subcells are preferred due to the considerations on the cost and fabrication time. More complicated structures with more subcells have also been developed to reach ultra-high efficiency especially for the applications in space or for concentrated photovoltaic applications where sunlight is usually concentrated to 10-100 times to a smaller area.

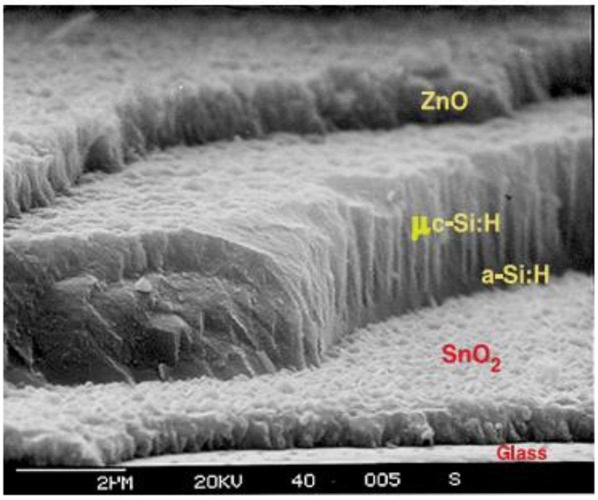

Fig. 1.3 Micromorph tandem solar cell structure [17].

### 1.1.2 Characterisation of solar cells

To characterise the solar cells properly, the understanding of how a solar cell works is important. The operation of a solar cell can be approximately represented using an equivalent circuit (Fig. 1.4) with the elements as follows: a current source (representing the flow of the photocurrent), a diode (representing the p-n junction), a shunt resistance (non-infinite values of which represent the parasitic current between the electrodes) and a series resistance (the sum of series resistances of the semiconductor, electrodes and external loads and circuitry) [23].

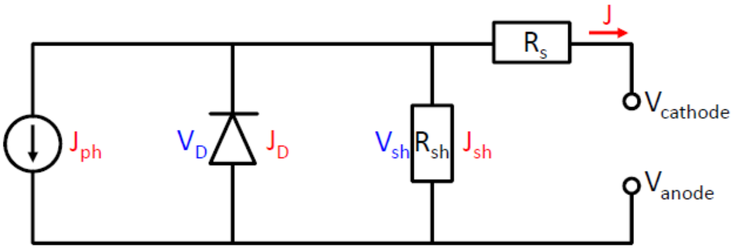

Fig. 1.4 The solar cell equivalent circuit. The current flowing through each of the components to represent the current-voltage characteristic of a solar cell [23].

To quantify the performance of the a-Si solar cell under light illumination, the current density voltage (I-V) characteristic and the external quantum efficiency (EQE) are standardised and must fulfil the following experimental conditions: (i) the spectral irradiance is relative to the *AM1.5* solar spectrum [34], (ii) the value of the irradiance is 1000 W/m$^2$, and (iii) the measurements are carried out at 25$^o$C.

The *J(v)* characteristic under illumination can be written as a linear superposition of the dark characteristics of the cell and the photogenerated current:

$$J(V) = J_0 \left[\exp\left(\frac{qv}{nkT}\right) - 1\right] - J_{PH} \tag{1.1}$$

where $J_{PH}$ is the photogenerated current density, $J_0$ is the saturation current density, q is the elementary charge, k is the Boltzmann constant, T is the absolute temperature and n is the ideality factor with n=1 standing for ideal p-n junctions, and n≈2 stands for p-i-n junctions.

Under the open circuit situation, $J(V)=0$, the open circuit voltage $V_{OC}$ can be deduced from (1), for a p-n junction

$$V_{oc} = \frac{kT}{q}\ln(\frac{J_{PH}}{J_0} + 1) \tag{1.2}$$

The efficiency of a solar cell is defined as the ratio of the max output power and input optical power $P_{in}$.

$$\eta = \frac{P_{out}}{P_{in}} = \frac{FF * V_{OC} * J_{SC}}{P_{in}} \tag{1.3}$$

*FF* is the fill factor, which is related to the recombination in the solar cell and defined as the ratio of maximum output power over the products of $V_{OC}$ and $J_{SC}$, as shown in Fig. 1.5.

$$FF = \frac{V_m * J_m}{V_{OC} * J_{SC}} \tag{1.4}$$

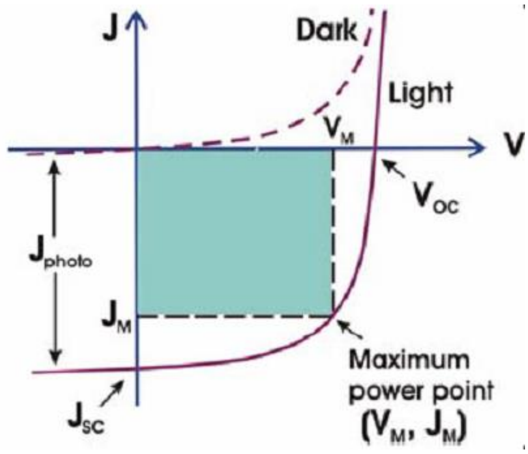

Fig. 1.5 The I-V curve of a solar cell [23].

The EQE is another important wavelength dependent value for the solar cell characterisation which measures the spectral response of a solar cell. For a-Si thin film solar cells, the EQE response is usually from 300 nm to 800 nm, which means that light with the wavelength above 800 nm could not contribute to the efficiency of an a-Si solar cell.

The incident photon flux $\Phi(\lambda)$ is defined as the number of photons per unit time, per unit area, and per unit wavelength:

$$\Phi(\lambda) = \frac{\lambda * P(\lambda)}{h * c} \tag{1.5}$$

where $h$ is the Planck constant and $c$ is the speed of light. The EQE can be defined as follows:

$$EQE(\lambda) = \frac{J_{PH}(\lambda)}{-q * \Phi(\lambda)} \tag{1.6}$$

It is the ratio of the number of electrons per unit time, per unit area, and per unit wavelength over the incident photon flux. And when integrating the $EQE\ (\lambda)$

with the corresponding *AM 1.5* spectrum (300 nm to 800 nm for the a-Si solar cell), the short circuit current density can be achieved. The applications of light management methods for thin film solar cells mainly influence $J_{SC}$. In the next chapters we will focus mainly on $J_{SC}$. Light trapping has a direct effect on the absorbance of solar cells and thus on the photogenerated current density. So when referring to the optical simulations in the following chapters, only the absorbance in the a-Si layer will be considered.

## 1.2 Nanoparticles and nanostructures enhanced solar cells

Regarding the traditional c-Si solar cells with a thickness around 250 μm, to achieve a good solar cell performance, usually pyramid surface textures are introduced on the front surface to scatter light into the solar cell over a large angular range, thereby increasing the effective path length in the cell [35-37]. However, the pyramidal geometry is not suitable for thin film solar cells as the surface roughness would exceed the film thickness. In addition, the large surface texture area will also increase the carrier recombination on the surface leading to the degraded solar cell performance. So, recently nanoparticles [38-40] and nanostructures [41-43] have attracted significant attentions for the applications in thin film solar cells as new and effective light trapping methods. In this Section, we will have a brief discussion about the nanoparticle and the nanostructure enhanced solar cells.

Both the metallic and the dielectric nanoparticles have been integrated with solar cells to achieve light trapping. Metallic nanoparticles that support localised surface plasmons can greatly enhance the light path length inside solar cells [44-52]. The resonances of noble metals are mostly in the visible or the infrared region of the spectrum, which is in the range of interest for thin film solar cells. The surface plasmon resonance is mainly affected by the size, shape and the dielectric properties of the surrounding media. By tailoring the geometry of the metallic nanoparticles, the surface plasmon resonance can be tuned based on the requirements of the applications [47, 52]. There are three main mechanisms that could be utilised for enhancing the performance of photovoltaic devices: (a) the scattering from the metal particles (far-field effect); (b) the near field enhancement from small nanoparticles, which directly enhance the absorbance of the semiconductor in the close vicinity of the nanoparticles due to the enhanced field; (c) for the plasmonic nanostructure enhanced solar cells, light can be coupled into surface plasmon polariton (SPP) modes or guided modes from a nanostructured metallic film on the back surface of a thin photovoltaic absorber layer [53-56]. The three main mechanisms for absorption enhancement in solar cells by plasmonics will be discussed in detail in Chapter 2, but a brief historical perspective will be provided here.

Rapid progress has been made in the field of plasmonic solar cells since 2008. Many nanostructure and nanoparticle fabrication methods have been explored. Till now, plasmonic effects have been investigated in almost all kinds of solar cells, such as c-Si based solar cells [46], a-Si solar cells [44, 49], GaAs solar cells [45], CdSe solar cells [57] and organic solar cells [58, 59]. Systematic numerical modelling for different structures of solar cells has been conducted towards new plasmonic nanostructure designs [60-62].

Among all the designs, metallic nanoparticles have been the most commonly used and simplest plasmonic nanomaterials in effectively enhancing the solar cell absorption. These nanoparticles acting as scatters have been integrated on the top or at the back surface of solar cells during the cell fabrication [43-51]. Both experiments and simulations have proven that the light absorption with the nanoparticle integrated solar cells can be improved compared to the reference solar cells especially in the longer wavelength range, where more light will be scattered due to the plasmonic enhanced scattering [44, 50, 52]. The disadvantage of applying metallic nanoparticles on top of the solar cells is that the nanoparticles must be optimised by changing the sizes, shapes and coverage densities to minimise the nanoparticle absorption loss so that light can be coupled into solar cells more efficiently.

To minimise nanoparticle absorption loss, in some cases, small metallic nanoparticles have been applied close to the active layers in a-Si or organic solar cells to boost the $J_{SC}$ value by utilising the near field enhancement from the nanoparticles [63-67]. In addition to the plasmonic nanoparticle enhanced solar cells, the metallic nanostructures such as the void structures [68-70], grating structures [71, 72] and nanocone structures [73-75] have also been widely explored in organic and a-Si thin film solar cells. The unique nanostructure designs can generate different guided modes or hybrid plasmon modes by controlling the geometries of the nanostructures thereby enhancing the absorbance of solar cells. However, one of the problems of these nanostructured solar cells is that normally the multilayered solar cells are fabricated on the nanostructured substrates. After the solar cell fabrication, the top layer morphology, which plays an important role in determining the light trapping effect, will not follow exactly the shape of the designed nanostructures in the substrate layer due to the increased thickness of the stacking films. Therefore it is challenging to directly engineer the morphology on top of a solar cell with the nanostructure textured rear surface of the substrate. In particular, it is challenging to achieve an entire band absorption enhancement for the a-Si layer using plasmonic nanoparticles or nanostructures due to the shadowing and the parasitic absorption.

To avoid the parasitic absorption of the metallic nanoparticles when applying them on top of the solar cells, dielectric nanoparticles can be used. $TiO_2$ nanoparticles have been demonstrated on top of the c-Si solar cells to act as anti-reflective coatings. Closely-packed $SiO_2$ were used to generate whispering gallery modes (WGMs) to enhance the absorbance in solar cells [76-80]. Dielectric nanoparticles can successfully avoid the shadowing problem and the parasitic absorption existing in the metal nanoparticles. In addition to the dielectric nanoparticles, nanoshells have also been demonstrated to be able to achieve effective light trapping by coupling the incident light into some particular modes or increasing the optical path length in the solar cells by utilising the WGM resonances [81, 82]. The above-mentioned dielectric nanoparticles and nanoshell structures can provide effective light trapping schemes for thin film solar cells.

In conclusion, the nanoparticles on the top surface and the nanostructures at the rear surface of the solar cells, respectively, have shown great potential to improve solar cell performance. However, the absorption enhancement is only focused on specific wavelength regions, such as the blue region of the spectrum for nanoparticle enhanced solar cells and the red region of the spectrum for nanostructure enhanced solar cells. To realise an even higher performance ultra-thin solar cell, the nanoparticles and the nanostructures need to be combined together in the solar cell design for an entire wavelength absorption enhancement. In this thesis, a novel solar cell geometry has been developed by the combination of low absorption loss nanoparticles on the top surface and conformal nanostructures at the back surface in a natural way.

## 1.3 Thesis objective and thesis preview

The objective of this thesis is to develop an ultra-thin a-Si solar cell architecture with high absorbance in the a-Si layer using novel nanoparticles and nanostructures. To achieve this objective, this thesis consists of four main parts. First, we compare the large plasmonic metallic nanoparticles with the closely-packed dielectric $SiO_2$ nanoparticles to find out which kinds of nanoparticles are more suitable for improving the solar cell performance when integrated on the top surface. Then the use of the near-field light concentration effects from small metallic nanoparticles for enhancing the absorbance and the efficiency of the normal thick solar cells is investigated. To further improve the solar cell performance with a thinner active layer thickness, the influence of closely-packed $SiO_2$ nanoparticles on a 150 nm thick solar cell is investigated by engineering the position of the nanoparticles. The dielectric nanoparticles are partially imprinted into the solar cells from the top surface to form conformal nanostructures at the rear surface of the solar cell naturally, thereby manipulating light in the interested wavelength region. At last, through combining the advantages of the large dielectric nanoparticles, small plasmonic nanoparticles and a-Si nanostructures together, a broadband light absorption enhancement for ultra-thin a-Si (20 nm) thin film solar cells is demonstrated. To achieve these goals, the studies have been conducted in the following sequences.

Chapter 2 reviews the current light management methods for thin film solar cells, which serves as a bench-mark for this thesis. In Section 2.2, we review the mechanisms for the plasmonic enhancement of absorption in thin film solar cells, mainly including metallic nanoparticles. The numerical modelling results of Al and Ag large metallic nanoparticles for the absorption enhancement in a-Si solar cells are conducted in this Section. In Section 2.3, we review the mechanisms of dielectric nanoparticles for improved thin film solar cells. The numerical modelling results of closely-packed $SiO_2$ nanoparticles on top of solar cells are shown in this Section. Through the comparison with the large metallic nanoparticles, we find that the dielectric $SiO_2$ nanoparticles can couple light more efficiently into the a-Si solar cells when integrated on top of the solar cells. In Section 2.4, several generally used nanostructures for advanced light trapping in thin film solar cells are reviewed and compared.

In Chapter 3, the experimental results of small metallic nanoparticles enhanced a-Si thin film solar cells are presented in Section 3.2. Both the small Au and the Ag nanoparticles with the diameter of around 10 nm are integrated into the a-Si solar cells by physical vapour deposition method. The performances of the solar cells with small metallic nanoparticles integrated are enhanced due to the near-field light concentration effects.

In Chapter 4, we systematically investigate the conformal structured solar cells induced by imprinting the $SiO_2$ nanoparticles. In Section 4.2, we first investigate the best position of $SiO_2$ nanoparticles for the highest absorption enhancement in a-Si solar cells by tuning the relative distance of nanoparticles inside the solar cells. Through calculation, we find the best position is with nanoparticles half embedded into the top surface of the solar cells. Then we systematically investigate different sizes of the nanoparticles and thicknesses of the AZO layer in the solar cells to find out the optimised condition for the new conformal solar cell geometry. In Section 4.3, we introduce a new fabrication method for the conformal structure solar cell and characterise the solar cells.

Based on the knowledge obtained from the previous chapters, to finally achieve high absorbance solar cells with an ultra-thin active layer (20 nm), a new nanoparticle model called the hetero-structured lumpy nanoparticle is set up in Chapter 5. This unique particle architecture combines large $SiO_2$ core particles and small metallic nanoparticles on the surface of the core nanoparticles. We investigate the size effects of the nanoparticles on the absorbance of a-Si solar cells when integrating them on top of the solar cells by numerical modelling in Section 5.2. Then we explore the conformal structure solar cells integrated with the hetero-structured lumpy nanoparticles by changing the relative distance and the sizes of the nanoparticles by both theoretical and experimental methods in Sections 5.3 and 5.4.

In Chapter 6, a conclusion of this thesis and the future work are presented. Section 6.2.1 suggests using plasmonic nanoparticles as well as the novel conformal structure and hetero-structured lumpy nanoparticles to enhance the performance of tandem thin film solar cells. In Section 6.2.2, we suggest applying the lumpy nanoparticles for solar cells with different active materials. In Section 6.2.3, we propose to combine metallic nanowires with traditional ITO layer together as a combined top electrode to enhance the electrical properties of the conformal structured solar cells.

# Chapter 2

## Literature review

### 2.1 Introduction

Before discussing what has been done in this thesis to improve the performance of a-Si thin film solar cells through novel light trapping geometry, this Chapter reviews the state-of-the-art thin film solar cells enhanced by nanoparticles and nanostructures to help to better understand the background and our motivation. Section 2.2 reviews the enhanced solar cells by plasmonic nanoparticles, localised surface plasmon excited by nanoparticles can be applied to solar cells to improve the absorbance through enhanced scattering and highly localised electric field. Finite difference time domain method (FDTD) is applied for the investigation of metallic nanoparticle integrated solar cells. Section 2.3 reviews the enhanced solar cells by dielectric nanoparticles, which provide an entirely different light trapping mechanism to enhance the absorbance in solar cells. Section 2.4 reviews the different nanostructures applied in thin film solar cells. The waveguide modes and surface plasmon polariton (SPP) modes are described in this Section. The challenge for the current nanophotonic solar cell research is to design the solar cell geometry with broadband light trapping schemes across the entire solar spectrum.

## 2.2 plasmonic nanoparticle enhanced thin film solar cells

Subwavelength metallic nanoparticles have been recently widely used to redirect light into different angles to enhance the light path in solar cells or localise the electric energy in the close vicinity of the nanoparticles thereby increasing the absorbance in the active layer. These nanoparticles are either on the front or the back surfaces of an absorbing layer which are shown in Figs. 2.1 (a) and (c), or embedded into the absorbing layer as shown in Fig. 2.1 (b). This can lead to higher short circuit current densities, in both relatively thick cells and thin solar cells on index-matched substrates due to the localised surface plasmon (LSP) effect from the metallic nanoparticles [39].

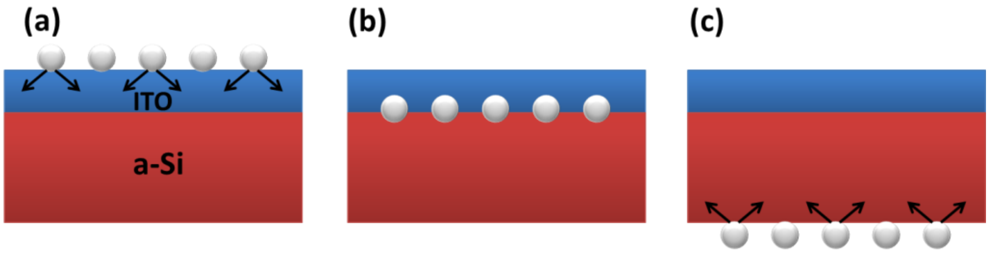

Fig. 2.1 Nanoparticles light trapping geometries for thin film solar cells. (a) Light trapping from metallic nanoparticles on top of solar cells. (b) Light absorption enhancement in the semiconductor by embedded nanoparticles due to the enhanced electric field around the nanoparticles. (c) Light trapping from metallic nanoparticles at the back of solar cells.

LSPs are non-propagating excitations of electron collective oscillations within a metallic nanoparticle. In the classic example of LSPs, a metallic nanoparticle is illuminated by external light, enhanced absorption and scattering can typically be observed at the resonance [83]. Fig. 2.1 shows the normal integration positions of metallic nanoparticles inside thin film solar cells. Two different mechanisms account for the absorbance enhancement in solar cells. One is the light scattering from the larger nanoparticles into the active layer when they are integrated on the top or back of the solar cells as shown in Figs. 2.1 (a) and (c). These nanoparticle arrays prefer scattering light into larger permittivity materials such as the a-Si when they are placed close to the a-Si layer [40, 44, 45]. The scattered light will be trapped in the a-Si layer, being bounced several times in the active layer and absorbed adequately. The other mechanism for absorption enhancement in solar cells comes from the near field concentration related to the LSP of small metallic nanoparticles when they are placed in the active layer as shown in Fig. 2.1 (b) [65-67]. By tuning the sizes and shapes of nanoparticles, particular frequency of optical excitation will lead to strongly enhanced fields in the close vicinity of nanoparticles. The absorbance in the active layer is proportional to the electric field enhancement, therefore significantly increase a-Si absorption can be achieved.

### 2.2.1 Localised surface plasmons of nanoparticles

To get better understanding of the theory of the nanoparticles plasmonics, we present the formalism for obtaining the quasi-static approximation for the resonant frequency of a spherical particle in a uniform external electric field [39, 40]. We can express the scattering and absorption cross-sections of the sphere respectively:

$$C_{sca} = \frac{k^4}{6\pi}|\alpha|^2$$

$$C_{abs} = k\mathrm{Im}(\alpha)$$

$$\alpha = 4\pi a^3 \frac{\varepsilon - \varepsilon_d}{\varepsilon + 2\varepsilon_d}$$

where K is the magnitude of the wave vector of the incident light, $\alpha$ is the polarisability and $a$ is radius of the sphere. The dielectric constants of the sphere and the dielectric medium are presented as $\varepsilon$ and $\varepsilon_d$ respectively [83, 84]. When $\varepsilon = -2\varepsilon_d$ the polarisability is at a maximum and the sphere exhibits a dipole surface plasmon resonance. If the medium surrounding the sphere is an ordinary dielectric material, $\varepsilon_d$ is positive and the real part of $\varepsilon$ must be negative to satisfy this condition. Obviously, it cannot be fulfilled with a dielectric sphere in a dielectric medium. However, in terms of metal materials, the real parts of dielectric constants $\mathrm{Re}[\varepsilon_d]$ can be negative at specific wavelengths. At these wavelengths, resonant scattering cross-section and absorption cross-section can be achieved. This is regarded as the localised plasmon resonance.

### 2.2.2 Plasmonic light scattering effect for active layer absorption enhancement

There are a number of good reviews about enhancing solar cell efficiency through the plasmonic interactions [38, 39, 85, 92], where in conclusion three methods on how plasmonics can be applied in thin film solar cells for light trapping were summarised: (i) Plasmonic scattering effect (ii) plasmonic near field effect (iii) SPP modes. In this Section, we will focus on the plasmonic scattering effect for improving the light path in the solar cells thereby increasing the absorbance.

Plasmonic in-coupling of scattered light from an external layer of metallic nanoparticles into the absorbing layer has been reported for different kinds of solar cells. In a typical configuration, metallic nanoparticles such as Ag, Au or Al can be deposited onto the front surface or the back surface of the solar cell, either embedded on the front electrode or electronically isolated by a transparent conductive oxide layer as shown in Figs. 2.1(a) and 2.1(c). The absorption enhancement in the active layer can be optimised by adjusting the nanoparticles sizes (in the order of 100 nm or more for light scattering) and the nanoparticles surface coverage density. This solar cell configuration has been applied to demonstrate the efficiency enhancements in crystalline silicon solar cells, gallium arsenide solar cells and organic solar cells [45, 86-88].

Recently, plasmonic light scattering mechanism has been widely implemented into a-Si thin film solar cells with similar geometries as shown in Figs. 2.1 (a) and 2.1(c). In terms of the concept with different nanoparticles located on the front surface of a-Si solar cells, the enhancement in the photocurrent and the efficiency have been achieved by a number of groups [44, 50, 76, 89, 90]. When metallic nanoparticles are placed on top of the solar cells, the incident light are preferentially scattered into the high permittivity materials [39]. For example, Ag nanoparticles have been applied on top of solar cells to increase the light path through the plasmonic light scattering, thereby increasing the efficiency by around 10% as shown in Fig. 2.2 [90]. In addition, Au nanoparticles have also been applied on top of a-Si solar cells achieving an 8.3% enhancement in the power conversion efficiency [44]. For the nanoparticles integrated at the rear side of the solar cells, many studies have been published, most of which with Ag nanoparticles fabricated by the thermal annealing method, chemical methods or the laser interference lithography method. V. E. Ferry *et.al* from California Institute of Technology have systematically investigated the rear surface located Ag nanoparticles fabricated by laser interference lithography for a-Si solar cells and shown a relative 46% $J_{SC}$ enhancement due to the plasmonic back scattering [91]. By optimising the particles sizes and pitches, solar cells with efficiency of 9.6% have been achieved with an only 90 nm thick active layer [93]. Recently, the nucleated Ag nanoparticle geometry was also demonstrated to be an effective way to achieve a broadband light trapping for a-Si thin film solar cells when they were integrated at the rear surface of the solar cell by introducing a large scattering cross section from the nanoparticles [49].

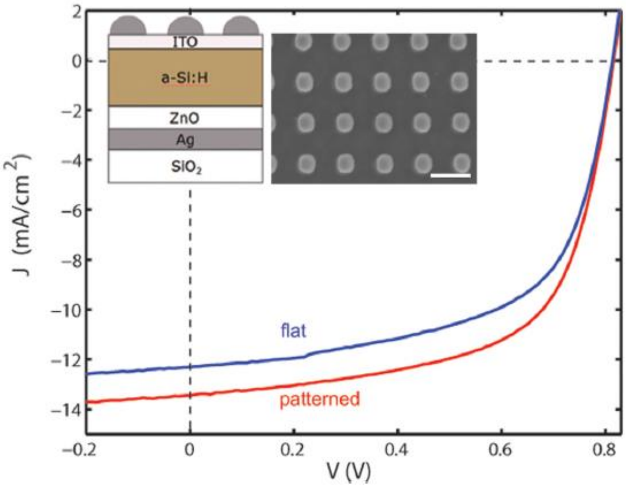

Fig. 2.2 I-V curves for the a-Si solar cell with Ag nanoparticles on top (500 nm pitch, 120 nm height and 120 nm radius, red) and a flat reference cell (blue). The insets show a schematic cross section of the solar cell structure and a top-view SEM image of the particle array (scale bar 500 nm) [90].

### 2.2.3 Numerical modelling of a-Si thin film solar cells integrated with large metallic nanoparticles on top

The light trapping effects from large metallic nanoparticles are also investigated by numerical modelling in this Section. We focus on investigating how the metallic nanospheres with different materials such as Ag and Al affect the absorption of a-Si solar cells when they are integrated on the top surface. Optimisation of plasmonic light scattering from large metallic nanoparticles in solar cells is a balancing process and several physical parameters must be taken into account. Here, we mainly focus on two materials for metallic large nanoparticles which are Ag and Al due to the consideration of the low particle absorption loss and the low material cost, respectively. To study and compare the performance of nanoparticle enhanced solar cells using metallic and dielectric nanoparticles, Lumerical FDTD software is used to simulate the case of an n-i-p a-Si solar cell structure. Ag or Al nanoparticles are set on top of an 80 nm ITO layer as shown in Fig. 2.3. The ITO layer is used as a transparent conductive top electrode and also an anti-reflection coating for a-Si solar cells. The thickness of the a-Si layer is set to be 300 nm as a normal case for the a-Si solar cell production. The ZnO:Al layer and the Ag back contact is set to be 100 nm and 180 nm, respectively. In our simulation, the shape of nanoparticles is sphere. Two flat power monitors are inserted between the top surface and the bottom surface of the a-Si layer to calculate the power absorbed in the a-Si layer, which can be defined as the power difference between the two monitors:

$$P_{abs} = T\ (monitor\_top) - T\ (monitor\_bottom)$$

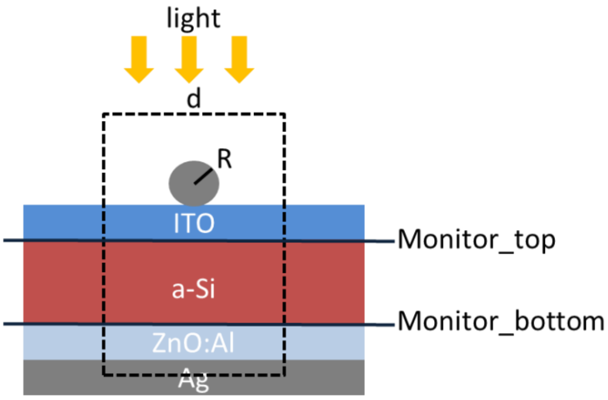

Fig. 2.3 Schematic of the cross section of the simulation model with a metallic nanosphere on top of an a-Si solar cell.

To quantify the effect of the nanoparticles on the absorbance of a-Si solar cells, the absorbance of the a-Si $A(\lambda)$ is first calculated, which is defined as the ratio of the absorbed power $P_{abs}(\lambda)$ to that of the incident light power $P_{in}(\lambda)$ within the a-Si film.

$$A(\lambda)=P_{abs}(\lambda)/P_{in}(\lambda), \tag{2.1}$$

By integrating the absorbance with the *AM 1.5* solar spectrum, we can obtain the area independent short circuit current density ($J_{SC}$), assuming that all generated electron-hole pairs can contribute to the photocurrent,

$$J_{SC}=e\int(\lambda/hc)A(\lambda)I_{AM1.5}(\lambda)d\lambda, \tag{2.2}$$

where $e$ is the electron charge, $h$ the Plank's constant, $c$ the speed of light in free space and $I_{AM1.5}$ *AM 1.5* solar spectrum. The absorption enhancement $G$ in the 300 nm thick a-Si film with/without nanoparticles is calculated as:

$$G=A_{with\ NP}(\lambda)/A_{ref}(\lambda), \tag{2.3}$$

where $A_{with\ NP}(\lambda)$ represents the absorbance of the a-Si film with the nanoparticles, and $A_{ref}(\lambda)$ the absorbance of the a-Si layer without the nanoparticles.

To find out the optimised parameters of the metallic nanoparticles for the largest absorption enhancement in the a-Si film, the diameter and the surface coverage (SC) are systematically investigated. SC is defined as the ration of the area of the nanoparticles to the area of the simulation region ($\pi R^2/d^2$ as shown in Fig. 2.3). The diameters are selected to be 100 nm, 150 nm, 200 nm, 250 nm and 300 nm while the SCs are changed from 10% to 30% with an interval of 5%. By calculating the absorbance as a function of the diameter of nanoparticles and the SC, the optimised condition for the absorption enhancement in the a-Si layer is shown in table. 2.1. Tables. 2.1 (a) and (b) show calculated $J_{SC}$ enhancements in the a-Si layer with the Al nanospheres and Ag nanospheres, respectively, which is normalised to the $J_{SC}$ (13.63 mA/cm$^2$) in the flat a-Si solar cells as a function of the diameter and the SC.

(a) With the Al nanosphere

| **SC**<br>**Radius** | **10%** | **15%** | **20%** | **25%** | **30%** |
|---|---|---|---|---|---|
| **50 nm** | 1.03637 | 1.03083 | 1.01271 | 0.990488 | 0.964318 |
| **75 nm** | 1.06332 | 1.0757 | 1.05975 | 1.02189 | 0.977132 |
| **100 nm** | 1.07522 | 1.06049 | 1.06324 | 1.02884 | 0.983118 |
| **125 nm** | 1.04143 | 1.10049 | 1.07982 | 1.04425 | 0.996497 |
| **150 nm** | 1.00722 | 1.01317 | 1.05765 | 1.05655 | 0.977453 |

(b) With the Ag nanosphere

| **SC**<br>**Radius** | **10%** | **15%** | **20%** | **25%** | **30%** |
|---|---|---|---|---|---|
| **50 nm** | 0.96352 | 0.931505 | 0.903264 | 0.874438 | 0.840227 |
| **75 nm** | 1.00721 | 0.959482 | 0.914967 | 0.869194 | 0.824285 |
| **100 nm** | 1.0808 | 1.03643 | 0.995401 | 0.923423 | 0.860234 |
| **125 nm** | 1.06259 | 1.11668 | 1.07791 | 1.00469 | 0.931288 |
| **150 nm** | 1.00635 | 1.0295 | 1.07013 | 1.03325 | 0.922627 |

Table 2.1 $J_{SC}$ enhancements with metallic nanospheres on top of an a-Si solar cell normalised to the cell without nanospheres (a) with Al nanosphere (b) with Ag nanosphere.

In table 2.1, the data above 1 means the a-Si absorption with the corresponding metallic nanospheres is enhanced. For the value below 1, the absorption is decreased. For example, for the radius of the 125 nm Al nanosphere with a 15% SC, the normalised enhancement is 1.10049, which means the absorption enhancement is 10.049%. From Table. 2.1 (a), we can find that the highest absorption enhancement of 10.049% is achieved under the optimised parameters of 125 nm in radius and 15% in SC for Al nanospheres. Lower enhancement value of G=1.075 and G=1.0757 can also be achieved with radius of 100 nm at 10% SC and radius of 75 nm at 15% SC respectively. For 50 nm radius, the best enhancement is only G=1.0363 with a 10% SC. When the radius is further increased to 150 nm, the highest enhancement obtained is G=1.0576 at 20% SC. It can be seen that as the SC increases to 30%, the absorption enhancement will be decreased mainly due to the increased parasitic absorption in metallic nanoparticles. The increased radius of metallic nanospheres from 50 nm to 125 nm can enhance the absorbance in the a-Si layer by the larger light scattering cross section and incoupling into waveguide modes in the a-Si layer [45, 47, 90]. When the radius is further increased to 150 nm, the best absorption enhancement is not as high as that with radius of 125 nm. This is mainly due to the less effective light coupling from larger Al nanospheres into a-Si solar cells [50]. In terms of larger nanoparticles, high absorption enhancements in the a-Si layer can be achieved with low SC because the scattering-cross sections are much larger than that of small nanoparticles [83]. The spectral absorbance of the a-Si active layer with Al nanospheres on top is shown in Fig. 2.4. Three radii of large nanoparticles are selected for the best absorption enhancement in each case.

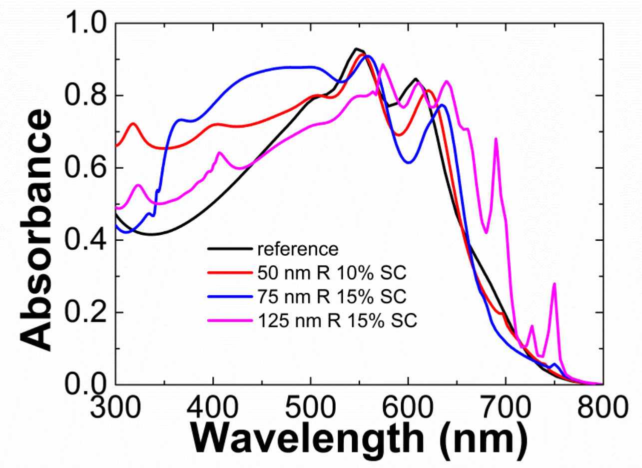

Fig. 2.4 The spectral absorbance in the a-Si layer with and without Al nanosphere arrays.

From the absorbance spectra in Fig. 2.4, we can find that for a-Si solar cells integrated with comparatively small Al nanoparticles (50 nm at a 10% SC and 75 nm at a 15% SC), the absorbance of the a-Si layer is mainly enhanced at the wavelengths below 500 nm compared to the reference case. This is mainly due to the forward scattering and the anti-reflection effect of the Al nanoparticles [40, 50]. However when the particle size is increased to 125 nm (at a 15% SC), the absorbance of the a-Si layer is mainly enhanced above 620 nm due to the wave-guide modes coupling [90]. Compared with the reference case, multiple peaks in the a-Si layer in the near infrared wavelength are generated due to the light coupling to the waveguide modes by the Al nanospheres. In the case of conventional noble metal plasmonic nanoparticles, such as Au and Ag, the resonant coupling of the incident light with the nanoparticle surface plasmons will lead to a significant parasitic absorption inside the nanoparticles thereby decreasing the absorbance in the a-Si layer [50]. However, for the Al nanospheres, the parasitic plasmon induced absorption does not reduce the absorbance in the a-Si layer because the plasmonic resonance peaks of Al nanospheres are located in the ultraviolet region outside the a-Si absorption band [50]. As the radius of the nanosphere increases, the plasmonic peaks redshift, which leads to the parasitic absorption shifted [83] to the a-Si absorption region decreasing the absorbance gain introduced by the anti-reflection effect of the Al nanosphere. As a result, for the 125 nm and 15% SC Al nanosphere, the a-Si absorbance enhancement in the short wavelength is not as high as that for the cases with radii of 50 nm and 75 nm. However, the absorbance in the longer wavelength is significantly increased due to the light coupling to the waveguide modes.

From table 2.1 (b), we can see that the largest absorbance enhancement G=1.1167 can be achieved with Ag nanospheres at 125 nm with a 15% SC. And in the case of 50 nm and 75 nm radius nanoparticles, the absorbance of the a-Si is decreased significantly under most of the conditions. For the cases with the radii of 100 nm and 150 nm, the best absorption enhancement can be obtained with the optimised SCs at 10% and 20%, respectively. As the SC increases, the absorbance of the a-Si is reduced due to the increased plasmon induced absorption from the dense Ag nanosphere arrays.

To find out the spectral distribution of the absorption enhancement in the a-Si layer, in Fig. 2.5 we plot the absorbance spectra of the a-Si solar cells integrated with 50 nm (10% SC), 75 nm (10% SC) and 125 nm (10% SC) Ag nanospheres. In the case of 50 nm (10% SC) shown as the red line, the overall absorbance of the a-Si is decreased mainly due to the parasitic plasmonic absorption of the Ag nanospheres in the short wavelength [89, 90]. For Ag nanosphere arrays with the radii of 75 nm at a 10% SC shown as the blue line, the absorbance of the a-Si is enhanced in the wavelength range from 420 nm to 500 nm because of the anti-reflection effect of the Ag nanospheres [88]. In the longer wavelength range above 700 nm, two waveguide modes at 710 nm and 740 nm are generated by the coupling of the scattered light from the Ag nanospheres. However, although the absorbance at some wavelengths is improved, the overall absorbance of the a-Si is still near the same compared to the reference flat solar cell. As a result, only 0.72% enhancement is observed as shown in Table 2.1 (b). For the 125 nm (15% SC) Ag nanospheres as shown in the purple line in Fig. 2.5, the absorbance in the short wavelength from 300 nm to 600 nm is decreased due to the plasmonic induced near field absorption and also the less effective light coupling into the a-Si layer due to the enhanced back scattering effect [85, 88-90]. However in the longer wavelength range above 600 nm, there exist several waveguide modes coupled from the plasmonic scattering of light from the Ag nanospheres into the a-Si layer [90]. The reason is that the large particles have larger scattering power. Therefore it can scatter more light into the waveguide mode of the a-Si. The longer wavelength absorbance enhancement overweighs the decreased light absorbance in the shorter wavelength range leading to an overall absorbance enhancement of 11.67%.

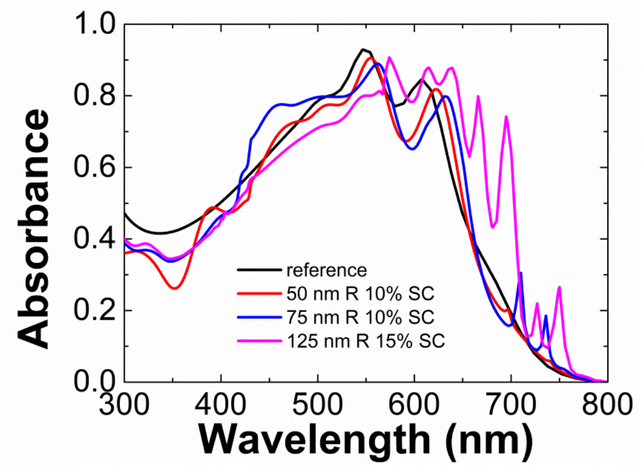

Fig. 2.5 The spectral absorbance of the a-Si layer with and without the Ag nanosphere arrays.

Through comparing the absorbance of a-Si layers integrated with the Al nanosphere arrays and the Ag nanosphere arrays, we can reach some conclusions. For smaller metallic nanosphere arrays with radii less than 75 nm and low SCs less than 15%, the nanospheres can act as an anti-reflection coating and couple more light in the short wavelength into the a-Si layer [40, 50]. The performance of Al nanospheres is better than the Ag nanospheres due to less particle absorption in the interested wavelength range. As for the larger nanospheres with low SCs less than 20%, the anti-reflection property of the nanospheres is compromised by the particle absorption due to the redshift of the LSP resonance with increased particle size. In the meantime, the plasmonic scattered light from the metallic nanospheres in the longer wavelength range can be strongly coupled to distinct waveguide modes in the a-Si layer, increasing the longer wavelength absorption [90]. The light coupling efficiency for the larger Ag nanospheres into the a-Si layer is stronger than that for the Al nanospheres. The achieved highest absorption enhancement is G=1.1005 for Al nanospheres with a 125 nm radius and a 15% SC and G=1.1167 for the Ag nanospheres with a 125 nm radius and a 15% SC, respectively.

Form the numerical modelling, it is challenging to realise a broadband light absorption enhancement by utilising metallic nanospheres due to the narrow band plasmonic resonant nature. To fulfil an entire band light absorption enhancement, the influence of the closely-packed dielectric nanospheres on the absorbance in a-Si solar cells is depicted in the Section 2.3.

### 2.2.4 Plasmonic near field effect for absorption enhancement

In comparison to the forward or back scattering from the comparative large nanoparticles to enhance the Si absorbance, small metallic nanoparticles can be applied in the close vicinity to the active layer as shown in Fig. 2.1(b) to make use of the LSP near field enhancement of the electromagnetic field, which can give rise to the absorption enhancement in the active layer around the nanoparticles. Numerous publications have been reported in recent years regarding the enhanced absorbance resulting from the embedded metallic nanoparticles in the active layer for thin film solar cells, especially in organic solar cells [63-67]. High efficiency plasmonic tandem solar cells have also been reported [64], achieving 20% enhancement in the efficiency from 5.22% to 6.24% due to the LSP near field absorption enhancement.

Theoretically embedding metallic nanoparticles in the active layer of thin film solar cells can lead to significant absorption enhancement. For instance, it was predicated an ideal conversion efficiency of 18% can be achieved by combining an Ag/a-Si nanocomposite layer with an only 20 nm thick active layer as shown in

Fig. 2.6 [65].

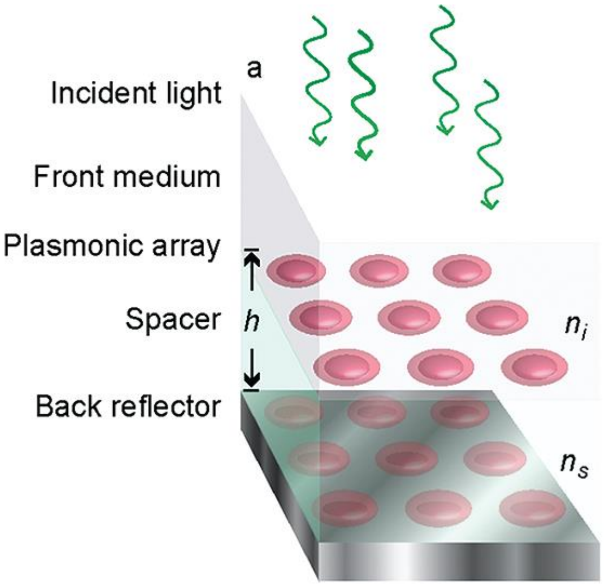

Fig. 2.6 Array of metal core/semiconductor shell nanoparticles represents a close to ideal plasmonic near-field absorber [65].

## 2.3 Dielectric nanoparticle enhanced thin film solar cells

To avoid the inherent loss issue associated with metallic nanoparticles, dielectric nanoparticles have been employed due to almost negligible absorption loss in the visible to near infrared range and broadband scattering cross sections which are beneficial for solar cells. Although their scattering cross sections are less than those of metallic nanoparticles at the resonance wavelengths, the absence of particle absorption leads to comparable light absorption enhancements in the active layer of solar cells. In addition, the refractive indices of the dielectric nanoparticles are normally from 1.5 to 2.0 making them competitive candidates for antireflection components in the solar cell geometry when they are incorporated on top of the solar cells.

Both simulation and experimental work has been reported on the solar cells with dielectric nanoparticles integrated on the top surface [76-80]. For instance, $SiO_2$ nanoparticles with a size of 150 nm and a density of $2.1\times10^{9}$ $cm^{-2}$ are incorporated on the top surface of the quantum-well solar cells by D. Derkacs leading to an increased *Jsc* of 12.9% and efficiency enhancement of 17% as shown in Fig. 2.7 [97]. The enhancements arose from the coupling of the incident light into lateral optical propagation, with optical confinement provided by the refractive index contrast of the quantum-well layers. In this case, due to the top layer of the solar cell is the 15 nm thick $SiO_2$, the $SiO_2$ nanoparticles do not obviously show the anti-reflection properties because of the small refractive index difference between the $SiO_2$ nanoparticles and the $SiO_2$ layer. To illustrate the anti-reflective properties of the dielectric nanoparticles, D. Wan implemented a closely-packed 65 nm $TiO_2$ nanoparticle film on top of Si solar cells using the spin-coating method [77]. After the nanoparticle integration, the reflectance of the substrate was reduced dramatically from 35% to less than 15% over the entire interested wavelength range, leading to a 30% improvement in the photocurrent. This was attributed to the antireflection effect of the $TiO_2$ nanoparticles for planar Si solar cells.

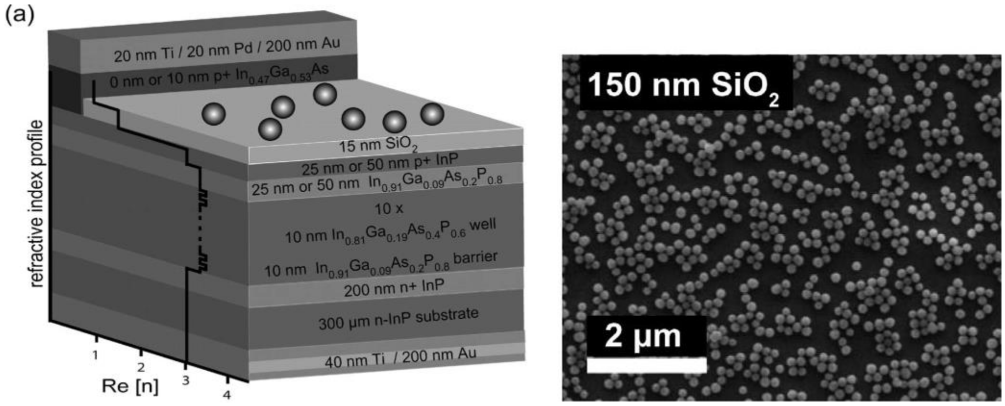

Fig. 2.7 The geometry of quantum-well solar cells with $SiO_2$ nanoparticles on the top surface [96].

Recently, a new concept for light trapping in a-Si thin film solar cells through the use of whispering gallery modes (WGM) generated by closely-packed $SiO_2$ nanoparticles has been proposed to enhance the absorption and the photocurrent [78, 79]. The $SiO_2$ nanoparticles are integrated on top of a standard a-Si solar cell as shown in Fig. 2.8 a. Closely-packed $SiO_2$ dielectric nanospheres are interesting photonic structures because they can diffractively couple light from air and support confined resonant modes inside the nanospheres. In addition, the periodic distribution of the nanospheres can result in light coupling between the adjacent spheres, leading to mode splitting. The coupling originates from the WGMs inside the spheres. When the resonant dielectric nanospheres are placed in the close vicinity of a high-index solar cell absorber layer, such as a-Si, the incident light from free space can be coupled into the high-index absorber layer thereby increasing the light absorbance in the solar cell. Another obvious advantage of these closely-packed $SiO_2$ nanospheres for photovoltaic application is the spherical geometry allows the acceptance of light from large angles of incidence.

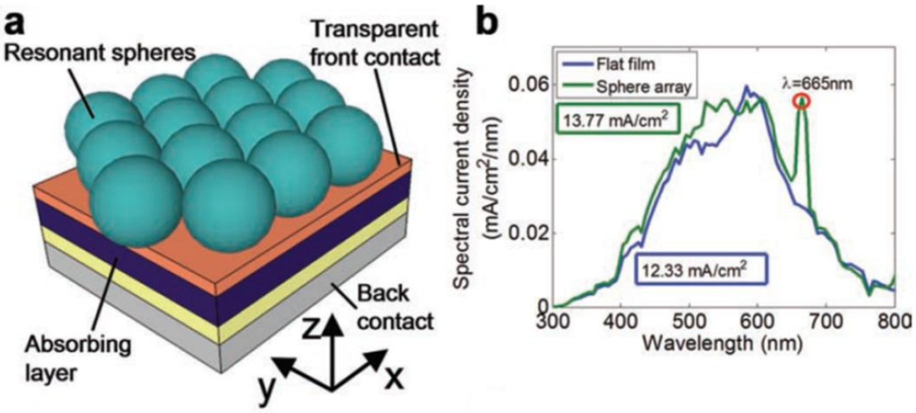

Fig. 2.8 (a) The solar cell geometry with the presence of closely-packed $SiO_2$ nanospheres. (b) Calculated current density in a 100 nm thick a-Si layer with and without the presence of nanospheres [78].

Through calculating the spectral current density generated from the a-Si layer with and without the 600 nm $SiO_2$ nanospheres, the light trapping effect on solar cell performance can be evaluated. The overall integrated current density in the a-Si with the nanospheres is 13.77 mA/cm$^2$ increased from 12.33 mA/cm$^2$ without the nanoparticles, which corresponds to an enhancement of 12% as shown in Fig. 2.8 b. The enhancement in the short wavelength below 600 nm can be explained by the textured anti-reflection coating induced by the spheres. The discrete enhancement at 665 nm is ascribed to the WGM mode coupling into the a-Si layer. The WGMs of the nanospheres can couple with each other due to their closely-packed geometry, which forms a 2D waveguide for light. This resonant guided mode can be finally leaked into the a-Si layer thereby increasing the absorption at this specific wavelength. G. Kang *et.al* experimentally observed broadband light trapping enhancement by placing periodic dielectric surface textured structures embedding closely-packed polystyrene (PS) nanospheres on top of a flat ultrathin a-Si absorber (100 nm) as shown in Fig. 2.9 [97]. By embedding the nanosphere structures the absorption of the a-Si layer increased from 23.8% to 39.9% due to the wave-guiding of the light inside the PMMA embedding layer and the coupling between free space light and resonant WGM.

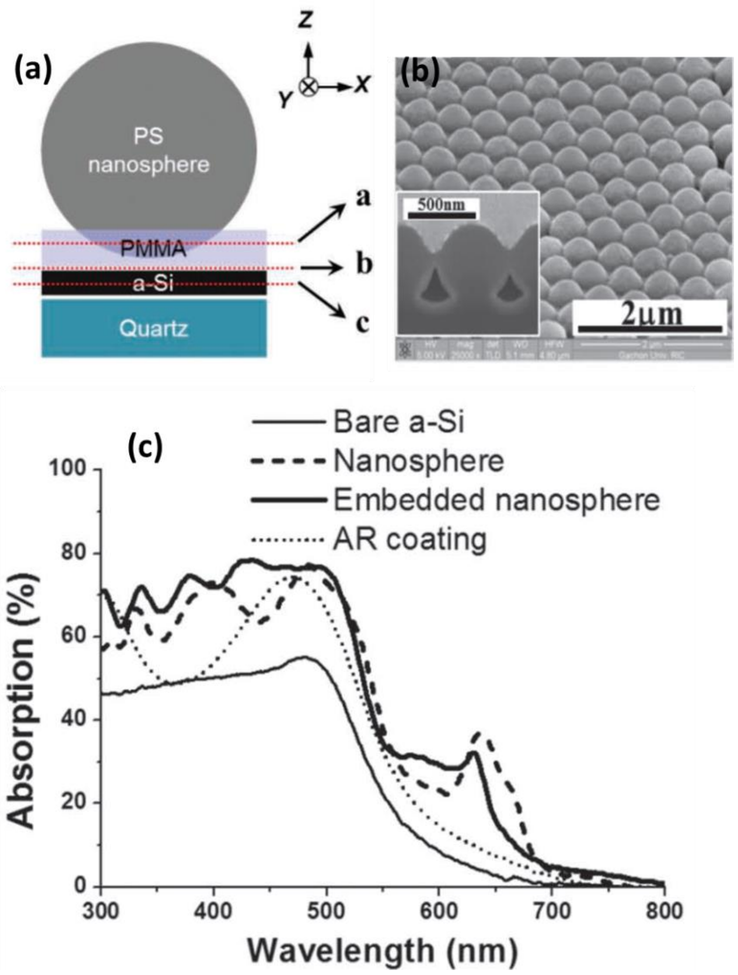

Fig. 2.9 (a) PS nanosphere partially embedded in a PMMA layer on top of a 100 nm thick a-Si absorber. (b) SEM image of the PS nanosphere array embedded partially in the PMMA layer on top of a-Si absorber. (c) Experimentally measured absorption curves as a function of wavelength [97].

To compare the plasmonic nanoparticles discussed in Section 2.2 with dielectric $SiO_2$ nanoparticles to find out which kinds of nanoparticles are more suitable for improving the solar cell performance when integrated on the top surface. We conduct numerical modelling with FDTD method. Fig. 2.10 depicts the a-Si solar cell geometry with the closely-packed $SiO_2$ nanospheres placed on top. In order to study the absorption properties of the solar cells, a 3D FDTD model (Lumerical) is built up. The solar cell parameters are the same as the one depicted in Fig. 2.3. $SiO_2$ nanospheres with a refractive index of $n$=1.46 are directly placed on the ITO layer as a close-packed monolayer array. The same formulas as discussed in Section 2.2.3 are used to calculate the short circuit current density with and without the presence of $SiO_2$ nanospheres. Due to the closely-packed geometry of the $SiO_2$ nanospheres, we only investigate the size effects on the absorption enhancement in the a-Si layer. Based on the estimation on the scattering wavelength, the diameters of the nanospheres in our simulation are changed from 100 nm to 700 nm with an interval of 100 nm.

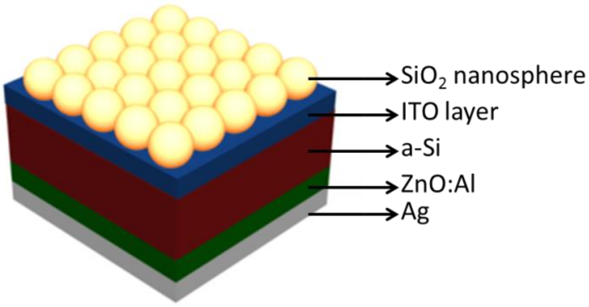

Fig. 2.10 Schematic of the closely-packed $SiO_2$ nanospheres on top of the a-Si solar cell.

| **Radius** | **100 nm** | **150 nm** | **200 nm** | **250 nm** | **300 nm** | **350 nm** |
|---|---|---|---|---|---|---|
| **$SiO_2$** | 1.04474 | 1.05779 | 1.10121 | 1.10636 | 1.14579 | 1.09699 |

Table 2.2 $J_{SC}$ enhancements of the a-Si solar cells with $SiO_2$ nanospheres on the top normalised to that without the nanospheres.

As can be seen from Table 2.2, for all the cells integrated with the nanospheres, the overall absorbance in the a-Si layer is enhanced. The highest enhancement G=1.1458 is achieved with the $SiO_2$ nanospheres of 300 nm in radius. We plot the calculated absorbance as a function of the wavelength for of the a-Si solar cells integrated with and without 200 nm, 500 nm and 600 nm $SiO_2$ nanospheres on the top as a function of the wavelength, as shown in Fig. 2.11.

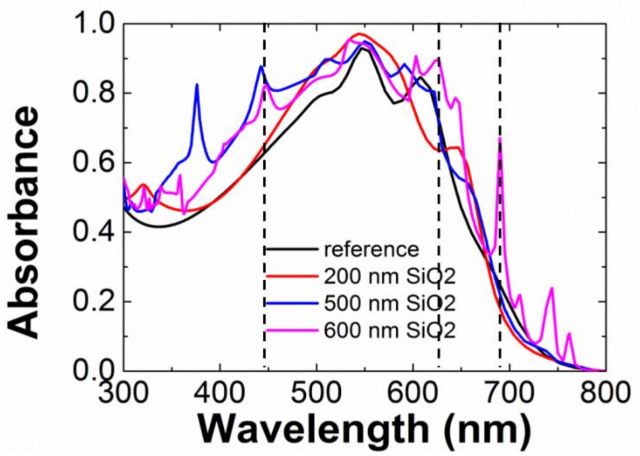

Fig. 2.11 Light absorbance of the a-Si solar cells integrated with $SiO_2$ nanospheres of 200 nm (red line), 500 nm (blue line) and 600 nm (purple line) in diameter. The reference is plotted as the black line.

From Fig. 2.11, we can clearly see that the absorbance in the a-Si solar cell with the 600 nm diameter $SiO_2$ nanospheres is improved in the entire wavelength range. Some distinct absorbance peaks can be found both in the short and long wavelength ranges. For the nanospheres with the diameter of 200 nm, the highest enhanced absorption is located in the short wavelength range. The absorption enhancement is mainly due to the Fabry-Perot resonance formed by the monolayer array of spheres acting as an effective textured antireflection coating. The absorbance peaks found with the 500 nm and 600 nm nanospheres are mainly due to the whispering gallery modes (WGM) coupled into localised modes in the a-Si layer as shown in Fig. 2.12 (a) [78, 79]. The reason we could not find any absorbance peaks in the a-Si solar cell with the 200 nm $SiO_2$ nanospheres is that the size of the nanospheres is not large enough to excite the whispering gallery modes in the interested wavelength region. In the longer wavelength range from 600 nm to 800 nm, we find that there exist several absorbance peaks for the case of 600 nm $SiO_2$. We attribute these enhancements to the coupling of the light to the in-plane leaky waveguide modes of the closely packed nanospheres and these modes only exist when the diameter of nanosphere is larger than 500 nm [79].

To further confirm the multiple optical coupling mechanisms of these $SiO_2$ nanospheres, we plot the electric field distributions of the solar cell integrated with nanospheres at three different wavelengths of 446 nm, 626 nm and 690 nm, corresponding to the absorbance peaks in the a-Si with 600 nm $SiO_2$ in diameter, as shown in Figs. 2.12 (a-c).

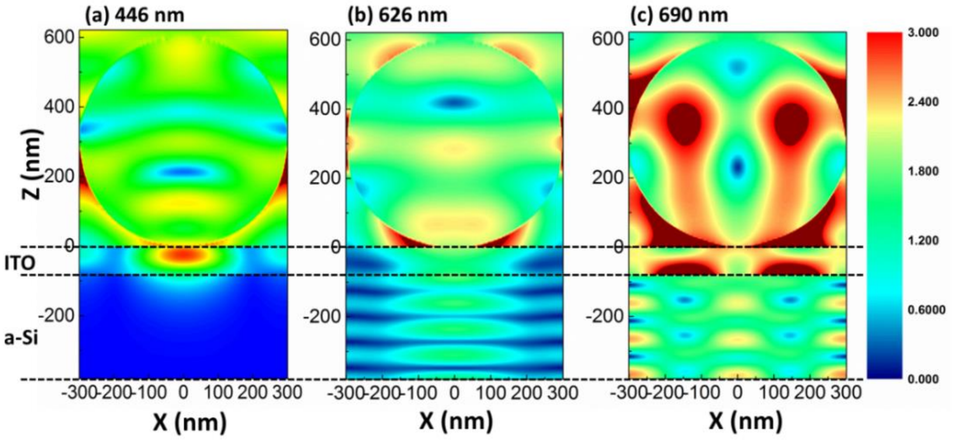

Fig. 2.12 Electric field distributions in a-Si solar cells integrated with 600 nm $SiO_2$ nanospheres at the wavelengths of (a) 446 nm, (b) 626 nm and (c) 690 nm.

From Fig. 2.12, we can see the two different coupling mechanisms accounting for the absorption enhancement. In Fig. 2.12 (a), a localised mode can be clearly found just under the $SiO_2$ nanosphere in the ITO layer. We attribute this mode to the coupling of light from the higher order mode of WGM at the short wavelength range [78]. In Figs. 2.12 (b) and (c), in-plane leaky waveguide modes can be found in the a-Si layer due to the coupling of light from the lower order WGM modes generated by the $SiO_2$ nanospheres. These waveguide modes contribute to the increased absorbance in a-Si solar cells in the long wavelength range. However, due to the atop position of the $SiO_2$ nanospheres on the solar cell, the generated WGMs cannot be fully utilised. In Fig. 2.12, we can find that only the WGMs generated near the top surface of a-Si solar cells can be effectively coupled into the solar cell and the modes which are away from the top solar cell surface will only be confined at the surface of $SiO_2$ nanospheres [78]. Through the comparison of $SiO_2$ nanoparticles with the large metallic nanoparticles, we find that the dielectric $SiO_2$ nanoparticles can couple light more efficiently into the a-Si solar cells when integrated on top of the solar cells.

The $SiO_2$ nanospheres can not only be applied on the top surface of solar cells for forward scattering, but also be utilised in the middle of the absorber layer to enhance the absorbance by the lateral scattering from the nanospheres. James R. Nagel et.al proposed a solar cell concept with embedded dielectric nanospheres within the semiconductor layer to increase the absorption [98]. The concept was demonstrated by the FDTD simulations of $SiO_2$ nanospheres embedded in a 1 μm c-Si film with a 75 nm $Si_3N_4$ anti-reflection coating. The total integrated absorption of the incident light across the visible *AM 1.5* spectrum was on the order of 5-10% higher than the same solar cell structure without any dielectric scatters as shown in Fig. 2.13. The enhancement arose from the scattered fields of the periodic nanospheres that interacted with each other and can be expressed as the lateral modes indicated as the regions of constructive and destructive interference as shown in Fig. 2.13 (b). These modes lead to an overall absorption enhancement in the absorber.

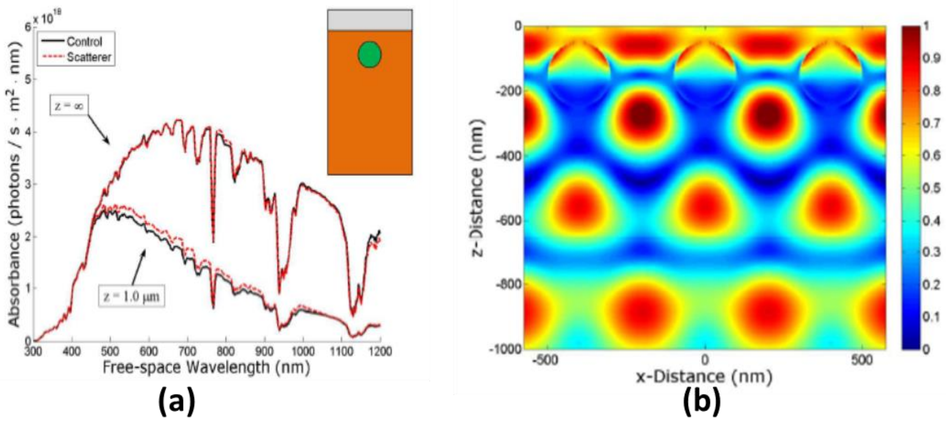

**(a)** **(b)**

Fig. 2.13 (a) Calculated photon absorbance of the thin-film silicon solar cell with an ARC and $SiO_2$ nanospheres embedded in the semiconductor layer. (b) Electric field intensity distribution at a wavelength of 700 nm for a periodic nanosphere arrays [98].

In the configuration of tandem a-Si/µ-Si solar cells, $SiO_2$ nanospheres can also be integrated experimentally between the top a-Si cell and the bottom µ-Si cell as an advanced intermediate reflector layer (IRL) for light management [99, 100]. The functions of the IRL are the back reflection of the visible light into the top a-Si cell and transmission of the near infrared light into the bottom µ-Si solar cell [101, 102]. Normal IRL can enhance the performance of the top cell through the reflection of the visible light but the fraction of near infrared (NIR) light for the bottom cell is often decreased. Replacing the normal IRL with $SiO_2$ nanospheres can solve this challenge. The $SiO_2$ nanosphere IRL provides enhanced NIR light absorption in the bottom cell by forward scattering. The cross-section profile of the solar cell with the $SiO_2$ nanosphere IRL is shown in Fig. 2.14 (a). The nanometer sized light scatters were placed at the interface between the top and the bottom cells. The incident NIR light was forward scattered from the nanosphere scatters (ray 1), and trapped by the subsequent internal reflection from the bottom cell (ray 2), which resulted in the enhanced NIR absorbance of the bottom cell. The incident red light was reflected by the scatterers (ray 3), improving the red response of the top cell which can be confirmed by the EQE measurement shown in Fig 2.14 (b). The corresponding top cell current increased from 10.1 mA/cm$^2$ to 11.0 mA/cm$^2$ due to the Fresnel reflection of the red light from the scatterers. The current density of the bottom cell was increased from 6.3 mA/cm$^2$ to 7.3 mA/cm$^2$. The total efficiency of the solar cell was enhanced by 16%, from 7.2% to 7.9% after incorporating the $SiO_2$ nanosphere light scatterers. Such improved NIR response results from the scattering of NIR light and subsequent internal light trapping. The different interference fringes in the QE response of the NIR region from the bottom cell are less obvious for the solar cell with the $SiO_2$ nanospheres, indicating the forward scattering of light.

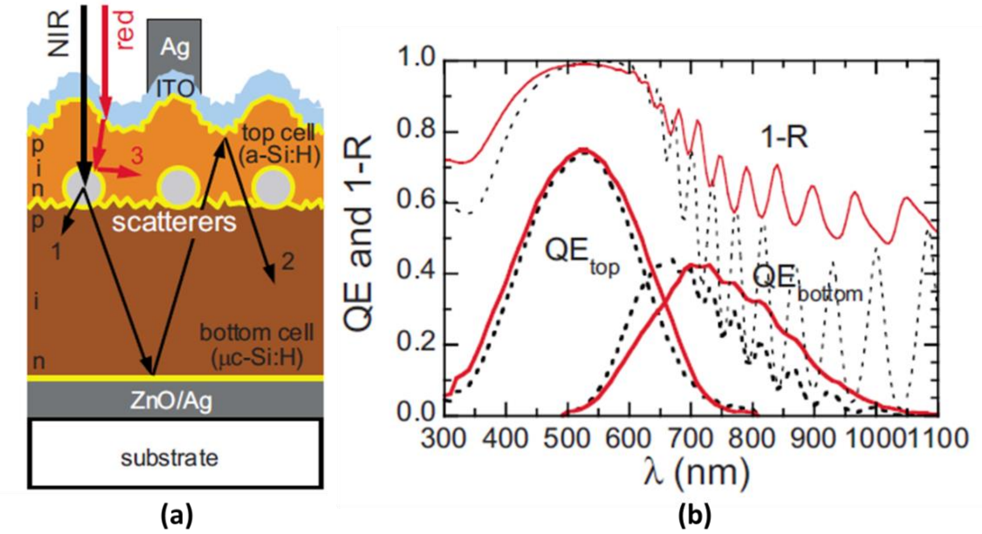

Fig. 2.14 (a) Schematic of the solar cell structure with $SiO_2$ nanospheres (b) EQE and 1-R spectrum for solar cells with/without nanospheres. Red solid line corresponds to the case with the nanospheres and the black dotted line corresponds to the reference solar cell [101].

## 2.4 Nanostructures for enhanced thin film solar cells

In the previous sections, nanoparticles including plasmonic nanoparticles and dielectric nanoparticles for the improvement of the efficiency in solar cells have been reviewed. In this Section, we will mainly review some new light management methods based on nanostructures.

For thin film solar cells, the traditional used surface textures on thick c-Si solar cells cannot be applied especially when the thickness of solar cells is comparable to the light wavelength. Therefore nanometric light trapping structures need to be developed to solve the problem of the mismatch between the minority-carrier diffusion length and absorption depth in thin film absorbers to realise ultrahigh efficiency thin film solar cells at low cost. Recently, research efforts have been focused on the investigation of different nanostructures for light management based on their strong scattering and light concentration properties. Both plasmonic nanostructures for the back electrode of the solar cells and dielectric or semiconductor nanostructures have been proven to be effective in light management and the influence have been experimentally demonstrated on realistic solar cell designs. We will describe these new developments in more details in the next few sections.

### 2.4.1 Plasmonic back electrode nanostructures for thin film solar cells

Plasmonic back reflector has been regarded as a promising candidate for light management in thin film solar cells, which can be naturally integrated with the metal back reflector in a standard design in the solar cell geometry. The concept of the solar cells with plasmonic back electrode nanostructures is shown in Fig. 2.15. The incorporated nanostructures for the back metal reflector can couple light into surface plasmon polaritons (SPP) modes or photonic waveguide modes at the metal/semiconductor interface if the nanostructures are periodic. There exist two modes of enhancement in a periodically plasmonic nanostructured back reflector [39]. One is the photonic modes travelling parallel to the layers in the long wavelength regions due to coupling of the incident light into the waveguide modes. The other is the SPP mode excited by plasmonics if the shape and size of the metallic nanostructures fulfil the coupling condition. Near the resonant frequency, the SPP modes travel parallelly to the interface of the metal/semiconductor to provide a strong near-field decaying into the semiconductor which leads to the increased light intensity in the semiconductor region close to metal and therefore increasing the absorption. These two modes can couple to each other and provide a higher enhanced absorption than when they act separately.

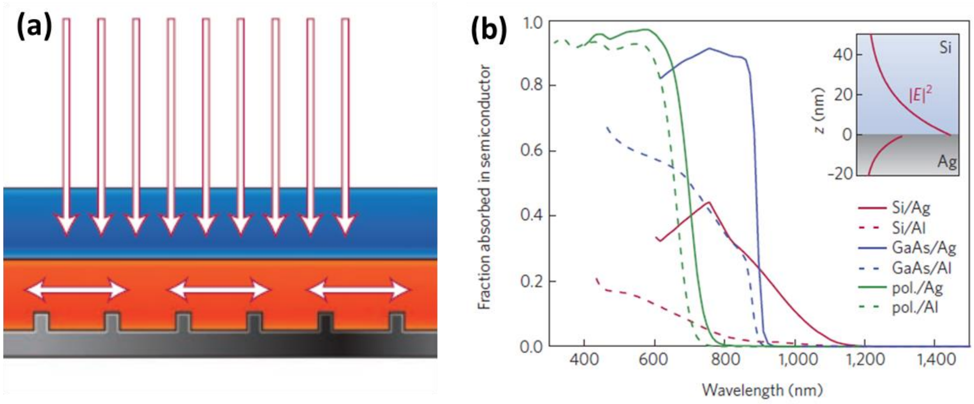

Fig. 2.15 (a) Solar cell concept with a plasmonic nanostructured back reflector. (b) Fraction of light absorbed into the semiconductor for SPPs modes between semiconductor layers of GaAs, Si and an organic semiconductor film, in contact with either Ag or Al [39].

In fact, there exists a competitive absorption process of the SPP modes between the semiconductor and the metal back electrode. This is shown in Fig. 2.15 (b), which illustrates the fraction of light absorbed by a silicon or GaAs film on top of Ag or Al. It can be seen that the absorption of SPP modes at the interface of Si/Ag is higher; however the plasmon absorption losses cannot be ignored. That is the reason that a nanostructured reflector is preferred for the back electrode of solar cells. Under such a circumstance, the light can be coupled into both the SPP modes and photonic modes inside the semiconductor layer by tuning the shapes and sizes of the nanostructures in solar cells to control the mode coupling. The coupling to photonic modes is preferred as they do not suffer from significant loss in the metal. A large amount of research efforts during the last few years have proven that a relative high absorbance enhancement can be achieved by incorporating nanostructured plasmonic back reflector into solar cells. The most commonly used nanostructures for plasmonic back reflectors for a-Si thin film solar cells are the nanocone [74] or nanodome [73] structures, nanocylinder induced conformal structures [91-93] and nanovoid structures [68, 70].

A novel nanodome a-Si solar cell structure was firstly proposed by J. Zhu *et.al*. Periodic nanostructures were implemented for solar cells from the bottom Ag substrate as shown in Fig. 2.16 [73]. This nanodome structured solar cell could absorb 94% of the light from 400 nm to 800 nm with an only 280 nm thick a-Si layer compared to the flat solar cell which can only absorb 65% of the light. The efficiency of the solar cell was enhanced from 4.7% to 5.9% with the nanodome structure. The enhancement mainly arose from an increased $J_{SC}$. The unique nanodome geometry of the solar cells provided an effective anti-reflection light trapping mechanism because the gradually increased effective refractive index led to a better matching with air effectively suppressing the reflection on the solar cell surface. The SPP modes coupled into the a-Si layer and the scattered light along the in-plane direction by the Ag nanocone structure of the back electrode increased the light traveling path, providing an additional plasmonic light trapping mechanism. This plasmonic absorption enhancement mechanism was also proved by V. E. Ferry who proposed to apply the rounded Ag hemiellipsoidal plasmonic back electrode for a-Si solar cells [93]. After the deposition of the a-Si solar cell over the plasmonic back reflector, the conformal hemiellipsoidal shape of the back electrode was transferred to the a-Si layer and the top ITO layer due to the ultrathin thickness of the a-Si solar cell. In their experiments, the performance of the solar cell was improved from 6.32% to 9.6% with a rounded Ag hemiellipsoidal plasmonic back reflector of 290 nm in diameter and 400 nm in periodicity, as shown in Fig. 2.17.

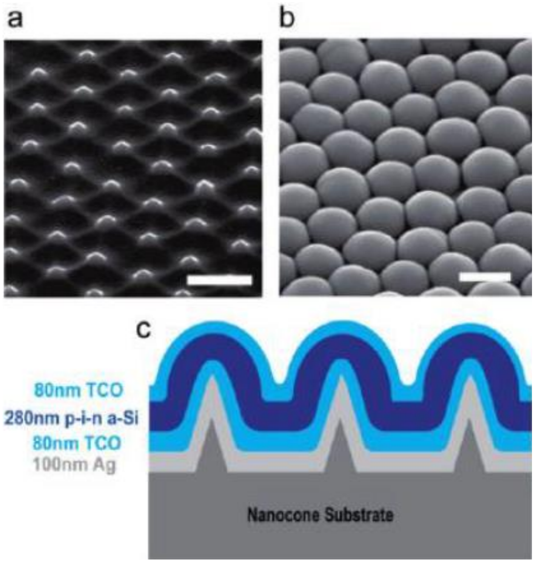

Fig. 2.16 SEM images of (a) the nanocone quartz substrate and (b) the a-Si nanodome solar cell after deposition multilayers of materials on nanocones. Scale bar: 500 nm. (c) Schematic of nanodome solar cells [73].

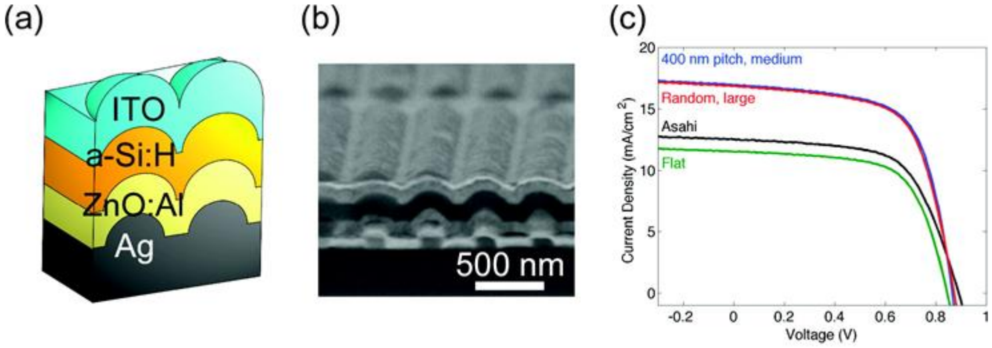

Fig. 2.17 (a) Schematic of the solar cell geometry. (b) SEM image of the cross section of the solar cell. (c) I-V measurement of the best cell with a 90 nm a-Si layer [93].

The EQE measurement demonstrated a broadband photocurrent enhancement in both the blue and the red regions of the spectrum. The enhanced photocurrent on the blue side was attributed to the top interface nanostructures formed by the conformal deposition of solar cells which could act as weakly coupled Mie resonators to forward scatter the incident light into the a-Si layer. On the other hand, the enhanced photocurrent in the red part of the spectrum was because of the plasmonic back reflector coupling light to the SPP modes and waveguide modes.

Another commonly used plasmonic back reflector is the nanovoid structure as shown in Fig. 2.18 (a). The optical properties of metallic nanovoid structures both in theory and in experiment have been investigated extensively [68, 70]. Hybrid modes can be excited inside the void structures, which mix the LSP modes with the Fabry-Perot cavity modes and the rim dipole modes associated with the charge build-up at the void rims. On the outer surface of the structure, SPP propagating modes can be excited. The nanovoid plasmonic back reflector can be fabricated by electrochemical deposition through a template of closely-packed self-assembled arrays of nanospheres. It was first introduced into organic solar cells in 2011 by N. N. Lal [68], demonstrating an enhancement of 3.5 times at the plasmonic resonance in the EQE measurement and a 4 times enhancement in the overall efficiency. Significant localised field enhancements as shown in Figs. 2.18 (c) and (d) in the void structure led to strong absorption enhancement in the active layer of the solar cell. Enhanced scattering from the textured surface in the void structure was also an important factor increasing the efficiency across the spectrum. Recently, similar void structured back reflectors fabricated by electrochemically anodizing the Al foil have also been applied to a-Si solar cells as shown in Fig. 2.18 (e). The efficiency of the solar cell with the nanostructured Ag back reflector was improved from 5.6% to 7.1%, mainly due to the $J_{SC}$ enhancement as shown in Fig. 2.18 (f) [70]. A broadband optical absorption enhancement was achieved on the nanostructured substrates. From experimental measurements and numerical calculations, it can be concluded that the enhancement was resulted from the efficient scattering of the light in the short wavelength region due to the textured surface and the excitation of the SPP modes, LSP resonances and the waveguide modes in the long wavelength region.

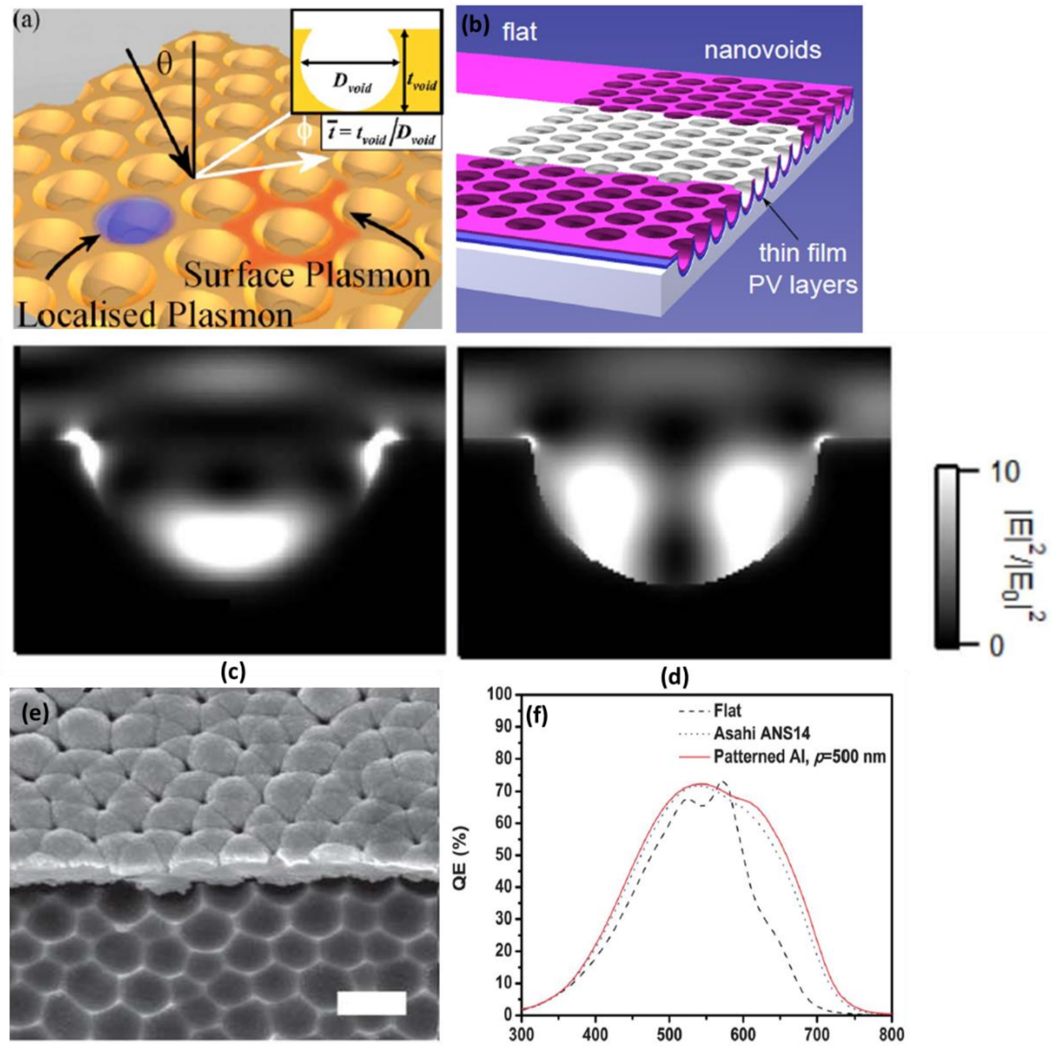

Fig. 2.18 (a) Schematic of different modes excited in the void plasmonic structure. (b) Solar cell geometry fabricated on the plasmonic void substrate. (c) Distribution of the plasmonic electric field intensity at 375 nm. (d) Distribution of the plasmonic electric field intensity at 496 nm. (e) SEM image of the void structured a-Si solar cell. (f) EQE comparison of solar cells with and without the void structures [68, 70].

### 2.4.2 Nanostructured absorbing layer in thin film solar cells

Introducing nanostructures in the active layer of a solar cell has an imperative influence on both the electric and optical properties. When the nanostructures of the absorber are optimised, strong optical resonances can be excited, which can significantly improve the light absorbance in the solar cell compared to a flat absorber. InP nanowire array thin film solar cell with p-i-n junction is a good example of this concept. As shown in Figs. 2.19 (a) and (b) enhanced light absorption exceeding the ray optics limit was demonstrated leading to a 13.8% efficiency [123]. Apart from the nanowire solar cell structures, systematic simulations have been conducted on the possible benefits from nanostructuring both sides of the ultrathin c-Si solar cell as shown in Figs. 2.19 (d) and (e) [122]. High light absorbance can be obtained through using high-aspect-ratio dense nanocone arrays at the front surface acting as an ARC structure and low-aspect-ratio sparse nanocone arrays at the back surface acting as a grating to couple light into the guided resonances in the absorber. The optimised structures with an only 2 μm thick absorber can result in significant absorption enhancement, leading to a photocurrent close to the Yablonovitch limit [122]. Similar nanocone array structure was also used for a-Si solar cells as shown in Fig. 2.19 (c), broadband absorption enhancement in the solar cell through the whole wavelength range was achieved compared to the flat reference solar cell due to the dramatically reduced reflection from the cone structure providing a gradient refractive index change from the air to the a-Si substrate.

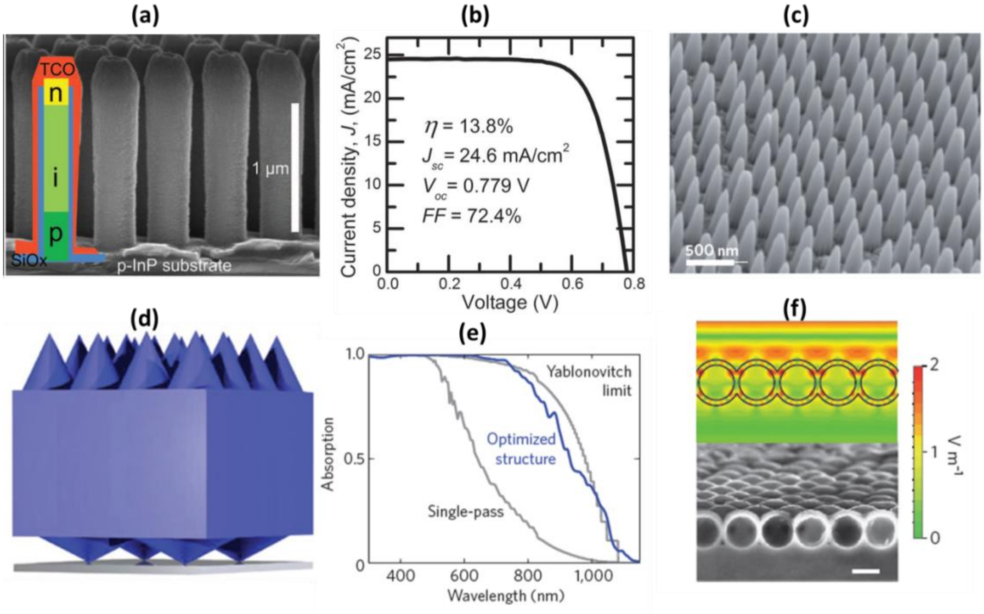

Fig. 2.19 (a) SEM image of the InP nanowire solar cells. (b) I-V measurement for the nanowire solar cell shown in (a). (c) SEM of nanocone array structures of the a-Si solar cell. (d) Schematic of the ultrathin c-Si solar cell with double sided nanocone structure design. (e) Calculated absorption curves of the optimised structures shown in (d). (f) Bottom: SEM cross section image of a monolayer of spherical nc-Si nanoshell arrays on a quartz substrate. Scale bar, 300 nm. Top: Full-field electromagnetic simulation of the electric field distribution inside the nanoshell showing the importance of the excitation of whispering gallery modes to enhance the absorption of light [73, 81, 122, 123].

Recently, a novel spherical nanoshell nano-crystalline (nc-Si) structures has been proposed by Y. Yao to improve the broadband absorbance dramatically due to the excited low-Q WGMs as shown in Fig. 2.19 (f) [81]. The geometry of the nc-Si solar cell was designed into nanoshell structures providing a 20-fold enhancement in the absorbance of the active layer compared to a flat reference.

This nanoshell nc-Si solar cell could couple incident light into the WGM modes inside the spherical shells and induce a profitable recirculation of light inside the shell shaped absorbers, leading to the increase of light path in the active layer and reduce of the amount of material demanded for comparable light absorbance. By optimising the shell thickness and inner shell radius, a relatively low-Q value of the Si nanoshell resonances could be excited, which not only allowed efficient light coupling to the resonant modes, but also spectrally broadened the resonant absorption peaks region to allow broadband enhancement. By theoretically calculating the electrical performance of a p-i-n solar cell, an 80 nm thick nc-Si shell solar cell with an outer radius of 225 nm based on the spherical nanoshell structure could yield an efficiency of 8.1% which is comparable to that of a flat solar cell with an active layer thickness of 1.5 µm.

Even though these novel nanostructures can significantly improve the overall absorbance of the solar cells in the entire wavelength range interested, a manufacturable solar cell based on these fancy nanostructures has not yet been demonstrated due to the technical limitations or the unrealistic designs of the solar cells. Take the nanoshell solar cell nanostructures for an example, there is no way to introduce a back electrode experimentally to extract the electricity out. So, practically, there is still a long way to go for solar cell engineering.

## 2.5 Chapter conclusion

This chapter introduces the necessary background for understanding the content and novelty of this thesis. First, the mechanisms and theory of plasmonic nanoparticles and dielectric nanoparticles for absorption enhancement in solar cells are reviewed for understanding the motivation for the light management. The plasmonic nanoparticles are compared with $SiO_2$ dielectric nanoparticles when integrated on top of the solar cells, finding that the $SiO_2$ nanoparticles can couple light more efficiently into the a-Si layer. Then, commonly used different nanostructures of solar cells are reviewed for understanding the mechanisms for absorption enhancement due to the anti-reflection properties and guided modes coupled from different nanostructured solar cells. Those are the benchmarks for investigating the benefits of the novel nanoparticles combined with a reverse hemi-nanoshell conformal a-Si nanostructures which we propose in this thesis for ultrathin solar cells with high absorbance.

# Chapter 3

## Effect of small metallic nanoparticles for the absorption enhancement in a-Si thin film solar cells

### 3.1 Introduction

Plasmonic nanoparticles have been proved to be highly effective in improving the performance of diverse solar cells, including organic solar cells [64, 103], dye sensitized solar cells [104], crystalline silicon solar cells [46, 105-106] and silicon thin-film solar cells [44, 49, 91]. The reported enhancement mechanisms are mainly due to two effects, one is the photocurrent improvement induced by the plasmonic resonant scattering associated with comparatively large nanoparticles (~100 nm), and the other one is the plasmonic near-field light concentration of the ultra-small nanoparticles predicted to be able to dramatically increase the charge-carrier generation in solar cells [107-109].

In this Chapter, first we incorporate ultra-small metallic nanoparticles of a few nanometers on the front side of the solar cells to harness the plasmonic near-field light concentration to improve the performance of a-Si solar cells. In

Section 3.2, the nanoparticle fabrication process is introduced. Ultra-small nanoparticles are prepared by the simple thermal evaporation method. Different sizes of nanoparticles are characterised by scanning electron beam microscope (SEM) and UV-VIS spectrometer. Then, the ultra-small metallic nanoparticle integrated solar cells are characterised and compared with different sizes of nanoparticles.

## 3.2 Small metallic nanoparticles for absorption enhancement in a-Si solar cells

Although the plasmonic near-field light concentration has been theoretically predicted to be able to dramatically increase the absorption in solar cells, experimental demonstration has been greatly limited. The challenges mainly lie in two aspects. First of all, the near-field light concentration is always accompanied by strong ohmic loss from the nanoparticles, which is dissipated as heat. To solve this problem the nanoparticles need to be designed to possess the highest possible localised field enhancement much exceeding the particle absorption loss. Secondly to fully utilise the large field concentration, the nanoparticles should be placed in the close vicinity of the photoactive layer, where the electron-hole pairs are generated. This often means that the nanoparticles need to be on the front surface or embedded in the active layer of the solar cells, which could lead to severe light absorption loss. In this Section, we propose to make use of the near field effect from ultra-small metallic nanoparticles on the top surface of a-Si solar cells to enhance the solar cell performance.

### 3.2.1 Small Ag and Au nanoparticle fabrication and characterisation

To fabricate ultra-small metallic nanoparticles, a simple thermal evaporation method is applied here. To control the particle size to be a few nanometers, metal films with sub-nanometer to a few nanometer thicknesses need to be deposited first. By carefully controlling the deposition speed, ultra-small nanoparticles with different sizes and surface coverages (SCs) can be formed. In our experiments, we deposited gold films with six different thicknesses (0.3 nm, 0.6 nm, 0.7 nm, 0.8 nm, 1 nm, and 1.8 nm, respectively) on top of a ZnO:Al layer coated on glass. Figs. 3.1(a-c) show the SEM images of a few selected uniformly deposited Au nanoparticles. To make a comparison of the influence of different metallic material on the solar cell performance, Ag films with five different thicknesses (0.3 nm, 0.6 nm, 1 nm, 1.3 nm and 1.8 nm, respectively) were also deposited on the ZnO:Al coated glass. Figs. 3.1 (d-f) show the SEM images of the selected uniformly deposited Ag nanoparticles. It can be observed that the sizes and SCs of the nanoparticles increase with increased film thickness. The mean sizes are approximately 7 nm (±2 nm) with 27% SC, 10 nm (±2.5 nm) with 49.7% SC and 14 nm (±3 nm) with 84.2% SC for Au films with 0.6 nm, 1.0 nm and 1.8 nm thicknesses, respectively. While the mean sizes are approximately 6 nm (±2 nm) with 10% SC, 9 nm (±2 nm) with 23% SC and 15 nm (±2 nm) with 86% SC for Ag films with 0.6 nm, 1.0 nm and 1.8 nm thicknesses, respectively.

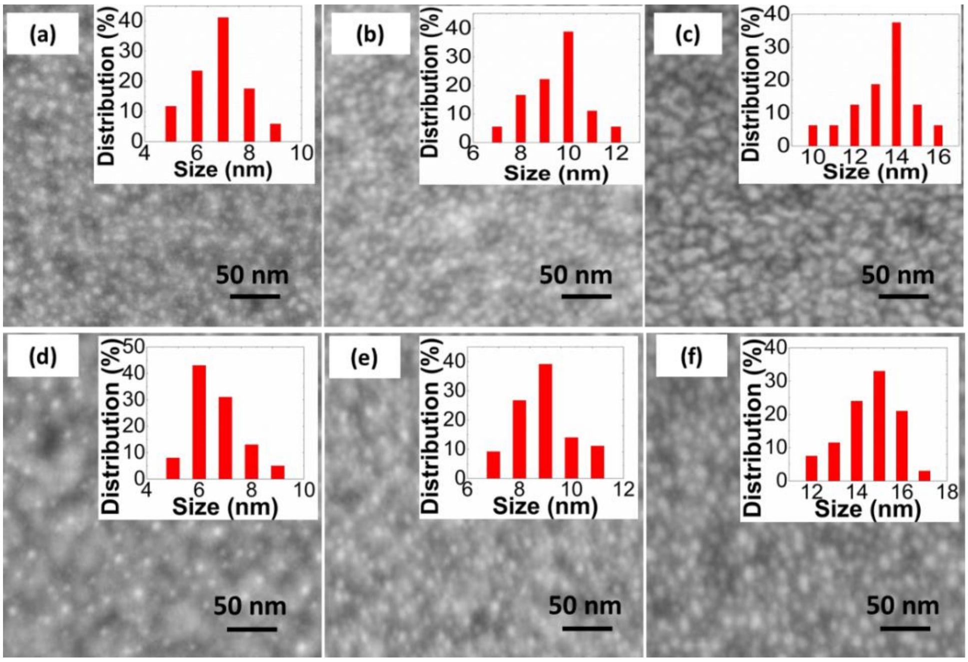

Fig. 3.1 SEM images of different sized metallic nanoparticles (a) Au ~7 nm (±2 nm), (b) Au ~10 nm (±2.5 nm), (c) Au ~14 nm (±3 nm), (d) Ag ~6 nm (±2 nm), (e) Ag ~9 nm (±2 nm), (f) Ag ~15 nm (±2.5 nm) on the surface of ZnO:Al layers on glass corresponding to film thicknesses of 0.6 nm, 1 nm and 1.8 nm, respectively.

To characterise the ultra-small metallic nanoparticles, the transmittance curves of the ZnO:Al coated glass integrated with ultra-small metallic nanoparticles of different sizes were measured with a spectrometer (Perkin Elmer, Lambda 1050). The results are presented in Fig. 3.2. From the transmittance curves shown in Fig. 3.2 (a), we can see that the localised surface plasmonic resonance (LSPR) peaks (corresponding to the dip in the transmittance) of Au nanoparticles redshift from 550 nm to 650 nm with increased thicknesses from 0.6 nm to 1.8 nm mainly because of the increase in particles size. For larger particle sizes and higher SCs of Au nanoparticles, the particle absorption becomes so strong that the light transmittance is reduced. And for Ag nanoparticles, the LSPR peaks redshift from around 430 nm to 510 nm with increased thicknesses.

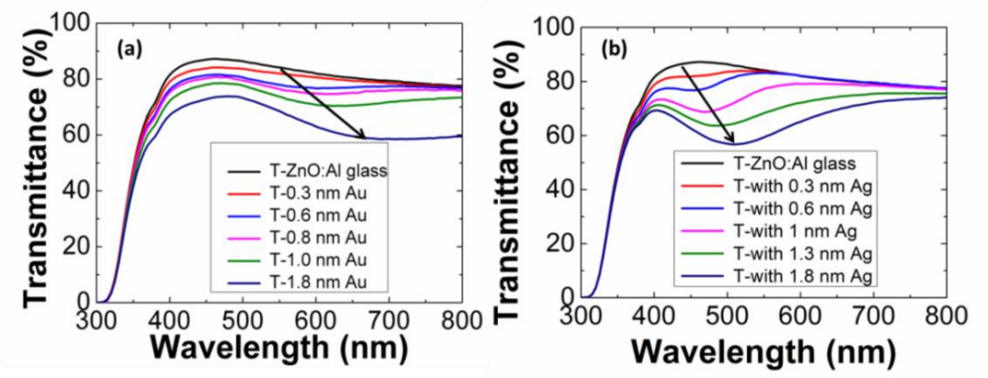

Fig. 3.2 (a) Transmittance of ZnO:Al glass with an Au layer of 0.3 nm, 0.6 nm, 0.8 nm, 1 nm, 1.8 nm in thickness. (b) Transmittance of ZnO:Al glass with an Ag layer of 0.3 nm, 0.6 nm, 1 nm, 1.3 nm, 1.8 nm in thickness.

### 3.2.2 Solar cells integrated with small Ag and Au nanoparticles characterisation

To examine the influence of the ultra-small nanoparticles on the solar cells performance, a-Si layers with an overall thickness of 260 nm were deposited by the plasma enhanced chemical vapour deposition (PECVD) method on top of the nanoparticle integrated TCO glass as shown in Fig. 3.3. At last a ZnO:Al layer with 100 nm in thickness and an Ag back reflector layer with 180 nm in thickness were deposited. The standard current density-voltage (I-V, Oriel Sol 3ATM class AAA, model 94023A) and external quantum efficiency (EQE, PV Measurements, Inc., Model QEX10) measurements were used to characterise the efficiency and spectral response of the solar cells.

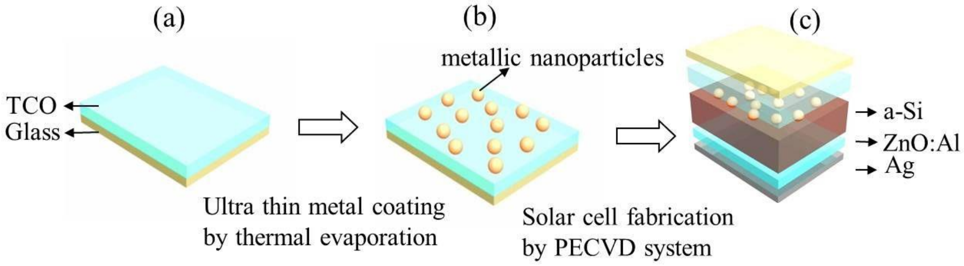

Fig. 3.3 The sketch of the a-Si solar cell with small metallic nanoparticles.

First, solar cells with small Au nanoparticles integrated on top of the a-Si are investigated. As shown in Figs. 3.1 (a)-(c), as the size and SC of the nanoparticles become too large, the particle absorption loss becomes non-ignorable, which leads to reduced photocurrent generation. However, the *FF* is expected to increase due to the reduced contact resistance between the TCO glass and the a-Si layer when Au nanoparticles are introduced. Therefore, there exists an optimised condition for the best values of $J_{SC}$ and *FF*. To find this condition, we plot the normalised values of $J_{SC}$, and *FF*, the open circuit voltage ($V_{OC}$) and efficiency of the solar cells integrated with the ultra-small Au nanoparticles to the reference cells as a function of the film thickness as shown in Fig. 3.4.

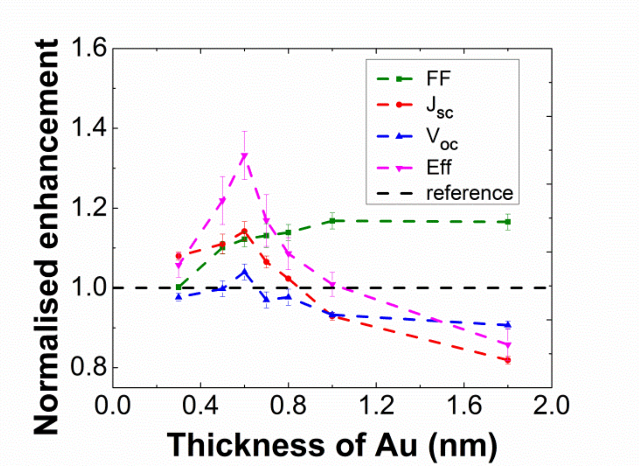

Fig. 3.4 Normalised enhancements of a-Si solar cell parameters with different thicknesses of Au nanoparticles.

It can be seen from Fig. 3.4 that *FF* increases steadily with increased Au film thickness as expected. In the meantime $J_{SC}$ and $V_{OC}$ decrease with increased Au film thickness except for the thickness of 0.6 nm. For a 0.3 nm Au film an enhancement of 7% in $J_{SC}$ is observed. When the thickness of the Au film increases to 0.6 nm, a peak enhancement in $J_{SC}$ of 14.1% is achieved. When the thickness is further increased, both the SC and the particle size become larger, which leads to the increased particle absorption loss overweighting the plasmonic near-field enhancement. Therefore $J_{SC}$ starts to reduce. So there is a competing process between the plasmonic near-field enhancement, which leads to the solar cell absorption enhancement, and the absorption loss by the Au nanoparticles, which reduces the light absorption in the a-Si solar cells.

From Fig. 3.4, we can also easily identify that the optimised film thickness to achieve the best solar cell efficiency enhancement is 0.6 nm. Under such a circumstance, $J_{SC}$ is improved from 12.4 mA/cm$^2$ to 14.15 mA/cm$^2$, while *FF* is improved from 34.88% to 39.16%. The Au nanoparticles effectively lower the Shorttky barrier height and provide a better ohmic contact to the a-Si than the TCO electrode [23]. The measured series resistance of the optimised solar cell with Au nanoparticles is 12.8 Ω compared with 17.1 Ω without the Au nanoparticles. To further analyse the mechanism of the enhancement, we measured the spectral response (EQE) of the solar cell with the highest enhancement, as shown in Fig. 3.5.

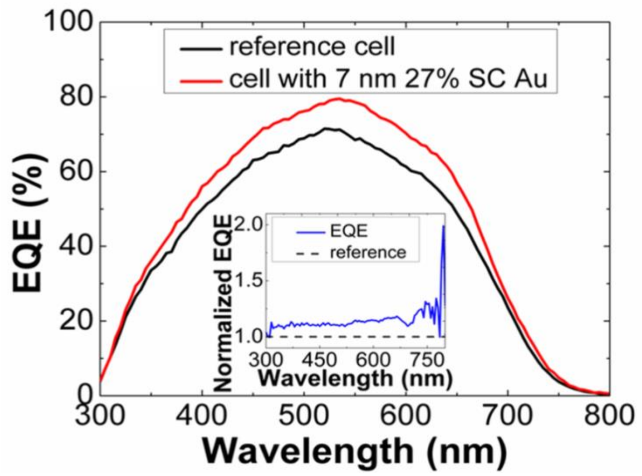

Fig. 3.5 EQE for solar cells with/without Au nanoparticles.

For a-Si solar cells, the largest value of EQE is around 550 nm, which is in accordance with the resonance peak of the Au nanoparticles shown in Fig. 3.2 (a). From the SEM image in Fig. 3.1 (a), the sizes of the 0.6 nm thick Au nanoparticles are less than 10 nm in diameter. So the plasmonic scattering effect can be ignored under such a situation. The light is strongly concentrated due to the localised surface plasmon resonance of Au nanoparticles, which increases the light absorption of the a-Si near the Au nanoparticles. In addition, the carrier mobility is increased due to the more conductive metallic nanoparticles than the

TCO materials [19], which may also lead to a broadband enhancement in the EQE curve.

To make a comparison of the influence of different metallic material on the solar cell performance, ultra-small Ag nanoparticles were also integrated in the a-Si solar cell with the same fabrication method. Ag films with four different thicknesses (0.3 nm, 0.6 nm, 1 nm and 1.3 nm, respectively) were integrated in a-Si solar cells. The normalised values of $J_{SC}$, and *FF*, the open circuit voltage ($V_{OC}$) and efficiency of the solar cells integrated with the Ag nanoparticles to the reference cells as a function of the film thickness are given in Fig. 3.6.

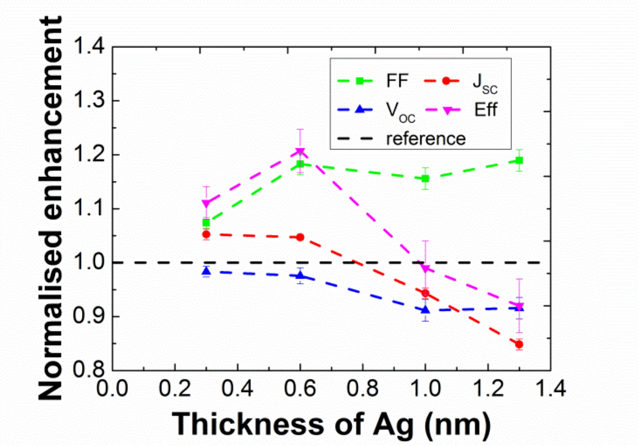

Fig. 3.6 Normalised enhancements of a-Si solar cell parameters with different thicknesses of Ag films.

It can also be seen from Fig. 3.6 that *FF* increases with increased Ag film thickness, while $J_{SC}$ and $V_{OC}$ decrease with increased film thickness. These trends are the same as those observed in the solar cell integrated with the Au nanoparticles. For a 0.3 nm thick Ag film, an enhancement of 5% in $J_{SC}$ is observed. When the thickness of the Ag film increases to 0.6 nm, a similar level of enhancement in $J_{SC}$ of 4.8% is observed compared with the case of 0.3 nm thickness. But the *FF* is increased by around 18% mainly due to the increased SC of Ag nanoparticles. When the thickness is further increased, both the SC and the particle size become larger, and the increased particle absorption losses overweigh the plasmonic near-field enhancement. Therefore $J_{SC}$ starts to reduce. The mechanism is similar to that with the Au nanoparticles. There exists a competing process between the plasmonic near-field enhancement from the Ag nanoparticles and the absorption loss by the Ag nanoparticles. For the best performance of the solar cell, the thickness of Ag film should be chosen at 0.6 nm. Through the comparison, both the Au and the Ag small nanoparticles can enhance the solar cell performance by optimising the sizes and SC of the particles due to the near field effect. The solar cell performance with Au nanoparticles integrated is better than that with Ag nanoparticles. However considering the cost issue, Ag is preferable.

### 3.2.3 Numerical modelling of light distributions around small metallic nanoparticles

To further confirm that the origin of the enhancement is due to the plasmonic near-field concentration, we conducted numerical modelling of the near-field light distribution of ultra-small metallic nanoparticles on the ZnO:Al substrate, which mimic the same condition as the experiment. Here in Fig. 3.7, we present the near-field intensity distribution results for the 10 nm Au nanoparticles under different wavelength light illumination for an example. In our simulation, the light incident direction is along the -Z direction. It can be seen that the light intensity around the Au nanoparticles is enhanced as high as 25 folds at 580 nm. The near field enhancement is around 10 folds at other wavelengths.

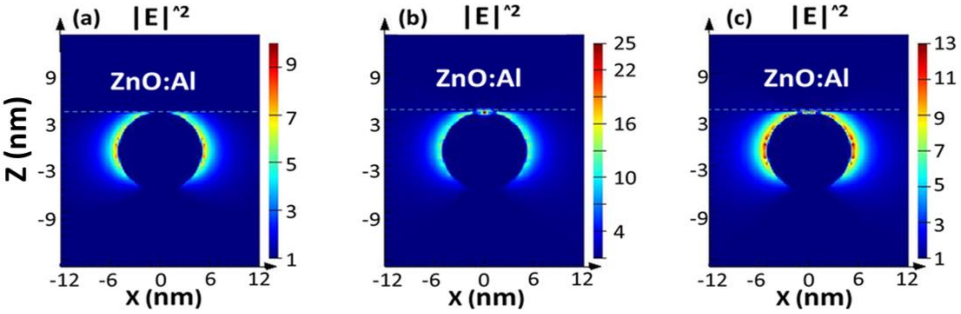

Fig. 3.7 The light intensity distributions around 10 nm Au nanoparticles on a ZnO:Al substrate at different wavelengths: (a) 400 nm (b) 580 nm (c) 650 nm.

The enhanced light intensity around the small nanoparticles contributes to the absorption enhancement in the solar cell. Tailored ultra-small metallic nanoparticles on the front side of solar cells are a simple solution that can effectively harness strong near-field enhancement leading to a significant performance improvement of a-Si solar cells. Both the short circuit current and the fill factor can be optimised. These findings offer a new approach to achieve a plasmonic near-field enhancement.

## 3.3 Chapter conclusion

In this Chapter, influence of different materials (Au and Ag) of small nanoparticles on the absorbance in a-Si solar cells is investigated both theoretically and experimentally. It has been unveiled that small metallic nanoparticles are effective in enhancing the a-Si layer absorption through the near-field concentration. Based on the analysis of the large metallic and dielectric $SiO_2$ nanoparticle integrated solar cells in Chapter 2, we find that closely-packed dielectric $SiO_2$ nanoparticles are more efficient to couple light into the solar cells when integrated on the top surface. To couple light more efficiently from the $SiO_2$ nanospheres into the a-Si layer and realise the high absorbance solar cell with a thinner active layer (150 nm), the position of the $SiO_2$ nanospheres need to be engineered. More details on this aspect will be discussed in Chapter 4. The potential to realise an even higher absorption enhancement in the ultra-thin a-Si layer (20 nm) by using the combination of closely-packed dielectric $SiO_2$ nanospheres and small metallic nanoparticles will be further investigated in Chapter 5.

# Chapter 4

## Ultrathin amorphous silicon solar cells by $SiO_2$ nanoparticle imprinting

### 4.1 Introduction

As mentioned in Chapter 1, amorphous silicon (a-Si) thin film solar cells are a competitive candidate for large scale manufacture of photovoltaics, due to the advantages of low cost, non-toxic and abundant material [17-19]. However, the key problem of the a-Si material is the existence of dangling bonds in the a-Si resulting in a short carrier diffusion length (<100 nm) and instability during the long term solar illumination (known as the light induced degradation) [28, 29]. The best way to solve these problems is reducing the thickness of the a-Si layer to realise an ultra-thin a-Si solar cell, thereby increasing the inner electric field to enhance the carrier separation rate and the collection efficiency. In addition, thinner a-Si solar cells can also reduce the impact of the light induced degradation, which often causes around 20% efficiency loss [16, 23]. However, at a reduced active layer thickness, the incident light cannot be harvested efficiently, especially in the wavelength range near the bandgap. Therefore, the trade-off between the ultra-thin thickness and the effective optical design of solar cells for broadband light trapping needs to be considered to design high efficiency solar cells.

Over the past decades, novel light trapping schemes have been demonstrated to have a great potential for improving the light absorbance in various thin film solar cells. Nanoparticles including plasmonic metallic nanoparticles [38-59, 63-67] and dielectric nanoparticles [76-82] have been investigated theoretically and experimentally to improve the solar cell performance. The mechanisms mainly lie in either the coupling of light into waveguide modes from large nanoparticles into the solar cells or the near field light concentration from small metallic particles [38, 39]. In addition to the nanoparticle light trapping, two dimension nanostructure arrays, such as nanodome, nanocone, nanovoid, plasmonic back reflectors, have been utilised to enhance the absorbance in solar cells [68-75]. The absorption enhancement mechanisms mainly lie in the gradient effective refractive index from the top of the structure to the bulk material and the increased optical path length induced by the plasmonic back scattering. However, there are some limitations for the aforementioned light management schemes. In case of the plasmonic metallic nanoparticle integrated solar cells, the nanoparticles can only enhance the absorbance in some specific wavelengths. On the other hand, dielectric nanoparticles on an ultrathin flat solar cell can offer a broadband absorption enhancement. But the overall integrated $J_{SC}$ is not as high as the solar cells with a thick active layer. As for the solar cells with various nanostructured plasmonic back reflectors, they can provide broadband light trapping schemes, but the cost for fabrication is high and scalability is low especially when using the electron bean or focused ion beam lithographic methods. In addition, these plasmonic nanostructures have the same problem as that in the traditional textured light trapping structures for the n-i-p solar cells. Only the nanostructures at the back side of the solar cell can be well controlled and optimised. The morphologies of the rest layers of the solar cell cannot be controlled due to the smear out of the fine structures with increased film thickness. Therefore, it is highly preferred that both the front and the back surface light trapping strategies can be combined to achieve the optimised solar cell performance. However there exist key challenges in designing and fabricating such light trapping structures with low-cost and scalable methods.

In this Chapter, we propose a novel solar cell geometry with closely-packed $SiO_2$ nanoparticles half embedded into the a-Si solar cell from the top surface to achieve a significantly higher absorption enhancement in an entire interested solar spectrum, which cannot be fulfilled by the solar cell design with the nanoparticle light trapping structure on the top surface presented in the Chapter 2 and the Chapter 3. By using this nanoparticle imprinting method, both the front and the back surface light trapping strategies can be combined to achieve the optimised solar cell performance. The conformal structures in both the a-Si layer and the Ag back reflector are formed in a natural way as shown in Fig. 4.1. The rest of the Chapter is arranged in the following way: First, a 3D solar cell model is set up to reveal the mechanism of absorption enhancement in the a-Si layer with this newly designed solar cell structure using the Lumerical FDTD software. The sizes of the nanoparticles, the positions of the embedment and the thicknesses of the AZO layer are investigated in the simulation. Then, the fabrication method of this new solar cell architecture is developed and demonstrated by the nanoparticle nanoimprinting method. The diameters of the $SiO_2$ nanoparticles are changed from 300 nm to 600 nm. The thickness of the a-Si layer is selected to be 150 nm, which is only half of the traditional thickness, for the demonstration of an ultra-thin solar cell case. At last, the solar cell is characterised by the reflectance measurement and the QE measurement.

## 4.2 Modelling of conformal structured a-Si solar cells induced by closely packed $SiO_2$ nanosphere arrays embedded in the top surface

In this Section, to achieve a broadband light trapping effect, a new a-Si solar cell structure is proposed in Fig. 4.1, which consists of a closely-packed $SiO_2$ nanosphere arrays and an n-i-p structured a-Si solar cell. Due to the partially embedded position of the $SiO_2$ nanosphere arrays in the solar cells, all the layers of the solar cell including the ITO, a-Si, AZO and Ag back reflector layers follow the hemispherical shape of the particles. The advantage of this geometry is to combine the closely-packed $SiO_2$ nanosphere front surface layer with the curvature of the a-Si layer and the Ag plasmonic back reflector to maximise the light trapping on both sides of the solar cell.

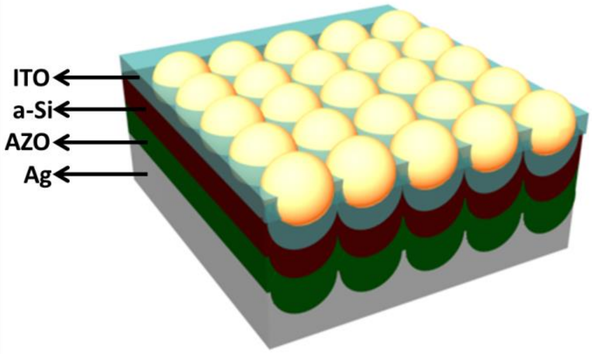

Fig. 4.1 Schematic of the front surface $SiO_2$ nanoparticle imprinted conformal solar cell.

### 4.2.1 Model set up

To account for the light absorbance in the front nanoparticle imprinted conformal solar cells, a 3D FDTD model was built up as shown in Fig. 4.1 with the Lumerical software. The cross section of the solar cell structure is shown in Fig. 4.2. The simulation region is set at the edge of the $SiO_2$ sphere since they are closely packed. We apply the periodic boundary conditions in the lateral directions to mimic the sphere array, and perfectly matched layers in the vertical direction. A broadband plane wave source (300 nm-800 nm) is used to simulate the light incident on the particles from the top.

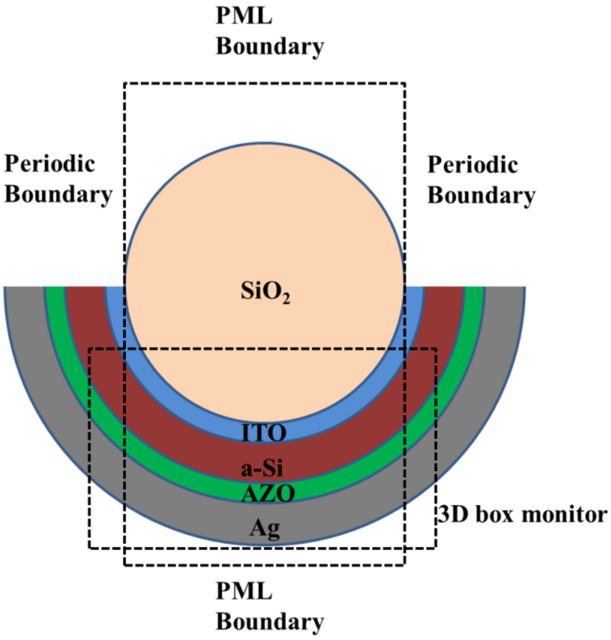

Fig. 4.2 The cross-section of the simulation model for the front surface nanoparticle imprinted conformal solar cell.

The thickness of each layer in the solar cell is set as 80 nm for the ITO layer, 150 nm for the a-Si layer, 100 nm for the AZO layer and 120 nm for the Ag layer, respectively. The diameter of the $SiO_2$ nanoparticle is changed from 300 nm to

600 nm according to the conditions obtained in Section 2.3. Due to the curvature of each layer in the solar cell, the flat 2D monitors cannot be used in this case to calculate the absorbance in the a-Si layer as discussed in Section 2.2.3. Here a 3D monitor box is utilised as shown in Fig. 4.2. Since the materials are defined explicitly in every mesh grid, it is straightforward to separate the absorption in parasitic materials such as ITO, AZO and Ag from the absorption in the a-Si material, even over the irregular curvature of the solar cell geometry. One of the advantages of this simulation technique is that the field distributions can be calculated explicitly everywhere in the model. This allows us to visualise the magnitude of the absorption in each layer.

To quantify the effect of the novel structure on the performance of the a-Si solar cell, we first calculate the absorbance of the a-Si layer $A(\lambda)$, which is defined as the ratio of the power of the absorbed light $P_{abs}(\lambda)$ to that of the incident light $P_{in}(\lambda)$ within the a-Si film.

$$A(\lambda)=P_{abs}(\lambda)/P_{in}(\lambda), \tag{4.1}$$

The power absorbed can be written as

$$P_{abs}(\lambda)=\frac{1}{2}\omega\varepsilon''|E|^2, \tag{4.2}$$

where $\omega$ is the frequency, $\varepsilon''$ the imaginary part of the permittivity, $E$ the electric field. The $P_{abs}$ is calculated over the whole structure and the index monitor data is used in the 3D box monitor to isolate the absorbance in the a-Si layer before integrated with the *AM 1.5* spectrum. By integrating the absorbance with the *AM 1.5* solar spectrum, we can obtain the area independent short circuit current density ($J_{SC}$) using the Equation (2.2) presented in the Chapter 2. The absorption enhancement $G$ in the 150 nm thick a-Si film with this novel structure is calculated and compared with the flat solar cell by changing the diameter of the $SiO_2$ nanosphere arrays,

$$G=A_{NP}(\lambda)/A_{ref}(\lambda), \tag{4.3}$$

where $A_{NP}(\lambda)$ represents the absorbance of the structured a-Si film with the $SiO_2$ nanosphere arrays, and $A_{ref}(\lambda)$ the absorbance of the flat a-Si solar cell.

### 4.2.2 Influence of the embedding position of $SiO_2$ nanoparticles on the absorbance of the a-Si layer

Before systematically investigating the optical performance of the solar cells based on the structures depicted in Fig. 4.1, the position of the closely-packed $SiO_2$ nanoparticles on the top surface of solar cells need to be optimised first. The nanoparticles can be embedded into the a-Si layer from the front surface with different embedding depths. We define a relative distance as the distance from the centre of the $SiO_2$ nanoparticles to the top surface of the a-Si solar cells. The diameter of the $SiO_2$ nanoparticle is selected to be 300 nm for demonstration while the relative distances are selected to be 150 nm (with nanoparticles on top of the solar cells), 75 nm (with one quarter of the nanoparticles embedded in the a-Si solar cells), 0 nm (with nanoparticles half embedded in the solar cells), and -75 nm (with three quarters of the nanoparticles embedded in the solar cells). The absorbance of a-Si solar cells with different relative distances is calculated based on the Equation (4.1) and the corresponding $J_{SC}$ value is calculated. Fig. 4.3 (a) shows the light absorbance in the a-Si layer with the 300 nm nanoparticles embedded into the a-Si layer by different relative distances.

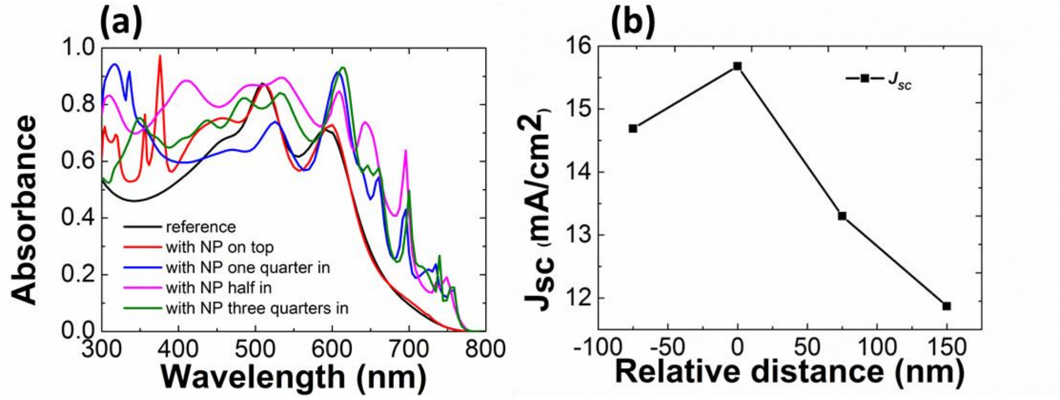

Fig. 4.3 (a) Light absorbance in the a-Si layer with 300 nm $SiO_2$ nanoparticles embedded. (b) $J_{SC}$ in solar cells with different relative distances of the embedded nanoparticles.

From Fig. 4.3 (a), we can clearly find that the absorbance in the a-Si layer is enhanced in the longer wavelength range when the nanoparticles are embedded into the a-Si solar cells. In some shorter wavelength ranges, the absorbance is decreased slightly when the nanoparticles are embedded by one quarter and three quarters of the diameter. However, a broadband absorption enhancement in the a-Si layer can be achieved with nanoparticles half embedded. Fig. 4.3 (b) shows the calculated $J_{SC}$ value by integrating the absorbance curve with the *AM 1.5* solar spectrum. The highest $J_{SC}$ value is obtained with the relative distance of 0 nm. From the calculation, it can be concluded that the best position of the nanoparticles in the solar cells for the highest absorbance enhancement is at 0 nm relative distance. So in the next Sections further simulations are conducted with the nanoparticles half embedded to find out the absorption enhancement mechanism.

### 4.2.3 Size effect of $SiO_2$ nanosphere arrays on the absorbance of the a-Si layer

First, we investigate the influence of $SiO_2$ nanosphere diameters on the absorbance of the a-Si. The diameters of $SiO_2$ nanoparticles are selected to be 300 nm, 400 nm, 500 nm and 600 nm according to our analyses in Section 2.3. The thickness of the a-Si layer is set to be 150 nm, which is half of the thickness of the normal case. The reason to set this value is that in reality it is technically challenging to make a solar cell with a smaller thickness because the quality of the a-Si layer cannot be guaranteed. For comparison, we calculate the absorbance of the flat a-Si solar cell as a reference case (the thicknesses of all the layers in the flat solar cell are the same as the nanoparticles imprinted solar cell). At last we use the Equation (2.2) to calculate the integrated $J_{SC}$ value to obtain the configurations that can offer the largest $J_{SC}$ value. Table 4.1 summarises the integrated $J_{SC}$ value and the absorption enhancement in a-Si solar cells with different sized $SiO_2$ nanospheres compared with the reference case.

| | **Reference** | **300 nm $SiO_2$** | **400 nm $SiO_2$** | **500 nm $SiO_2$** | **600 nm $SiO_2$** |
|---|---|---|---|---|---|
| **$J_{SC}$ (mA/cm$^2$)** | 11.41 | 15.68 | $\underline{17.82}$ | 16.71 | 16.10 |
| **Enhancement** | 1 | 1.374 | $\underline{1.561}$ | 1.464 | 1.411 |

Table 4.1 $J_{SC}$ and $J_{SC}$ enhancement of the $SiO_2$ nanoparticle embedded solar cells compared with the reference.

As can be seen from Table 4.1, the highest $J_{SC}$ value achieved in the $SiO_2$ nanosphere imprinted solar cell is 17.82 mA/cm$^2$ when the particle size is at 400 nm, increased from 11.41 mA/cm$^2$ compared to the flat case. A relative enhancement of 56.1% is obtained under this condition. We attribute this enhancement to three reasons. First, the closely packed embedded $SiO_2$ nanospheres can act as an effective textured antireflection coating between the a-Si solar cell and the air. In addition they can also scatter light and couple the whispering gallery mode (WGM) generated by the $SiO_2$ arrays into the a-Si layer [78, 79]. Secondly, the combination of the $SiO_2$ nanospheres and the gradient indexed conformal structure can act as a good anti-reflection structure for the solar cell similar to the nanocone solar cell structure [73]. Specific waveguide modes can be excited in by the front conformal structure of the a-Si layer leading to the absorbance enhancement [62, 93]. Thirdly, the plasmonic nanostructured Ag back reflector is playing an important role. Hybrid plasmon modes (mixture of the LSP modes, SPP modes and the rim modes [110]) near the metal surface can be generated, which can efficiently feed the electromagnetic energy into the a-Si layer thereby increasing the absorbance [68-70].

To further investigate the influence of the solar cell structure on the absorbance in the a-Si layer, we plot the light absorbance of the 150 nm thick a-Si layer dependent on the diameters of the $SiO_2$ nanosphere from 300 nm to 800 nm wavelength regions in Fig. 4.4. To make a comparison, the absorbance of a 150 nm thick flat a-Si solar cell is presented as a reference. In addition, to find out the relationship between the absorption enhancements of the a-Si and the plasmonic Ag back reflector, absorption of the Ag back reflector is also calculated in each structure of solar cells.

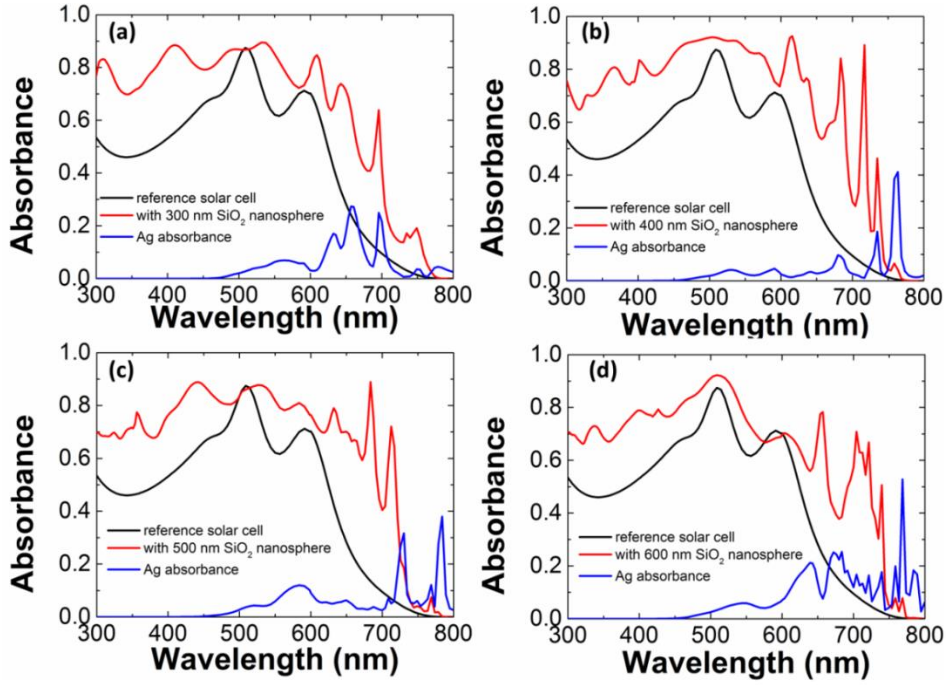

Fig. 4.4 Calculated absorbance of the a-Si layer (red line) compared with the flat reference solar cell (black line) and the nanostructured Ag back reflector (blue line) with $SiO_2$ nanoparticles of different sizes (a) 300 nm (b) 400 nm (c) 500 nm (d) 600 nm as a function of wavelength.

Fig. 4.4 shows the absorbance of the nanostructured a-Si layer (red curve) and the Ag back reflector layer (blue curve) with different $SiO_2$ nanoparticle diameters (from 300 nm to 600 nm) compared with the reference case (black line). An entire band absorption enhancement in the a-Si layer has been achieved by integrating the nanoparticle imprinted conformal nanostructures in every layer of the solar cell. In addition, there also exist some isolated absorbance peaks in the longer wavelength range which we believe is due to the void plasmon modes excited by plasmonic Ag back reflector [110].

To conform that the isolated absorbance peaks in the a-Si layer are due to the plasmonic absorptions in the nanostructured Ag back reflector, the absorbance of the Ag back reflector is also calculated in each figures shown as the blue lines. The absorbance of the Ag back reflector starts to show up from 450 nm indicating the light with wavelengths above 450 nm cannot be fully absorbed after the first pass in the solar cell. This portion of light reaches the Ag back reflector and is absorbed generating plasmon modes in the structured Ag back reflector. Due to the complex structures of the Ag back reflector, the generated plasmon modes cannot be simply depicted as the SPP modes or LSP modes. They are the hybrid plasmon modes which are coupled by the void modes (SPP modes, LSP modes) with the rim dipoles generated by the edge of the nanostructured Ag [110-112]. At some of the absorbance peaks of the Ag back reflector in the longer wavelength range, the void mode can dominate the hybrid plasmon modes such as the case at the wavelength of 735 nm for the 400 nm $SiO_2$ nanospheres [110]. Through the comparison of the absorbance between the a-Si and the Ag back reflector, we can find that at some specific wavelengths where the void modes are excited, the absorbance of the a-Si is enhanced by several folds. We attribute the enhancement to the coupling of these void modes into the a-Si layer by the AZO space layer.

To further illustrate the absorbance enhancement in a more intuitive way, the electric field distributions of the cross section of the 400 nm $SiO_2$ nanoparticle imprinted a-Si solar cell are plotted and compared with the flat solar cell in Fig. 4.5. The polarisation of the incident light is along the X direction and the field component of the light in the a-Si layer is also along the X direction. The reason we choose 400 nm $SiO_2$ particles as an example is that the highest overall absorbance and $J_{SC}$ can be obtained under such a circumstance.

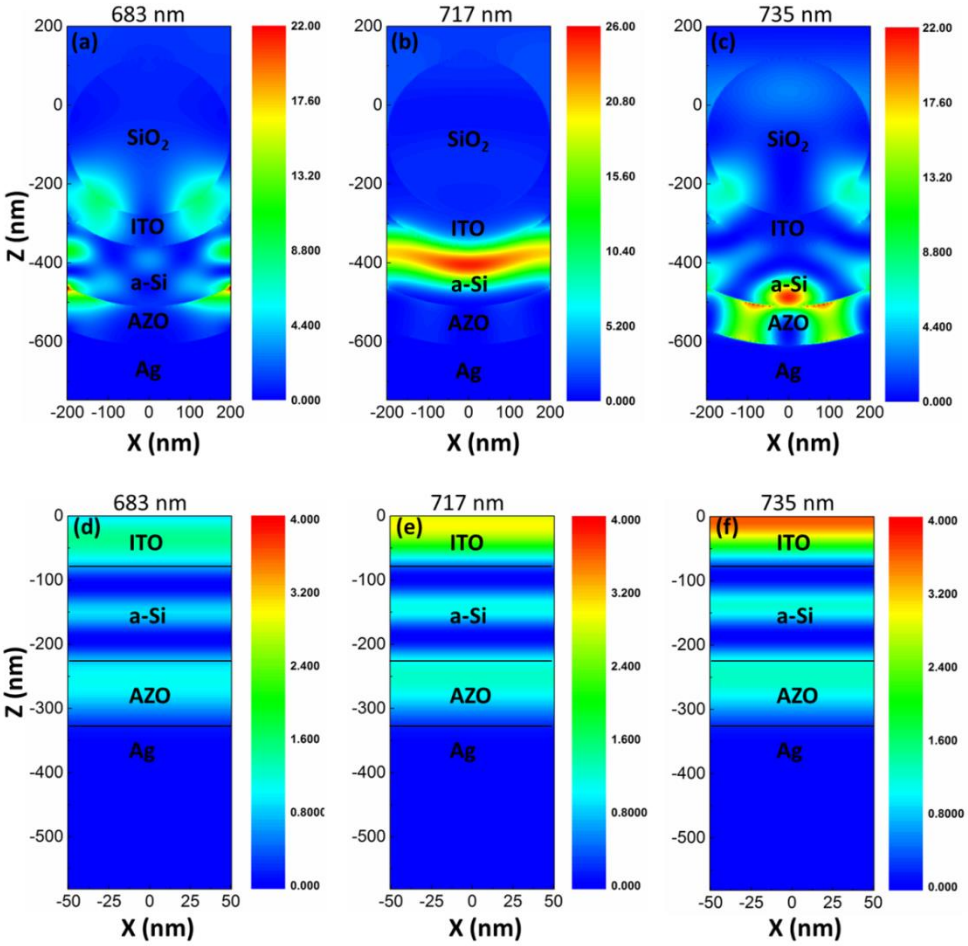

Fig. 4.5 Electric field intensity distributions in nanoparticle imprinted solar cells (a-c) and planer solar cells (d-f) with a 150 nm thick a-Si layer at wavelengths of (a and d) 683 nm, (b and e) 717 nm and (c and f) 735 nm, corresponding to the absorbance peaks of the a-Si as shown in Fig. 4.4 (b).

The calculation results show that two main physical mechanisms are responsible for the observed absorption enhancement in the a-Si layer. First of all, specific waveguide modes are excited within the conformal patterned multi-layer solar cell structure induced by the SiO$_2$ nanospheres at the wavelength of 683 nm and 717 nm. These modes are mainly confined within the a-Si layer especially at the wavelength of 717 nm where 90% of the incident light is confined within the a-Si layer. Secondly, at the wavelength of 735 nm corresponding to the absorbance peak of Ag, void plasmon modes at the metal-dielectric interface are excited and coupled into the a-Si layer, leading to a further absorbance enhancement in the a-Si layer. For comparison, the electric field intensity distributions of flat solar cells are also plotted in Figs. 4.5 (d-f). Without nanostructure induced void plasmons and waveguide modes, only interference fringes can be observed. Electric field cannot be effectively confined within the a-Si absorbing layer, and most of the incident light passes through the a-Si layer and is reflected back by the Ag reflector.

In addition to the absorption enhancement induced by the conformal structures, the presence of the $SiO_2$ nanoparticles on the structured a-Si solar cell can also lead to enhanced light trapping. Taking the 400 nm $SiO_2$ case as an example, the absorbance of the nanostructured a-Si layer and the Ag back reflector with and without the nanoparticles are calculated and compared with the flat reference solar cell as shown in Fig. 4.6.

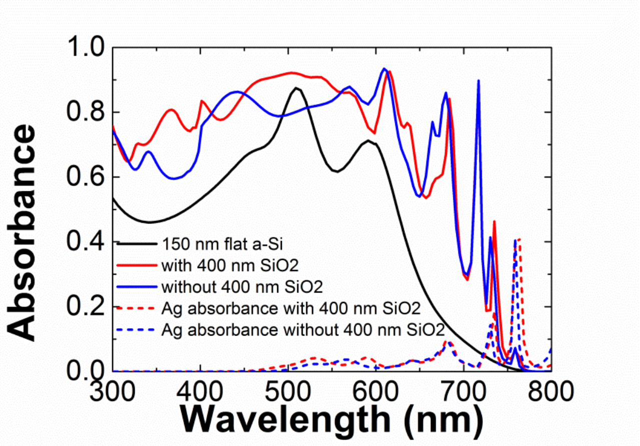

Fig. 4.6 Absorbance of the a-Si layer (solid line) and the Ag back reflector (dash line) in the conformal structured solar cell with (red line) and without (blue line) the 400 nm $SiO_2$ nanospheres compared with the flat reference solar cell (black line).

When the front $SiO_2$ nanospheres are not presented, the absorbance of the a-Si layer reduces significantly in the wavelength range from 300 nm to 550 nm leading to a decrease in the integrated $J_{SC}$ value from 17.82 mA/cm$^2$ to 16.84 mA/cm$^2$. We attribute this absorbance decrease to the less effective refractive index matching between the ITO layer and air which increases the top interface reflection [97,113]. The slight difference of the a-Si absorbance curves in the longer wavelength with and without the $SiO_2$ nanoparticles mainly arises from the different coupled waveguide modes and scattering properties of the nanospheres. In addition, we can also see that at the wavelength above 720 nm, the absorbance peaks of the a-Si redshift in accordance with the redshift of the Ag back reflector absorbance peaks. This confirms that the enhanced absorbance in the a-Si layer at these wavelengths arises from the void plasmon generated by the nanostructured Ag back reflector.

In conclusion, from the comparison of the conformal structured a-Si solar cell without the presence of $SiO_2$ nanospheres to the flat reference solar cell, the $J_{SC}$ value is improved from 11.41 mA/cm$^2$ to 16.84 mA/cm$^2$. The presence of $SiO_2$ nanospheres can further increase the absorbance of the a-Si solar cell (from16.84 mA/cm$^2$ to 17.82 mA/cm$^2$).

### 4.2.4 Effect of the AZO thickness on the absorbance in the a-Si layer

In a normal flat a-Si solar cell design, AZO is used for two purposes. Firstly, it is an electrical protection of the a-Si layer from the Ag back reflector [23]. During the fabrication process of the a-Si solar cell, the increased temperature of a-Si deposition can lead to the diffusion of Ag into the a-Si layer, causing defects in the a-Si material degrading the solar cell performance. In this case, the AZO layer can serve as a buffer layer to prevent the Ag diffusion. Secondly the AZO layer can enhance the back reflection from the rear surface [23]. For our nanostructured a-Si solar cells, this AZO layer can also play a key role in determining the void plasmon modes generated by the structured Ag back reflector [113-115]. In addition, different waveguide modes in the a-Si layer can also be excited by changing the thickness of the AZO layer. So in this Section, we mainly investigate the effect of the AZO layer thickness on the absorbance of nanoparticle imprinted a-Si solar cells.

The thickness of the AZO layer is changed from 25 nm to 250 nm with an interval of 25 nm considering the balance between the optical and electrical properties. The diameter of the $SiO_2$ nanospheres is selected to be 400 nm as with this size of nanospheres the highest $J_{SC}$ value is obtained. The absorbance of the Ag and the a-Si layer with different thicknesses of the AZO layer is calculated and compared to the AZO layer with a normal thickness of 100 nm. $J_{SC}$ of the nanoparticle imprinted solar cell with different AZO thicknesses is shown in Fig. 4.7.

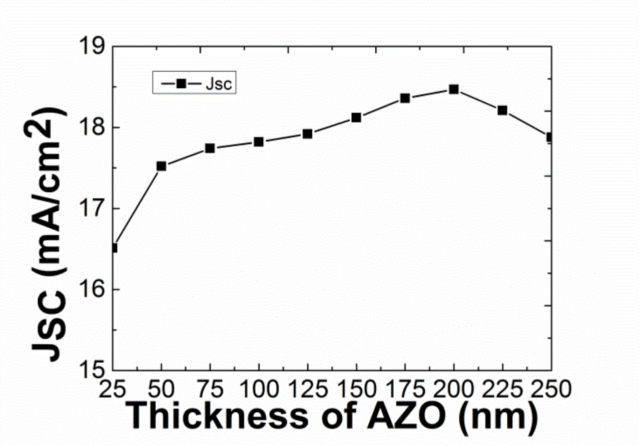

Fig. 4.7 $J_{SC}$ of nanoparticle imprinted solar cells with 400 nm $SiO_2$ nanospheres as a function of different AZO thicknesses.

From Fig. 4.7, we can find that with increased AZO thickness from 25 nm to 250 nm, the $J_{SC}$ value is first increased from 16.51 mA/cm$^2$ to 17.52 mA/cm$^2$ for a 50 nm thick AZO layer. Then it reaches the highest value of 18.47 mA/cm$^2$ with a 200 nm thick AZO layer and finally decreases to 17.88 mA/cm$^2$ when AZO is 250 nm thick. To investigate the reason for this phenomenon, the absorbance of the a-Si and the Ag layer in solar cell with different thicknesses of the AZO layer are calculated and plotted in Fig. 4.8.

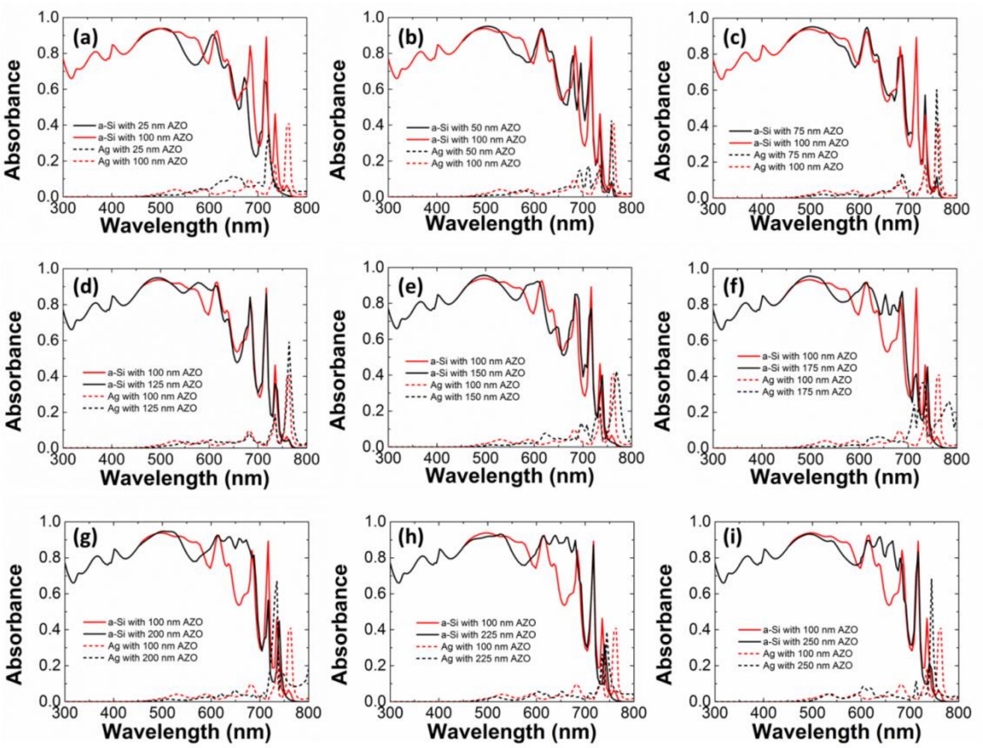

Fig. 4.8 Absorbance of the a-Si (solid line) and the Ag back reflector layer (dash line) in nanoparticle imprinted solar cells with different thicknesses of the AZO layer at (a) 25 nm, (b) 50 nm, (c) 75 nm, (d) 125 nm, (e) 150 nm, (f) 175 nm, (g) 200 nm, (h) 225 nm, (i) 250 nm, compared to the case with a standard thickness of 100 nm AZO.

Fig. 4.8 shows the absorbance of the a-Si and the Ag back reflector layer in nanoparticle imprinted solar cells with different thicknesses of the AZO layer at 25 nm (a), 50 nm (b), 75 nm (c), 125 nm (d), 150 nm (e), 175 nm (f), 200 nm (g), 225 nm (h) and 250 nm (i) compared to the case with a standard AZO thickness of 100 nm. In Fig. 4.8 (a), the main difference between the two a-Si absorbance curves lies in the longer wavelength range where the absorbance of the a-Si with a 25 nm of AZO layer is decreased. We attribute this decrease to two reasons. One is that with 25 nm of the AZO layer, the optical thickness of the AZO layer is reduced; thereby supporting less waveguide modes than the solar cell with 100 nm of the AZO layer. The other one is that the reduced thickness of the AZO layer leads to fewer void plasmon modes generated by the Ag back reflector, evidenced by the Ag absorbance with the dash line. For the 100 nm AZO layer, there exist two distinct absorbance peaks in the Ag back reflector layer above 700 nm wavelength as shown with the red dash line representing two different void plasmon modes. These two modes are both coupled into the a-Si layer through the 100 nm thick AZO layer leading to the two absorbance peaks in the absorbance curve of the a-Si layer. In comparison, there only exists one absorbance peak in the Ag absorbance curve above 700 nm in the black dash line when the AZO thickness is at 25 nm. In addition, this void plasmon modes cannot be coupled into the a-Si layer as there is no corresponding absorbance peak presented in the a-Si absorbance curve at this wavelength.

When the AZO layer is increased further from 125 nm to 200 nm, the light coupling to the waveguide modes starts to dominate the absorption enhancement in the a-Si layer. This is due to the increased optical thickness of the AZO layer. In Fig. 4.8 (e), when the thickness of the AZO layer reaches 150 nm, the absorbance in the a-Si layer between 560 nm to 600 nm is enhanced compared to the 100 nm AZO reference layer. When the thickness is further increased to 175 nm and 200 nm as shown in Figs. 4.8 (f) and (g), the absorbance in the a-Si layer between 580 nm to 680 nm is enhanced. Some isolated peaks can be found in this wavelength range, which illustrate that more guided modes are coupled into the a-Si layer. However in the meantime, the a-Si absorbance from around 530 nm to 580 nm is decreased, which offsets slightly the enhancement achieved in the longer wavelength region. When further increasing the AZO thickness to 250 nm, $J_{SC}$ can no longer be improved. The optimised thickness of the AZO layer for the highest $J_{SC}$ value in the a-Si solar cell is at 200 nm.

To illustrate the light confinement in the AZO layer, the electric field intensity distributions in the solar cell are calculated and compared to that with a 100 nm AZO layer at the void plasmon resonance as shown in Fig. 4.9. For the case of 25 nm of the AZO layer (Fig. 4.9 (a)), the void plasmon is generated at the wavelength of 721 nm and confined within the thin AZO layer. While for the case of 100 nm of the AZO layer (Fig. 4.9 (b)), the void plasmon is coupled into the a-Si layer. Figs. 4.9 (c) and (d) show the electric field intensity distributions in the solar cells with a 200 nm thick AZO layer compared to that with a 100 nm thick AZO layer at 656 nm. We can find that more light are coupled into the a-Si layer with thicker AZO layers leading to the higher absorption enhancement. Thus we have demonstrated that the optical performance of the nanoparticle imprinted solar cells can be further enhanced by optimising the thickness of the AZO layer.

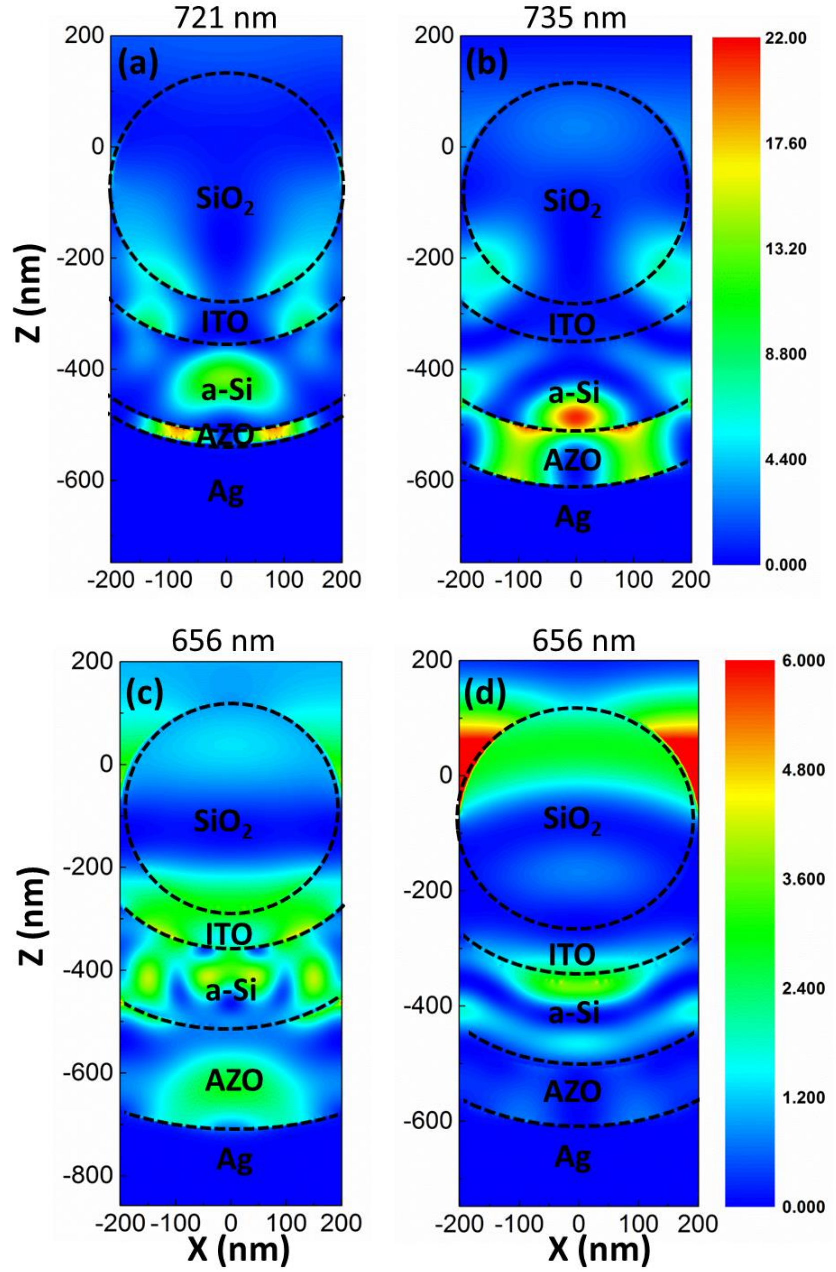

Fig. 4.9 The electric field intensity distributions in the nanostructured solar cells at the void plasmon resonance wavelength of 721 nm with the thickness of AZO layers at: (a) 25 nm, (b) 100 nm and at the wavelength of 656 nm with thickness of AZO layers at: (c) 200 nm, (d) 100 nm.

In conclusion, we investigate the influence of the thickness of the AZO layer on the absorbance in nanostructured a-Si solar cells. We find that by tuning the thickness of the AZO layer, the hybrid plasmonic modes and guided modes can be adjusted and coupled into the a-Si layer to achieve a higher absorbance for thinner a-Si solar cells.

## 4.3 Fabrication and characterisation of the nanoparticle imprinted a-Si solar cells

In this Section, we discuss the fabrication process of the nanoparticle imprinted a-Si solar cells as well as their optical and electrical properties.

Usually, metal nanovoid structured substrate can be fabricated by electrochemical deposition through a template of close-packed self-assembled spheres [68]. After the dissolve of the spheres an ordered array of nanovoid metal substrate can be achieved, which can then be used to fabricate the void structured solar cells. However, by using this method, the void shape is smoothed out at the front surface by multilayer film deposition leading to less efficient light trapping. In addition, there is no way to embed $SiO_2$ nanospheres on top of this kind of solar cell to achieve anti-reflection. In this Thesis we propose and demonstrate the use of the nanoparticle imprinted method to simultaneously form the conformal structured solar cell and the half-embedded $SiO_2$ nanospheres on the front to realise significantly enhanced light trapping.

### 4.3.1 Characterisation of closely-packed $SiO_2$ nanospheres

In our experiments, we first closely pack the $SiO_2$ nanospheres on the glass surface to investigate their optical properties. The closely-packed $SiO_2$ nanospheres are known to be able to excite the WGMs [78, 79], which can be coupled into the guided modes within the a-Si layer when they are integrated on top of a-Si solar cells. To investigate the WGMs from the nanospheres, the transmittance and the reflectance of the closely-packed nanospheres on top of the glass is measured as shown in Fig. 4.10. The sizes of the nanospheres are from 280 nm to 600 nm.

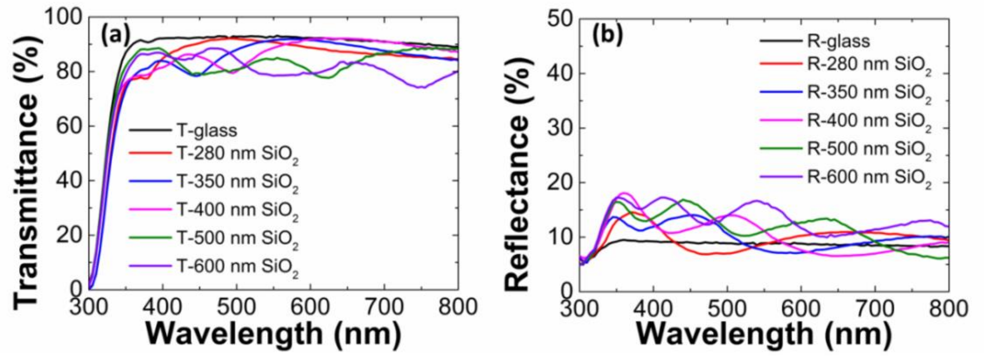

Fig. 4.10 Measured transmittance (a) and reflectance (b) of closely-packed $SiO_2$ nanospheres on glass with the diameters from 280 nm to 600 nm.

From the transmittance curve in Fig. 4.10 (a), we can find that there exist some distinguished valleys which should originate from the WGMs [82] in the $SiO_2$ nanospheres. The WGM from the nanospheres can produce a broad angle scattering of the incident light, which presents as a dip in the transmittance spectra near the resonance wavelength [82]. These valleys in the transmittance curves can also be confirmed from the peaks in the reflectance curves in Fig. 4.10 (b). By comparing the transmittance and reflectance curves with different sizes of the $SiO_2$ nanospheres, we can find that smaller nanospheres at 280 nm, only excite one WGM mode at the wavelength of 370 nm. With increased sizes of the nanospheres, more modes can be generated at the longer wavelengths. For example, for the 350 nm nanospheres, two peaks can be found from the reflectance curve at the wavelengths of 350 nm and 450 nm, respectively. But for the 600 nm nanospheres, there exist four resonance peaks in the reflectance curve at wavelengths of 355 nm, 420 nm, 540 nm and 760 nm, respectively, corresponding to different orders of WGM modes. By embedding these nanospheres half into the a-Si solar cell, the WGM modes are expected to increase the absorbance in the a-Si layer around these resonance wavelengths.

In the next Section, we will present the fabrication process for imprinting these closely-packed nanoparticles into the top surface of the solar cells.

### 4.3.2 Fabrication methods

To achieve our designed thin film solar cell structure in Fig. 4.1, we develop a new fabrication process using the nanoparticle-imprinting technology as shown in Fig. 4.11. First, closely packed $SiO_2$ nanospheres are fabricated by using the dip-coating or Langmuir–Blodgett (LB) method, which has been developed years ago [79]. In our experiments, commercial closely-packed $SiO_2$ nanoparticles on top of the glass substrate are purchased (Nanosyslab Company) as a template for a reverse nano-imprinting lithography process.

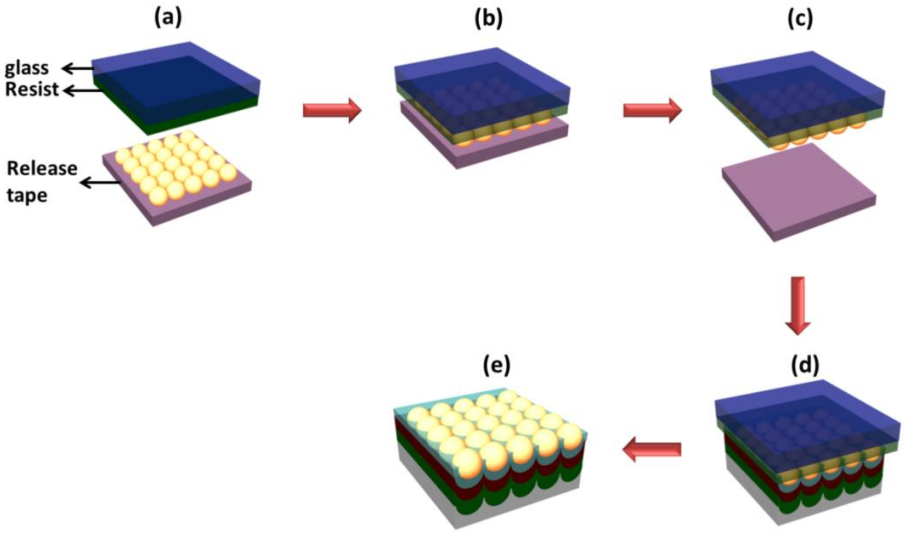

Fig. 4.11 Fabrication process of conformal nanostructured solar cells via embedding $SiO_2$ nanospheres half in the top surface of the solar cell.

Before the solar cell fabrication, in order to imprint $SiO_2$ nanospheres half into the a-Si solar cell, we need to prepare a substrate coated by a thin resist layer with the $SiO_2$ nanospheres half embedded in. The fabrication process is shown in Figs. 4.11 (a)-(c). First, a thermal release tape (Revalpha tape from Nitto Denko) is softly pressed onto the $SiO_2$ nanosphere packed glass substrate using a roller and then is gently peeled off. Thus, the closely-packed $SiO_2$ nanosphere structures are transferred onto the thermal-release tape as a release layer. Then we deposit a layer of thermal nanoimprinting resist (NXR-1025) on a clean glass substrate with the same thickness as the radius of the $SiO_2$ nanospheres using a spin-coater as shown in Fig. 4.11 (a). The glass needs to be cleaned by Acetone and IPA for 10 mins separately and then followed by a 5 mins cleaning in Oxygen plasma. Secondly, we bring the thermal nanoimprinting resist coated glass into direct contact with the closely-packed $SiO_2$ nanoparticles on the thermal-release tape, as shown in Fig. 4.11 (b). Under a pressure of 200 psi and a temperature of 130$^o$C for 5 mins in nanoimprinter, the thermal release tape can be peeled off by baking at 150$^o$C for several seconds. These nanoparticles are half embedded in the thermal resist layer as shown in Fig. 4.11 (c). The embedding depth of the $SiO_2$ nanospheres can be adjusted by changing the thickness of the resist layer. After that, this glass substrate with the $SiO_2$ nanospheres is used as a substrate for solar cell fabrication. First, an 80 nm ITO layer is deposited on the substrate serving as the top electrode. The p-i-n a-Si layers are then deposited on the ITO layer by the plasma enhanced chemical vapour deposition (PECVD) method. The n-type and p-type doped layers are 20 nm thick, while the thickness of the intrinsic a-Si layer is 110 nm (total thickness of a-Si is 150 nm). Then the AZO layer and the Ag layer are sputtered serving as the back reflector and the back electrode as shown in Fig. 4.11 (d). In the last step, after finally peeling off the thermal resist and the glass substrate from the solar cell, the designed solar cell with closely-packed $SiO_2$ half embedded in can be developed as shown in Fig. 4.11 (e).

### 4.3.3 Characterisation of the nanoparticle imprinted solar cells

The top surface morphology of our designed solar cells with embedded nanoparticles is characterised by scanning electron microscope (SEM) as shown in Fig. 4.12. The diameters of the closely-packed $SiO_2$ nanoparticle arrays are changing from 300 nm to 600 nm. To demonstrate that the nanoparticles are partially embedded into the top surface of the a-Si solar cells, the nanoparticles are peeled off to show the void structures in the insert images. The scale bar in the images is 500 nm. From the SEM images, we can find that the mean sizes of the nanoparticles are approximately 290 nm ± 10 nm, 340 nm ± 10 nm, 400 nm ± 10 nm, 500 nm ±10 nm and 610 nm ±10 nm.

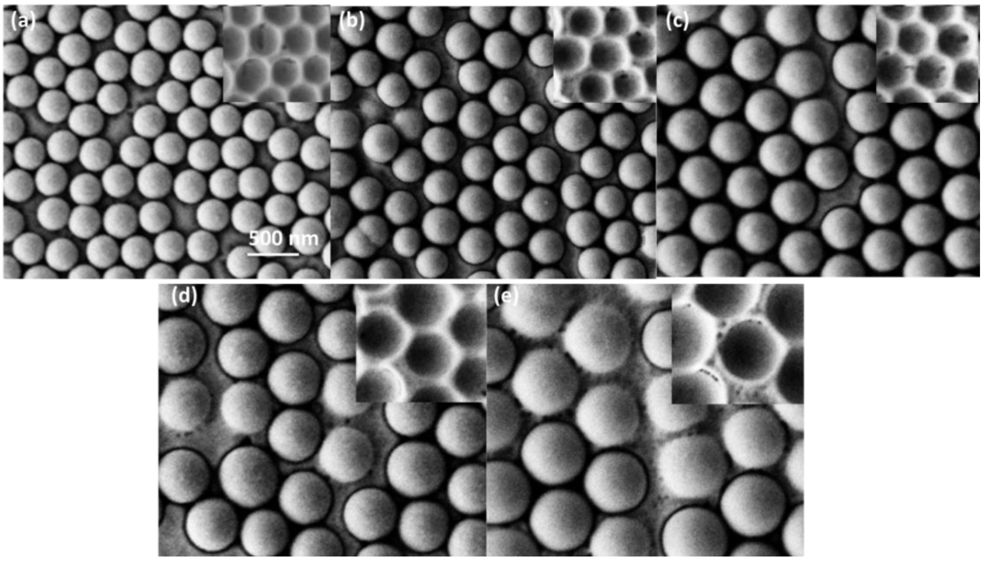

Fig. 4.12 SEM images of front surface nanoparticle imprinted solar cells with different sizes of embedded $SiO_2$ nanoparticles: (a) 290 nm ±10 nm, (b) 340 nm ±10 nm, (c) 400 nm ±10 nm, (d) 500 nm ±10 nm, (e) 610 nm ±10 nm. Insert figures are the a-Si nanostructures with the $SiO_2$ nanospheres peeled off.

It is worthwhile to know the depth of the void structure induced by the imprinted $SiO_2$ nanoparticles to determine the best light coupling efficiency. The depth of the void structures depends on the diameter of nanoparticles and the thickness of the thermal resist as shown in Fig. 4.11 (c). If the thickness of the resist layer is the same as the radius of the nanoparticles, we can accurately control the nanoparticles to be half embedded into the a-Si solar cells. From Fig. 4.12, we can also measure the diameters of the void structures in the a-Si solar cells. The embedding depth of the void structures can be roughly calculated by the formula:

$$d = R_{NP} - \sqrt{R_{NP}^2 - R_{void}^2} \tag{4.5}$$

where d is the depth of void, $R_{NP}$ and $R_{void}$ the radii of the nanoparticles and void structures, respectively. Through the calculation, the embedding depths of the void structures with different sizes of $SiO_2$ nanoparticles are obtained and listed in Table 4.2.

| **Sizes of NP** | **290 nm** | **350 nm** | **400 nm** | **500 nm** | **610 nm** |
|---|---|---|---|---|---|
| **Depth (nm)** | 108 nm | 112 nm | 134 nm | 210 nm | 266 nm |

Table 4.2 Depth of the void structures with different sizes of nanoparticles.

As can been seen from Table 4.2, the $SiO_2$ nanoparticles are approximately half embedded in the a-Si layer. The reflectance curves of the nanoparticle imprinted solar cells are measured using a UV-VIS spectrometer (Perkin Elmer, Lambda 1050) fitted with an integrating sphere and compared to a flat reference solar cell with the same thickness of the a-Si layer. The experimentally achieved reflectance spectra are depicted in Fig. 4.13 (a) and compared to the simulation results as shown Fig. 4.13 (b).

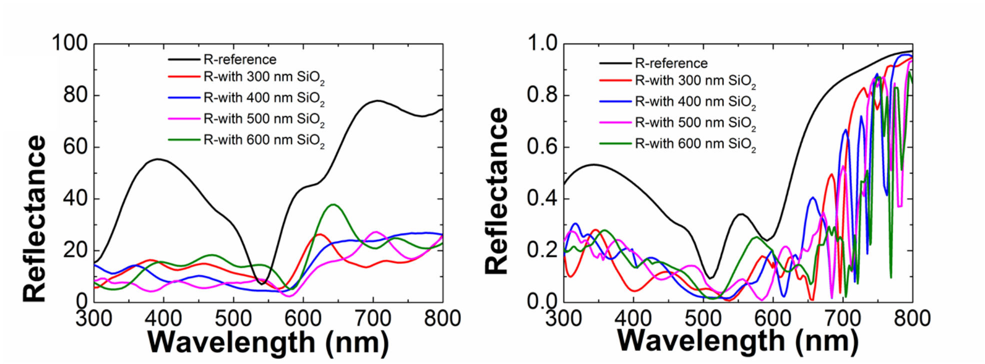

(a)

(b)

Fig. 4.13 (a) Measured and (b) calculated reflectance of 150 nm thick a-Si solar cells with different sizes of imprinted $SiO_2$ nanoparticles.

From Fig. 4.13 (a), we can find that the reflectance of all the nanoparticle imprinted solar cells is significantly reduced over the entire a-Si absorption band compared to the flat solar cell. The reduction of the reflectance indicates that more light is trapped inside the solar cell systems. The enhancement mechanism has been discussed systematically in Section 4.2 in this Chapter. It is worth noting that this enhanced absorbance (reduced reflectance) involves the entire solar cell devices, not only including the a-Si absorbing layer but also the ITO layer and the nanostructured Ag back reflector. That is why the reflectance in the longer wavelength around 800 nm can be dramatically reduced. In fact, there is a large amount of parasitic absorption loss due to the metal structure absorption. Therefore, in Section 4.2 numerical modelling was conducted to deduce the real absorption enhancement in the a-Si absorbing layers. Here, we only introduce the calculated reflectance curves of the solar cells in Fig. 4.13 (b) for the comparison with the measured reflectance curves. Due to the strong resonances occurring in the perfectly ordered nanostructures in the simulation model, sharp peaks can be observed in both the longer and the shorter wavelength regions with nanoparticles.

The slight difference between the experimental and simulation results can be ascribed to the factors such as the small offset in the incident angle, and the imperfectly matched material data between the experiments and simulation such as the refractive index (n) and extinction coefficient (k) values. In spite of these deviations, the simulation results can reproduce the experimental trends well, thus further confirming that the optical performance of the absorbing layer calculated previously is reliable.

To confirm that the enhanced absorbance from our designed solar cells contribute to the electricity generation, the quantum efficiencies (QE) are measured and compared to the flat reference solar cell which is deposited on the same glass substrate. From the QE measurements in Fig. 4.14, broadband improvements from the entire wavelength range are illustrated in all of the QE responses with nanoparticle imprinted solar cells. $J_{SC}$ of the solar cells with and without nanoparticles are calculated from the QE response curves and listed in Table 4.3. The relative enhancements of 30%-50% in $J_{SC}$ are obtained with the nanoparticle imprinted solar cells. From the simulation results discussed previously, the optimised size of the embedded nanoparticles in the solar cells for the highest absorbance should be 400 nm in diameter. However, from the experiment results in QE measurements, we cannot identify this optimised size of nanoparticles because of the unstable quality of the a-Si thin film during the different deposition cycles. However, the results are highly comparable within one large sample formed in one deposition, which contains both the sample cells and the reference cells.

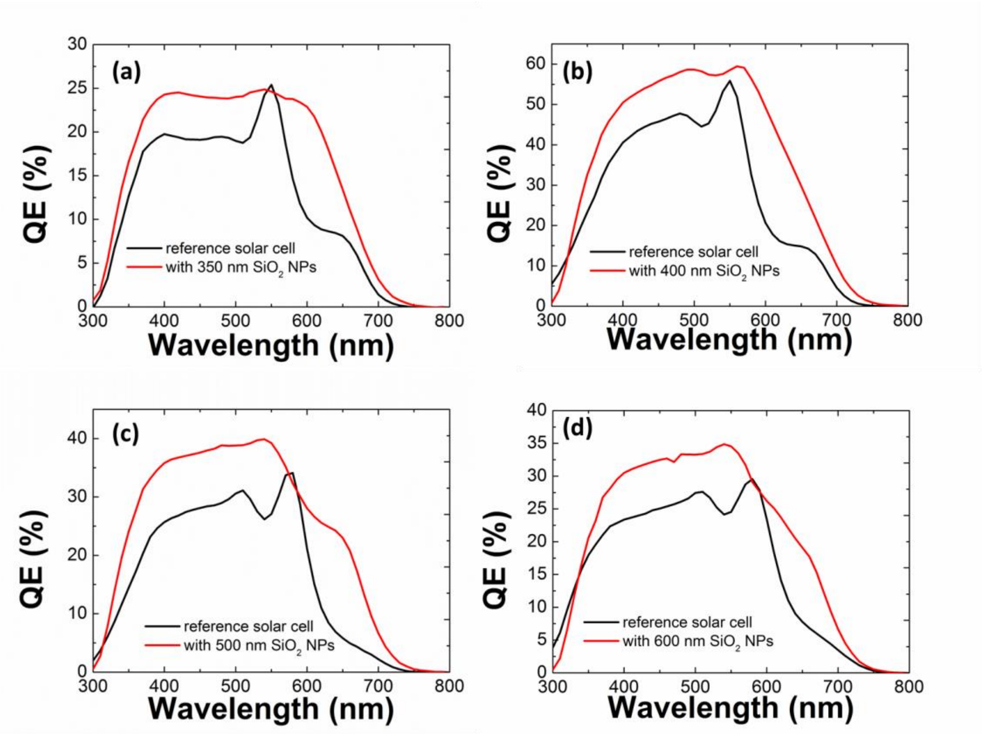

Fig. 4.14 QE comparison of 150 nm thick solar cells with different sizes of $SiO_2$ nanoparticles (a) 350 nm (b) 400 nm (c) 500 nm (d) 600 nm compared to the flat reference solar cells.

| | Reference $J_{SC}$ (mA/cm$^2$) | $J_{SC}$ with NPs (mA/cm$^2$) | Enhancement (%) |
|---|---|---|---|
| Solar cell with 350 nm $SiO_2$ NPs | 2.99 | 4.11 | 37.4 |
| Solar cell with 400 nm $SiO_2$ NPs | 6.6 | 9.5 | 43.9 |
| Solar cell with 500 nm $SiO_2$ NPs | 4.23 | 6.3 | 48.9 |
| Solar cell with 600 nm $SiO_2$ NPs | 4.09 | 5.55 | 35.7 |

Table 4.3 $J_{SC}$ of the solar cells with different sizes of $SiO_2$ nanoparticles (NPs) compared to the reference solar cell.

In Table 4.3 we can find that $J_{SC}$ of the reference solar cells are quite variable, changing from 2.99 mA/cm$^2$ to 6.6 mA/cm$^2$. The unstable quality of the a-Si film is attributed to the thin thickness (only 150 nm), which can be addressed by further optimising the solar cell fabrication process. From the comparison of the $J_{SC}$ values, a conclusion can be drawn on the basis of the evidence that the optical performance of the solar cells can be dramatically improved by nanoparticle imprinted structures from both the reflectance measurement and the QE measurement. It should be noted that the highest $J_{SC}$ value of 9.5 mA/cm$^2$ is achieved with the size of $SiO_2$ nanoparticle at 400 nm with an only 110 nm thick intrinsic a-Si layer, which shows the potential of further optimisation.

To confirm the comparable light trapping ability of the nanoparticle imprinted ultrathin solar cell with the traditional p-i-n textured 300 nm thick solar cell, the reflectance of our designed solar cell is measured and compared to the p-i-n textured solar cell as shown in Fig. 4.15.

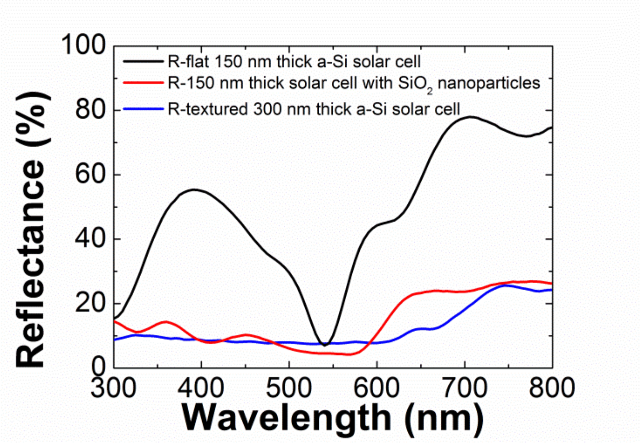

Fig. 4.15 Reflectance comparison between 150 nm thick a-Si solar cells with/without 400 nm $SiO_2$ nanoparticles imprinted and a 300 nm thick textured p-i-n a-Si solar cell.

From Fig. 4.5 we can see that the reflectance of the nanoparticle imprinted 150 nm thick solar cell is comparable with the traditional 300 nm thick p-i-n textured solar cell in the wavelength range below 600 nm and even lower from 480 nm to 600 nm. For the wavelength longer than 600 nm, the reflectance of the designed solar cell is not as good as that of the p-i-n textured solar cell, which is mainly due to the thinner active layer. The comparable reflectance curves between our designed ultrathin solar cell and the 300 nm thick textured p-i-n a-Si solar cell show the great potential of high performance with efficient light management via the nanoparticle imprinting.

## 4.4 Chapter conclusion

In this Chapter, we propose a new solar cell structure concept with closely packed $SiO_2$ nanoparticles partially imprinted in a-Si solar cells from the top surface. This structure introduces the conformal structures into the a-Si and the Ag back reflector layers in a natural way. Then we systematically investigate the influence of these nanoparticles on the absorbance in the 150 nm thick a-Si solar cells by numerical modelling. Through optimising the embedding depth and sizes of the $SiO_2$ nanoparticles, $J_{SC}$ can be increased from 11.41 mA/cm$^2$ for a flat reference solar cell to 17.82 mA/cm$^2$ for 400 nm $SiO_2$ nanoparticle imprinted solar cells. After that, the influence of the AZO layer thickness on the absorbance in the structured solar cells is also investigated. The optimised thickness of the AZO layer is around 200 nm, which can result in a further increase of $J_{SC}$ from 17.82 mA/cm$^2$ to 18.47 mA/cm$^2$. At last, a new fabrication method of the designed solar cells is developed using the nanoimprinting method. Through the characterisation of the solar cells by measuring the reflectance and the QE response curves, approximate 30%-50% $J_{SC}$ enhancements are achieved compared to the flat reference case. These results indicate the great potential of improving the thinner solar cell performance with the proposed novel nanostructures without compromising the optical property.

# Chapter 5

## Hetero-structured lumpy nanoparticle for high absorbance of ultrathin film amorphous silicon solar cells

### 5.1 Introduction

As previously discussed in Chapter 3 and Chapter 4, both the small metallic nanoparticles and $SiO_2$ nanoparticle imprinted solar cell structures show great potential to achieve entire band absorption enhancement in a-Si solar cells. However, how to combine the advantages of these nanoparticles and nanostructures together by designing novel nanoparticle and solar cell architecture seems to be challenging. Recently, the nucleated nanoparticle geometry (or the lumpy geometry) was demonstrated to be an effective way to mitigate these challenges in thin film solar cells [49,119,120]. Through combining a large core Ag particle with a number of small Ag surface nanoparticles, the strong scattering effect and the near field effect can be enabled leading to a significant enhancement of more than 20% in the solar cell conversion efficiency. However, the intrinsic absorption and the light blockage from the silver nanoparticles cannot be avoided, limiting the integration of the nucleated nanoparticles only to the back contact layer of the thin film solar cells.

In this Chapter, based on the understanding we achieved from the ultra-small metallic nanoparticles in the Chapter 3 and the large dielectric nanoparticles in the Chapter 4, we first propose a hetero-structured lumpy nanoparticle model in Section 5.2, as shown in Fig. 5.1, to address the challenges associated with the plasmonic nanoparticles in amorphous silicon (a-Si) thin film solar cells. For the core particles, metallic materials are replaced by dielectric materials to achieve strong broadband scattering with negligible particle absorption. Nanometer sized metal nanoparticles are used as the surface particles to enable the near field concentration. Through the optimisation of the position and size of the nanoparticles, we can also achieve similar value of $J_{SC}$ with only 20 nm thick a-Si layer as that with the 300 nm thick a-Si layer as discussed in Section 5.3. Then, the fabrication method of this kind of nanoparticle is developed by coating ultra-small Ag nanoparticles on the surface of the closely-packed $SiO_2$ nanospheres and characterised by the UV-VIS spectrometer in Section 5.4. The performance of the solar cells integrated with the hetero-structured nanoparticles is characterised by the I-V and EQE measurement.

## 5.2 Modelling of a-Si thin film solar cells with the hetero-structured nanoparticles

In this Section, a model of a-Si solar cells integrated with the proposed hetero-structured lumpy nanoparticles is built up using the FDTD method as shown in Fig. 5.1. It has been found that the relative distance of the centre of the hetero-structured nanoparticles to the top surface of the a-Si layer and the size of the core dielectric particles play a crucial role in the light absorption enhancement.

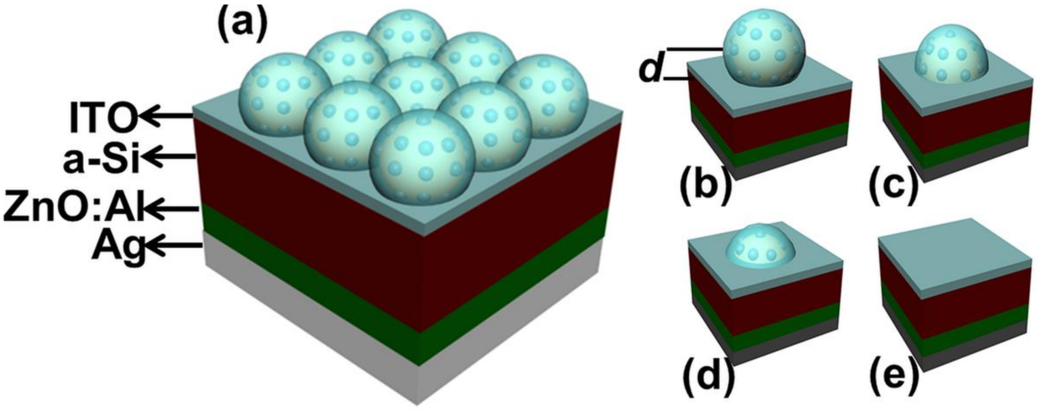

Fig. 5.1 (a) The scheme of the simulation model. (b)-(e) The solar cell structures with the hetero-structured nanoparticles sandwiched between the top surface of the a-Si layer and the ITO layer with different relative distances.

### 5.2.1 Model set up

In the design of the hetero-structured lumpy nanoparticles, 26 small metallic spheres are evenly anchored half embedded surrounding the outside of the large dielectric core particles. Due to the minimised nanoparticle absorption and the light blockage, these hetero-structured lumpy nanoparticles can be closely packed between the front surface of the a-Si layer and the indium tin oxide (ITO) layer to enhance the absorption in the solar cell. The benefit of the closely packed hetero-structured lumpy nanoparticles on the front surface of solar cells also lies in the effective anti-reflection effect in the far field to further improve the light trapping [77-80]. Fig. 5.1 shows the schemes of the model for the a-Si thin film solar cell integrated with the closely packed hetero-structured lumpy nanoparticles sandwiched between the a-Si layer and the ITO layer. The model was simulated with the Lumerical FDTD software and the dielectric functions were from the

Palik handbook [121]. The solar cell was set up according to the common silicon thin film solar cell geometry (ITO: 20 nm, a-Si: 300 nm, ZnO:Al: 100 nm and Ag: 180 nm) [50]. A broadband plane wave source (300 nm-800 nm) was used to simulate the light incident on the particles from the top. Periodic boundary conditions (PBCs) were used at the lateral boundaries of the simulation model to mimic the infinite periodic arrays of nanoparticles.

$SiO_2$ nanoparticles have been proven to be effective in light trapping and anti-reflection as discussed in Chapter 4. In Chapter 3, the near field light concentration of Ag nanoparticles has been proven to lead to the enhanced electric field and result in photogeneration excitation increase in a-Si solar cells. We select Ag nanoparticles with 10 nm radius as the surface metallic particles according to our analyses in Chapter 3.

To quantify the effect of the hetero-structured nanoparticles on the absorbance of a-Si solar cells, we first calculated the absorbance of the a-Si $A(\lambda)$, using the Equations (4.1) and (4.2) depicted in Chapter 4. The $J_{SC}$ is calculated by integrating the absorbance with the *AM 1.5* solar spectrum using the Equation (3.2). The absorption enhancement $G$ in the 300 nm thick a-Si film with/without the hetero-structured nanoparticles is calculated by Equation (4.3).

### 5.2.2 Relative distance and the size ratio effect of nanoparticle arrays on the absorbance of the a-Si layer

The relative distance $d$ and the radius ratio $\alpha$ (the ratio of the radius of the dielectric core to that of the metallic particles) were investigated in the simulation. $d$ was changed from $-R$ to $R$ ($R$ is the effective radius of the hetero-structured nanoparticle), as shown in Figs. 5.1(b-e). The radius ratio $\alpha$ was changed from *50/10* to *200/10*.

To find out the optimised hetero-structured nanoparticles and the best position of the particles to the solar cells for a maximum absorption enhancement in the a-Si layer, we systematically investigated two parameters: the radius ratio $\alpha$ and the relative distance $d$. Based on the scattering effect from dielectric nanoparticles and our previous results with Ag nanoparticles on the front surface of solar cells for enhanced near-field effect, the radius ratios are selected to be *50/10*, *75/10*, *100/10*, *125/10*, *150/10*, *175/10* and *200/10*. The relative distance is changed from $R$ to $-R$, as shown in Figs. 5.1(b-f). By mapping the absorbance as a function of the radius ratio and the relative distance, the optimised condition for the largest absorption enhancement in the a-Si layer is found as shown in Fig. 5.2(a). It can be seen that the highest absorption enhancement of $G=1.507$ is located at the purple star point under the optimised parameters with $d=0$ and $\alpha=150/10$. It can also be seen that when the particles are partially embedded in the a-Si layer, the absorption enhancement is larger than the case when the particles are on the top of the a-Si surface or totally embedded in the a-Si layer. That is mainly because that the forward scattering from the hetero-structured nanoparticles is improved when they are partially embedded in the a-Si layer. In addition they can act as a high performance anti-reflection coating due to the graded RI matching. The light absorbance as a function of the wavelength is calculated and shown in Fig. 5.2 (b). It can be seen that compared with a reference a-Si layer without the hetero-structures nanoparticles the absorption enhancement is over the entire investigated wavelength range and the integrated absorbance can be enhanced as much as 50.7%.

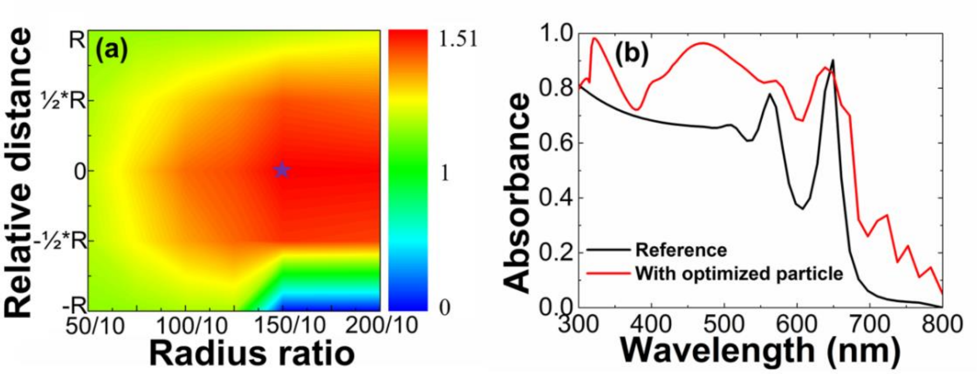

Fig. 5.2 (a) Absorption enhancement in the a-Si layer with/without the hetero-structured nanoparticles as a function of the relative distance *d* and the radius ratio $\alpha$. (b) Light absorbance in the a-Si layer with/without the hetero-structured nanoparticles at the optimised position in (a).

## 5.3 Modelling of conformal structure solar cell with hetero-structured lumpy nanoparticles

### 5.3.1 Design of the conformal geometry for ultrathin film solar cell

The achieved large absorption enhancement allows us to further investigate the solar cells with a reduced active layer thickness. Based on the above optimisation results, we propose a conformal structure to investigate the light absorbance in the ultrathin a-Si layer as shown in Fig. 5.3. As can be seen from Fig. 5.3, the a-Si layer and the other layers in the solar cell follow the hemispherical shape of the hetero-structured particles half embedded in the a-Si layer. The geometry is similar to the one we discussed in the previous Chapter 4, however, the main difference lies in the position of the ITO layer. In this new geometry design, the ITO layer are set on top of the nanoparticles in order to completely make use of the near field light concentration from the small metallic nanoparticles as discussed in Chapter 3 to enhance the absorbance of the a-Si layer. The thickness of the a-Si layer is changed from 20 nm to 100 nm.

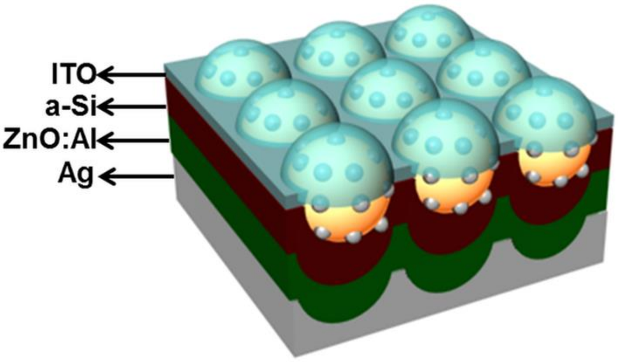

Fig. 5.3 The schematics of the conformal structure for the ultrathin a-Si solar cell.

### 5.3.2 $J_{SC}$ enhancement in conformal structure solar cells with different a-Si thicknesses

In this Section, we will discuss the absorbance in the a-Si layer with different solar cell thicknesses and investigate the influence of small Ag nanoparticles on the absorbance in the a-Si layer at different wavelengths. First the $J_{SC}$ in the conformal solar cells of the a-Si layer with different thicknesses (from 20 nm to 100 nm) is calculated and compared to the standard solar cells with a 80 nm ITO anti-reflection layer on the top, as shown in Fig. 5.4(a). It can be observed that the $J_{SC}$ is tripled in the conformal structure compared with that of a standard solar cell configuration with the same active layer thickness due to the enhanced light trapping effect. At the point of the 20 nm thickness of the a-Si layer, the $J_{SC}$ is increased from 4.11 mA/cm$^2$ to 13.5 mA/cm$^2$, which is comparable with the maximum achievable *Jsc* in the standard flat 300 nm thick a-Si solar cell (13.8 mA/cm$^2$), as indicated by the dashed horizontal line in Fig. 5.4(a). The boost in $J_{SC}$ is attributed to a combination of the scattering effect, the anti-reflective properties of the closely packed dielectric nanoparticles, which are half embedded in a-Si layer and also the enhanced electric field in the vicinity of the small Ag nanoparticles due to the near field light concentration.

Fig. 5.4(b) shows the absorbance of the 20 nm and 40 nm thick a-Si layers in the conformal solar cells as a function of the wavelength compared with a standard solar cell structure with the same thicknesses of the a-Si layer. In Fig. 5.4(b) the absorbance of a standard 300 nm thick a-Si solar cell is also presented for comparison. It can be seen from Fig. 5.4(b) that the absorption of the a-Si layer in the conformal structure is enhanced through the overall wavelength range compared with those in the standard cells due to the comprehensive role of the hetero-structured lumpy nanoparticles. The enhancement in the shorter wavelength range is the highest because of the low absorption loss from the $SiO_2$. The absorbance of a 20 nm thick a-Si conformal solar cell is comparable with that for a standard 300 nm thick flat a-Si solar cell. Thus, it can be concluded that the conformal structure with the hetero-structured nanoparticles can offer a more effective light trapping strategy than the traditional anti-reflection coating of a-Si solar cell.

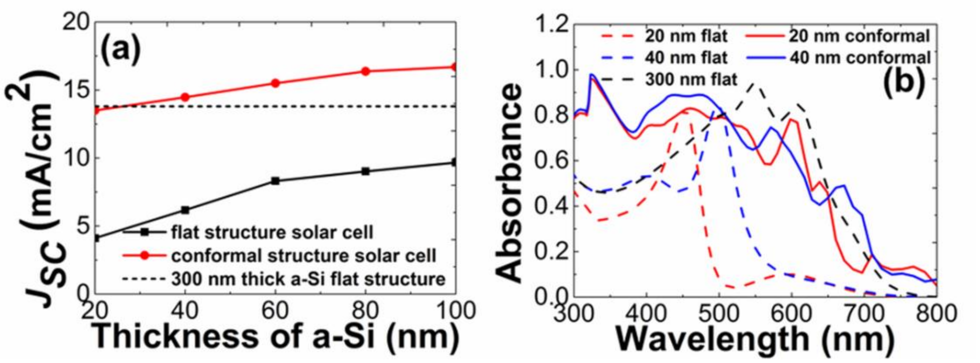

Fig. 5.4 (a) $J_{SC}$ in the conformal solar cell structure as a function of the a-Si thickness. (b) Absorbance in the a-Si layers as a function of the wavelength for different thicknesses.

To further confirm the mechanism for the enhanced absorption, the electromagnetic field intensity distributions in the 20 nm conformal a-Si layer with and without the small Ag nanoparticles are calculated and shown in Fig. 5.5. The polarisation of the incident light is in the X direction and the field component of light is also along the X direction. The calculation results clearly show that two main physical mechanisms are responsible for the observed absorption enhancement in the a-Si layer. First of all, the conformal structure induced by the $SiO_2$ leads to strong near-field coupling to guided modes supported by the multi-layer solar cell structure. This can be observed even without the presence of the Ag nanoparticles in Figs. 5.5(a-c). Secondly, the surface Ag nanoparticles introduce the strong local field concentration in the close vicinity of the nanoparticles leading to further absorption enhancement in the a-Si layer as compared to Figs. 5.5(a-c), in particular at 500 and 600 nm, where the peak of the solar spectrum is located. Therefore both the dielectric core particle and the surface Ag particles in the hetero-structured nanoparticles play an important role in achieving the significant absorption enhancement in the a-Si layer.

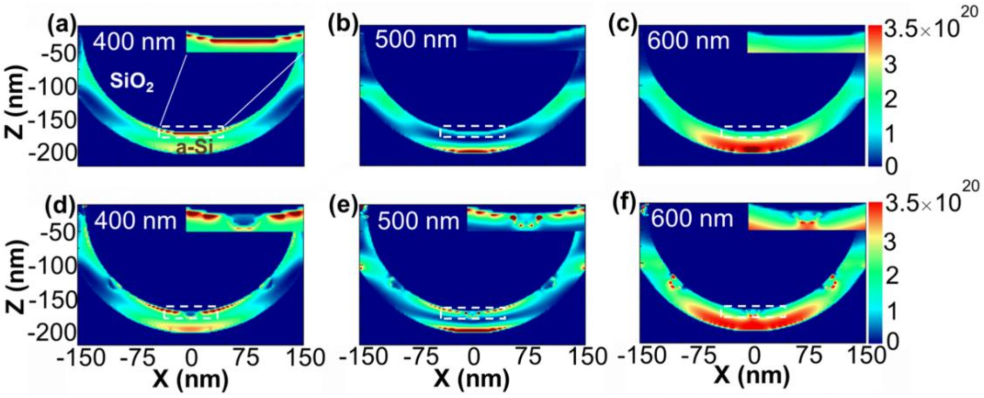

Fig. 5.5 Electric field intensity distributions of a-Si solar cells with (a-c) $SiO_2$ core only conformal geometry and (d-f) hetero-structured lumpy nanoparticle conformal geometry. Insets: highlight of the close vicinity of the Ag nanoparticles.

To illustrate the effect of lumpy nanoparticles on the ultrathin solar cells, the absorbance of a 20 nm thick solar cell with optimised lumpy nanoparticles in this Chapter is compared to the absorbance of solar cell with optimised $SiO_2$ nanoparticles of the same thickness of absorber in Chapter 4 in Fig. 5.6. From the absorbance and $J_{SC}$ calculation, the $J_{SC}$ value of the 20 nm thick solar cell with $SiO_2$ nanoparticles can be improved from 10.13 mA/cm$^2$ to 13.5 mA/cm$^2$ when the lumpy nanoparticles are replaced. From the absorbance curves, it can be found that the absorbance of the solar cell designed in this Chapter with lumpy nanoparticles is higher than that with just $SiO_2$ nanoparticles in the Chapter 4.

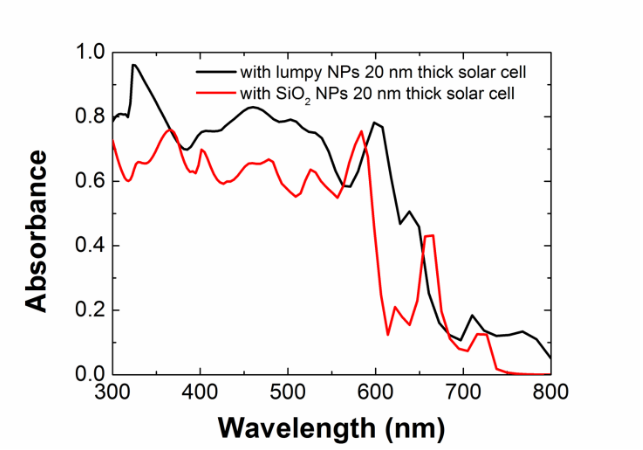

Fig. 5.6 Absorbance comparison of a 20 nm thick solar cell with lumpy and $SiO_2$ nanoparticles

### 5.3.3 Effect of the refractive index of the core particles on the absorbance in the 20 nm thick a-Si layer

In the hetero-structured nanoparticle design, the dielectric core particles are important in determining the strength of the light scattering and anti-reflection when integrated into a-Si solar cells. In addition to the size and geometry, the refractive index also plays an important role in the light trapping strategy.

To further optimise the design of the hetero-structured nanoparticles on the absorbance of the a-Si layer in conformal structure, the refractive index of the core particles is investigated from 1.25 to 4.0 and the thickness of the a-Si layer is set at 20 nm. Fig. 5.6(a) shows the $J_{SC}$ enhancement as a function of the refractive index of the core particles. The optimised refractive index of the core particles to achieve the best enhancement of $J_{SC}$ is 1.5 with a relative absorption enhancement of 229.8% compared with that in the flat 20 nm thick a-Si solar cell case. By further increasing the refractive index of the core particles, the $J_{SC}$ enhancement decreases due to the reduced anti-reflection and scattering effect. Fig. 5.7(b) shows the absorbance as a function of the wavelength with the refractive index of the core particles at 1.25, 1.5 and 4.0, respectively. From Fig. 5.7(b) we can see that the absorption in the ultrathin a-Si layer with the core particles of a higher refractive index decreases at the wavelength above 450 nm, leading to a reduction in the absorption enhancement due to the inefficient light trapping effect while in the short wavelength range below 400 nm, the absorbance in the a-Si layer with high refractive index of core particles is increased mainly due to that the refractive index is at 4 which is close to the refractive index of a-Si leading to a better anti-reflection from the graded refractive index matching between the a-Si and the ITO layer.

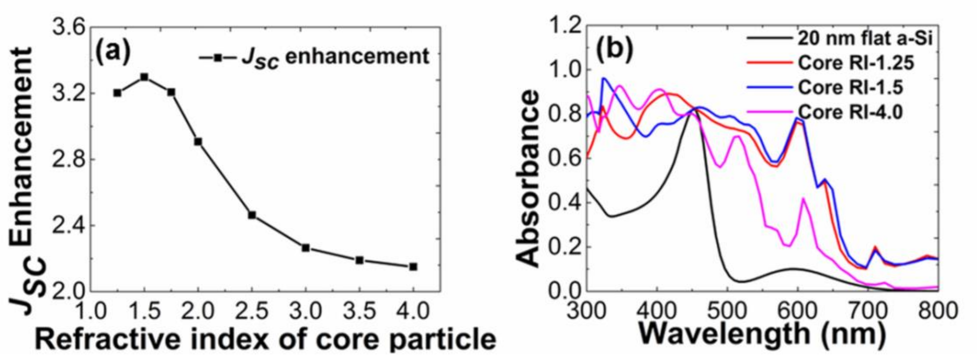

Fig. 5.7 (a) Normalised $J_{SC}$ enhancement in the conformal structure solar cell with the 20 nm thick a-Si layer as a function of the refractive index of the core particles (b) Absorbance in the 20 nm thick a-Si layer in the conformal structure for core particles with different refractive index as a function of the wavelength.

In summary, here we introduce an approach for a broadband absorption enhancement in the a-Si thin film solar cells by placing the hetero-structured nanoparticles on the front side of solar cells. The proposed conformal structures enable significant $J_{SC}$ gains of 229.8% in the 20 nm thick a-Si solar cell by simultaneously harnessing the strong scattering from large dielectric nanoparticles with a refractive index at 1.5 and near field light concentration from small Ag nanoparticles. The absorbance of an optimised 20 nm thick a-Si conformal solar cell with the hetero-structured nanoparticles can be comparable with a 300 nm thick standard a-Si solar cell with the conventional anti-reflection coating.

## 5.4 Fabrication and characterisation of the solar cell integrated with the hetero-structured lumpy nanoparticles

In this Section, the method of fabricating the hetero-structured lumpy nanoparticles is introduced first. We use the scanning electron microscope (SEM) and UV-VIS spectrometer to characterise the properties of the nanoparticles. We transfer the nanoparticles from the glass substrate to the top surface of the a-Si solar cells. Around 7% enhancement is achieved due to the anti-reflection from the nanoparticles compared with the reference solar cell. Then we imprint 350 nm hetero-structure nanoparticles into the a-Si solar cells, achieving an enhancement of 62.5% in $J_{SC}$ from the QE measurement compared with the reference solar cell, which is even 18% higher than that with the same size of $SiO_2$ nanoparticles.

### 5.4.1 Fabrication of hetero-structure lumpy nanoparticles

Different from the chemical synthesis method, here we introduce an easy process for nanoparticle fabrication. The closely-packed hetero-structured lumpy nanoparticles are fabricated using the self-assembled $SiO_2$ nanoparticles as substrate combined with e-beam evaporation technology as shown in Fig. 5.8. Commercial closely-packed $SiO_2$ nanoparticles on top of the glass substrate are purchased from Nanosyslab, with the diameters of 350 nm, 500 nm and 600 nm. To decorate the $SiO_2$ nanoparticles with ultra-small metallic nanoparticles to harness the near field light concentration effect, a simple physical vapour deposition method is introduced instead of the chemical synthesis method. The advantage of using physical deposition method is that the sizes and the distributions of the metallic nanoparticles are easily controlled on the surface of the core dielectric nanoparticles. According to Chapter 3, the metallic nanoparticles with ultra-small sizes and low coverage densities can be fabricated by controlling the metal film thickness to the sub-nanometer scale. The SEM images of the lumpy nanoparticles are presented in Fig. 5.9.

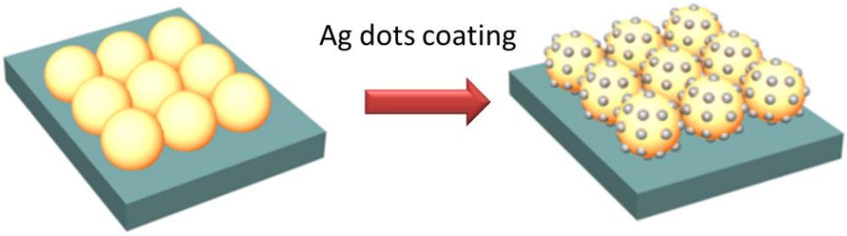

Fig. 5.8 Fabrication process of the lumpy nanoparticles.

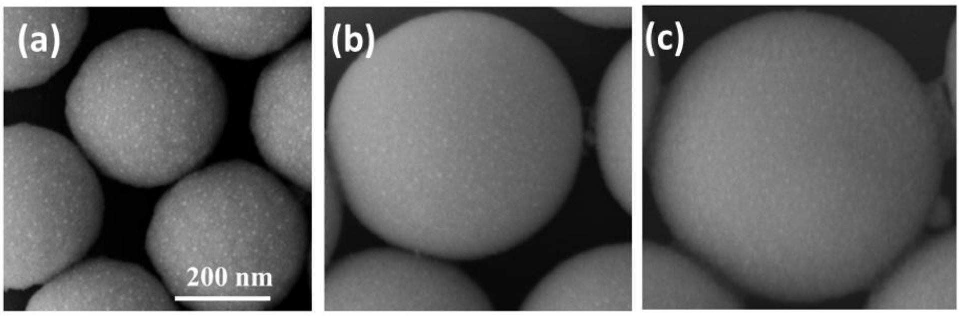

Fig. 5.9 SEM images of hetero-structured lumpy nanoparticles with different sizes of core $SiO_2$ nanoparticles (a) 350 nm (b) 500 nm (c) 600 nm in diameter. The size of Ag nanoparticles is around 10 nm.

From Figs. 5.9(a)-(c), we can see that the lumpy nanoparticles with the $SiO_2$ cores are decorated with small Ag nanoparticles after a thickness of 0.3 nm Ag film deposition using the e-beam evaporation method. The size of the Ag nanoparticles fabricated by this method is around 10 nm. The nanoparticles are distributed evenly on the surface of the $SiO_2$ nanoparticles. The nanoparticles are fabricated on the glass substrate to allow the characterisation of the transmittance and the reflectance using the UV-VIS spectrometer. Fig. 5.10 shows the transmittance and reflectance of the $SiO_2$ core nanoparticles on the glass substrate with and without the decorated small surface Ag nanoparticles. The reason we measure the transmittance and the reflectance of the $SiO_2$ core nanoparticles without Ag decorated is that we want to calculate the plasmonic resonance of small Ag nanoparticles in the hetero-structured lumpy nanoparticle geometry.

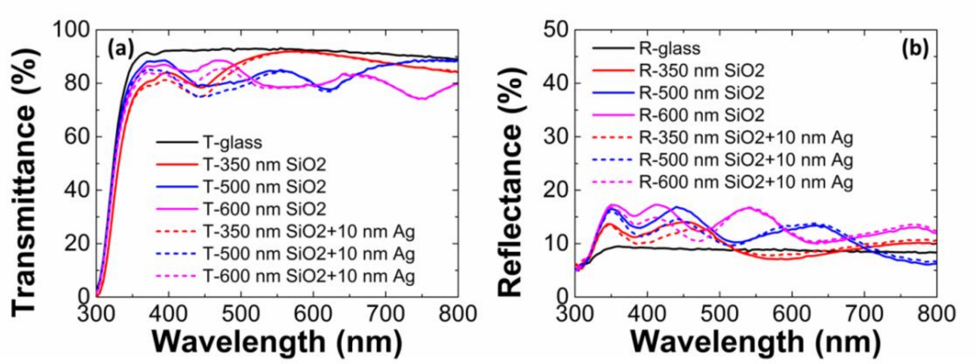

Fig. 5.10 Transmittance (a) and reflectance (b) of the $SiO_2$ nanoparticles and lumpy nanoparticles with different diameters on the glass substrate.

From Fig. 5.10, we can find that there exist higher order modes for larger $SiO_2$ nanoparticles corresponding to the valleys in the transmittance curve or the peaks in the reflectance curves as shown in the solid lines. However, when deposited small Ag nanoparticles on the outer surfaces of the $SiO_2$ nanoparticles, the transmittance and the reflectance are both decreased in the short wavelength range as shown in the dash line. This is due to the excitation of the plasmonic resonances of the small Ag nanoparticles in the short wavelength range leading to the Ag particle absorbance. The plasmonic resonance (A) of the Ag nanoparticles can be calculated by using the formulas shown as below:

$$A=A_1-A_2 \tag{5.5}$$

$$A_1= 100-T_1-R_1 \tag{5.6}$$

$$A_2= 100-T_2-R_2 \tag{5.7}$$

$A_1$ represents the absorbance of the hetero-structured lumpy nanoparticles while $A_2$ represents the absorbance of the $SiO_2$ nanoparticles. $T_1$ and $T_2$ represent the transmittance of the $SiO_2$ particles with and without the decorated Ag nanoparticles respectively. $R_1$ and $R_2$ represent the reflectance of the $SiO_2$ particles with and without the Ag nanoparticles.

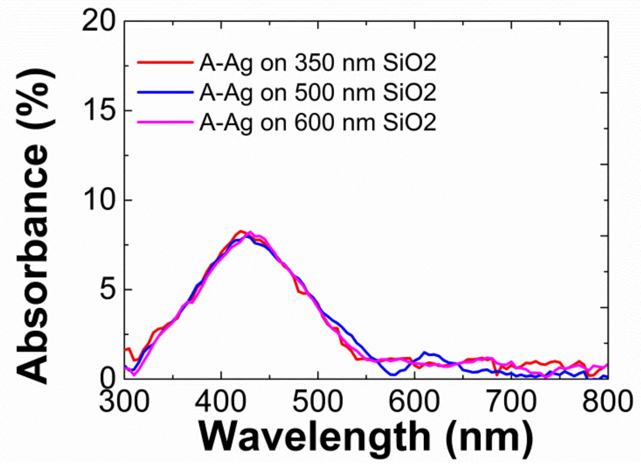

Fig. 5.11 Plasmonic resonance of small Ag nanoparticles in the hetero-structured lumpy nanoparticles.

Fig. 5.11 shows the plasmonic resonance of small Ag nanoparticles in the hetero-structured nanoparticles. The resonance peaks of Ag nanoparticles on different sizes of $SiO_2$ core particles are nearly the same at round 425 nm. The absorbance curves are not narrow because of the size distribution of the Ag particles. From the characterisation of the hetero-structured nanoparticles, we can see that these structured nanoparticles can generate the WGMs from the core particles as described in Chapter 4 together with the plasmonic effect from the small surface decorated Ag nanoparticles as detailed in Chapter 3.

### 5.4.2 Characterisation of solar cells integrated with lumpy nanoparticles

After the fabrication of the lumpy nanoparticles on the glass substrate, we transfer the nanoparticles from the glass substrate to the top surface of n-i-p structure solar cells and characterise the solar cell performance by measuring the reflectance, I-V and QE curves. To successfully transfer the nanoparticles from the glass substrate to the top surface of the solar cells, we use a reverse nano-imprinting procedure with a thermal release tape as shown in Fig. 5.12.

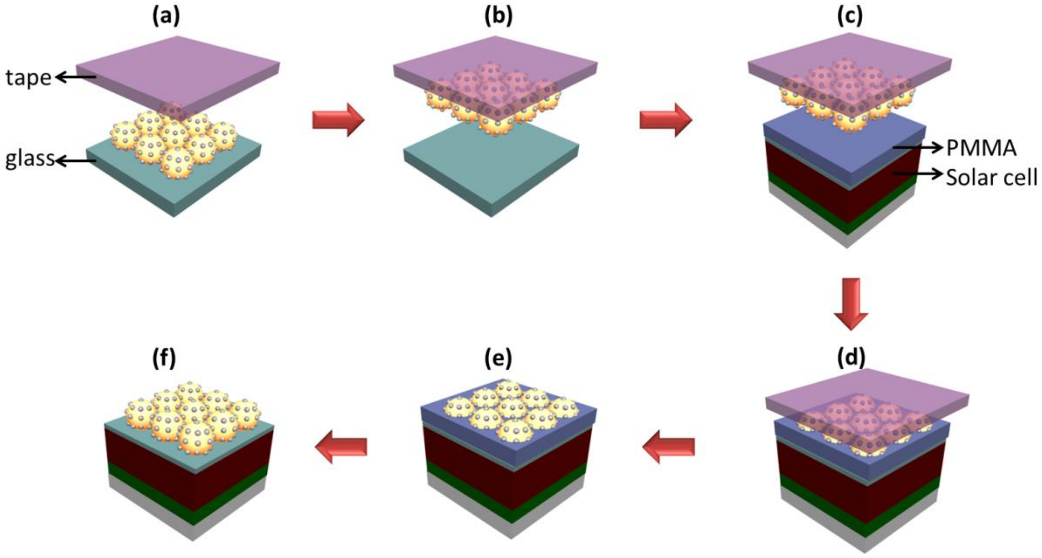

Fig. 5.12 Schematic diagram of fabrication process of solar cell with lumpy nanoparticles on top using a reverse nano-imprinting method with thermal release tape.

First, we softly press the thermal release tape onto the nanoparticles which are fabricated on the glass substrate and then gently peel off the tape from the glass as shown in Figs. 5.12 (a) and (b). Thus the packed nanoparticles are transferred onto the tape as a release layer. Secondly, we coat a 100 nm thick PMMA layer on top of the a-Si solar cell by spin-coating. And then we bring the unbaked PMMA layer into the direct contact with the nanoparticles on the thermal release tape, as can be seen in Figs. 5.12 (c) and (d). After using nano-imprinter to imprint the nanoparticles into the PMMA layer, we bake our samples under 150$^{o}$C. Under these conditions, the thermal release tape loses the adhesion to the nanoparticles and can be peeled off automatically. In the end we dissolve the PMMA layer using acetone and the close-packed nanoparticles are left on the top surface of the solar cell as shown in Fig. 5.12(f). Fig. 5.13 shows a selected SEM image of 500 nm lumpy nanoparticles on top of an n-i-p structured a-Si solar cell. It can be seen that the nanoparticles after transferred onto the solar cell are still closely packed using the method we depict as above.

To examine the influence of the nanoparticles on the solar cells, we first measure the reflectance of the solar cell with and without the nanoparticles using a spectrometer (Perkin Elmer, Lambda 1050). The reflectance curves are shown in Fig. 5.14.

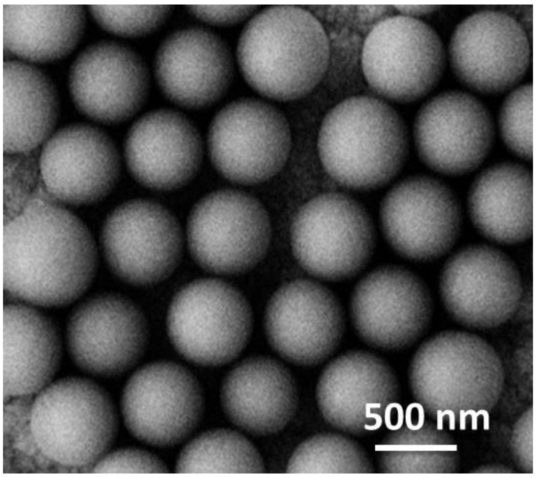

Fig. 5.13 SEM image of 500 nm lumpy nanoparticles on top of a-Si solar cells.

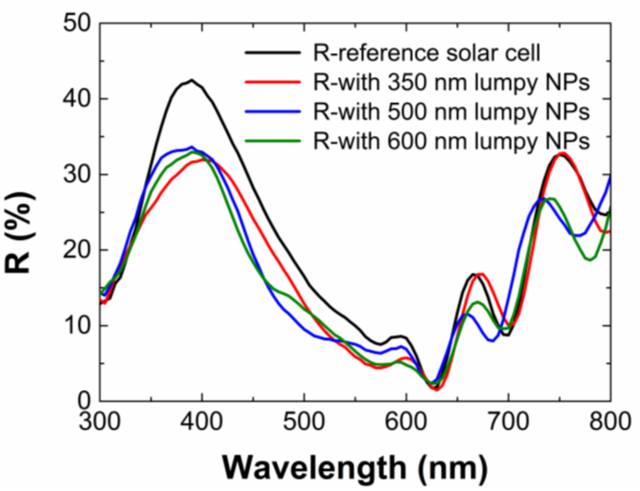

Fig. 5.14 Comparison of reflectance of n-i-p solar cells with and without the integrated lumpy nanoparticles.

From Fig. 5.14, we can find that the reflectance curve of the solar cell without nanoparticles shown as black line is decreased after the nanoparticles integration, especially in the short wavelength range. This is mainly due to the anti-reflection effect and the plasmonic effect from the lumpy nanoparticles. These reflectance decrease leads to the absorbance enhancement in the a-Si layer, which can also be proven in the EQE curves of the solar cells as shown in Fig. 5.15.

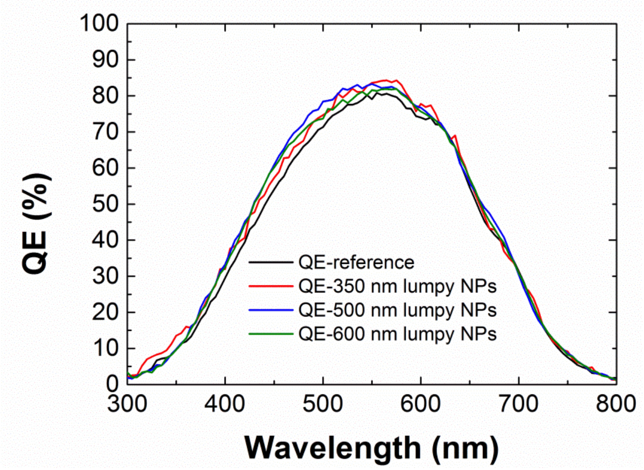

Fig. 5.15 QE comparison for solar cells with/without lumpy nanoparticles (NPs) on the top.

From the QE comparison, we can find that the QE curves from 300 nm to around 620 nm are all enhanced with nanoparticles integrated on top of the solar cell compared to the reference solar cell. In the longer wavelength, the EQE curves are slightly enhanced mainly due to that the nanoparticles do not reduce the reflectance well in these wavelength ranges. The overall performance of the solar cell is characterised by measuring the I-V curves as shown in Fig. 5.16 and Table 5.1.

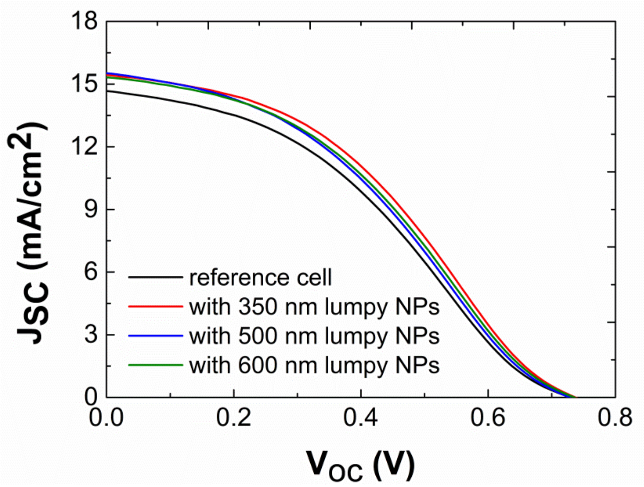

Fig. 5.16 I-V curves for the solar cells with/without lumpy nanoparticles on top.

Table 5.1 Parameters for solar cells with/without nanoparticles on top.

| | $V_{OC}$ (mV) | $J_{SC}$ (mA/cm$^2$) | *FF* (%) | *Eff* (%) |
|---|---|---|---|---|
| **Reference** | 731 | 14.6 | 36.9 | 3.957 |
| **With 350 nm NPs** | 736 | 15.3 | 37.9 | 4.27 |
| **With 500 nm NPs** | 730 | 15.5 | 37.01 | 4.19 |
| **With 600 nm NPs** | 733 | 15.35 | 37.2 | 4.18 |

From table 5.1, we can find that $V_{OC}$ and *FF* in the reference solar cell do not change much after applying the lumpy nanoparticles on top. This is because the nanoparticles are integrated onto the completed solar cells and will not change the solar cell electrical properties. We can also see that the $J_{SC}$ value is increased from 14.6 mA/cm$^2$ to 15.5 mA/cm$^2$ with the 500 nm lumpy nanoparticles on top, which is the highest among the three cases with nanoparticles integrated. This $J_{SC}$

improvement results from the anti-reflection effect of the nanoparticles in the short wavelength range and the light trapping effect in the longer wavelength range. The total efficiency is enhanced by around 7% with 350 nm lumpy nanoparticles integrated on top compared with the reference case.

To examine the influence of the half embedded lumpy nanoparticles on the performance of the solar cells, we use the same fabrication method as discussed in Chapter 4 except that we exchange the $SiO_2$ nanoparticles with the lumpy nanoparticles. The size of the core $SiO_2$ nanoparticles we use is 350 nm, which is close to the optimised lumpy nanoparticles size from the simulation results as presented in the Section 5.3. To demonstrate the better influence of 350 nm lumpy nanoparticles on the solar cells, we also apply 350 nm $SiO_2$ nanoparticles embedded into solar cells for a comparison. The thickness of the solar cell is reduced to around 150 nm (20 nm p type layer, 110 nm i-layer and 20 nm n type layer), which is comparatively thin but still maintains the electrical property of the solar cells. We measure the QE response of the solar cells with the 350 nm lumpy and 350 nm $SiO_2$ nanoparticles, and compare to the flat solar cell as shown in Fig. 5.17. The calculated $J_{SC}$ from the QE curves is shown in Table 5.2.

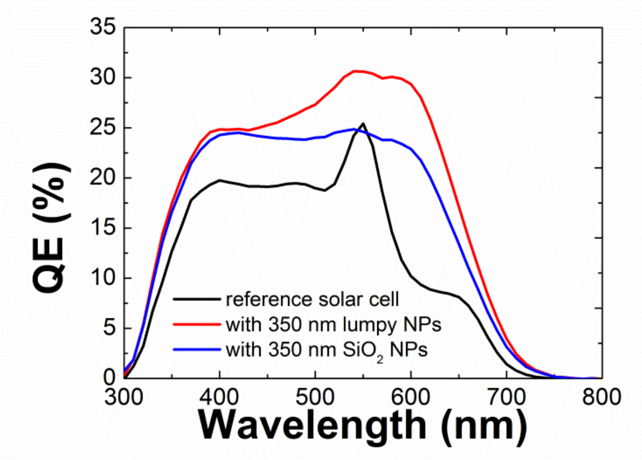

Fig. 5.17 QE comparison of 150 nm thick solar cells with 350 nm $SiO_2$ nanoparticles and lumpy nanoparticles to the flat reference solar cell.

| | Reference | With 350 nm $SiO_2$ NPs | With 350 nm lumpy NPs |
|---|---|---|---|
| **$J_{SC}$ (mA/cm$^2$)** | 2.99 | 4.11 | 4.86 |

Table 5.2 $J_{SC}$ of the solar cell with 350 nm $SiO_2$ NPs, lumpy NPs compared to the reference solar cell.

In Fig. 5.16, compared to the flat reference cell with the $J_{SC}$ value of 2.99 mA/cm$^2$, the QE response with the 350 nm $SiO_2$ nanoparticle embedded solar cell is improved both in the short wavelength range and long wavelength range with the $J_{SC}$ value of 4.11 mA/cm$^2$. The enhancement in the short wavelength results from an excellent antireflection effect of the top surface due to the imprinted $SiO_2$ nanoparticles; while the enhancement in the long wavelength region originates from the guided modes and the hybrid plasmon modes from the conformal nanostructured solar cell geometry. When the $SiO_2$ nanoparticles are replaced by lumpy nanoparticles with the same particle size, the QE response is further improved especially above the wavelength of 450 nm with the $J_{SC}$ value of 4.86 mA/cm$^2$. This is mainly due to plasmonic near field effect of the small Ag nanoparticles of the lumpy nanoparticles. This can be confirmed from Fig. 5.10, which shows that the LSP resonance of the small Ag nanoparticles lies in the wavelength of around 425 nm. And the resonance peak will redshift when the higher refractive index environment is applied such as a-Si. In fact, the different shapes of the QE curves also indicate the different solar cell top surface morphology originated from the half embedded nanoparticles inside the solar cells. Although the value of $J_{SC}$ is not as high as it should be from the simulation results, we can still conclude that the performance of the solar cell with the lumpy nanoparticles imprinted in the top surface is better than those with only the $SiO_2$ nanoparticles. Both of the solar cells incorporated with the lumpy nanoparticles and $SiO_2$ nanoparticles show better QE response than that of the un-patterned reference solar cell.

## 5.5 Chapter conclusion

In this Chapter, first we propose a new hetero-structured lumpy nanoparticle model which combines a large dielectric core particle with small metallic Ag nanoparticles on the surface of core particle. By optimising the size and position of the lumpy nanoparticles in a-Si solar cells, the absorbance of a 20 nm thick a-Si conformal solar cell with the hetero-structured nanoparticles can be comparable with a 300 nm thick standard a-Si solar cell with the conventional anti-reflection coating. Secondly, we develop a new method to fabricate the lumpy nanoparticles by simply depositing Ag nanoparticles on the surface of $SiO_2$ core nanoparticles. By successfully integrating the nanoparticles on top of the solar cell, we find that these nanoparticles can improve the solar cell efficiency by around 7%. At last, we experimentally demonstrate that the QE response of 150 nm thick conformal solar cells with 350 nm lumpy nanoparticles embedded is higher than that with 350 nm $SiO_2$ nanoparticles embedded. And compared to a flat reference solar cell, relative $J_{SC}$ enhancements of 62.5% and 37.4% are achieved, respectively.

# Chapter 6

## Conclusion and future work

### 6.1 Conclusion

The aim of this thesis is to develop an ultra-thin a-Si solar cell without compromising the optical properties. On one hand, the absorber layers in the a-Si thin film solar cells need to be kept thin to minimise the light induced degradation effect. On the other hand, light absorption in the absorber layers need to be maximised to maintain the current density. To realise an ultra-thin solar cell with high absorbance, a novel solar cell structure is proposed in this Thesis by applying the hetero-structured lumpy nanoparticles and conformal nanostructures.

In this thesis, we first develop a numerical model using the FDTD method to investigate the plasmonic scattering effect from large metallic nanoparticles and closely-packed $SiO_2$ nanoparticles in Chapter 2. The model is built up with large Ag and Al nanoparticles on top of completed n-i-p solar cells (300 nm thick a-Si layer) with different sizes and surface coverage (SC) densities. We find that under the optimised condition with both Ag and Al nanoparticles, the overall absorbance can be increased with largest enhancement of around 10%. However, the a-Si absorption decrease in short wavelength cannot be avoided due to the plasmonic absorption from the metallic nanoparticles. To fulfil an absorption enhancement across a broad range of wavelengths, we replace the large metallic nanoparticles with dielectric $SiO_2$ nanoparticles. Through the comparison between the plasmonic nanoparticles and $SiO_2$ nanoparticles, it is found that higher absorption enhancement in the a-Si layer is achieved with the closely-packed $SiO_2$ nanoparticles on top.

In Chapter 3, the near field light concentration effects from small metallic nanoparticles are investigated when the particles are integrated on the top surface. We develop a simple fabrication method to integrate small metallic nanoparticles in the close vicinity to the normal thick a-Si solar cells by coating sub-nanometer thick metal films. By harnessing the near field light concentration from the small metallic nanoparticles, significant performance enhancement in a-Si can be obtained including $J_{SC}$ and $FF$. The findings in Chapter 2 and Chapter 3 allow us to achieve an even higher absorption enhancement in the a-Si layer in the entire solar spectrum by using the combination of closely packed $SiO_2$ resonant nanospheres and small metallic nanoparticles which is named as the hetero-structured lumpy nanoparticle and is discussed in Chapter 5.

Before the discussion of the lumpy nanoparticles in Chapter 5, the closely-packed $SiO_2$ nanoparticle integrated solar cells are further investigated with the reduced thickness of the a-Si layer. To fully utilise the closely-packed $SiO_2$ nanoparticles for optimum absorbance enhancement in thinner a-Si solar cells, we systematically optimise the size and position of the $SiO_2$ nanoparticles. In Chapter 4, we develop a thinner solar cell model (150 nm in thickness) with closely-packed $SiO_2$ nanoparticles embedded partially into the a-Si layer from the top surface. Through the numerical modelling, the optimised position of the nanoparticles for the highest absorption enhancement is found to be where the particles are half embedded in the solar cells. The integrated $J_{SC}$ value calculated from the structured solar cell with 400 nm $SiO_2$ nanoparticles is 17.82 mA/cm$^2$, which is 56.1% higher with respect to the $J_{SC}$ (11.41 mA/cm$^2$) of the flat solar cell. It is also demonstrated that scattering and anti-reflection effects are introduced in the absorber layer to enhance the absorbance and the overall absorbance could be made even higher by optimising the AZO layer thickness. $J_{SC}$ can be further increased to 18.42 mA/cm$^2$ under the condition when the AZO thickness is at 200 nm. To experimentally confirm the designed model, we develop a fabrication process by imprinting the closely-packed $SiO_2$ nanoparticles half into the a-Si solar cells. From the optical and the electrical characterisation, the reflectance of the nanoparticle imprinted solar cell is reduced in the entire wavelength range with respect to the flat solar cell, leading to a strongly enhanced photocurrent (approximate 30%-50% enhancement) which is confirmed from the QE measurements. The calculated reflectance in the nanoparticle imprinted solar cells reproduces well the measured reflectance, validating the effectiveness of the new solar cell concept. The results demonstrate that by carefully designing the nanostructures of solar cells, high performance solar cells can be achieved in ultrathin thickness to overweigh the flat solar cells with normal thickness.

Finally in Chapter 5, we combine the advantages of the small metallic nanoparticles and large dielectric nanoparticles together to propose the hetero-structure lumpy nanoparticle geometry. This new nanoparticle concept consists of a large dielectric core nanoparticle decorated with ultra-small metallic nanoparticles on the outside surface of the core particles. Nanometer sized metal nanoparticles are used as the surface particles to enable the near field concentration. Through the optimisation of the position and size of the nanoparticles from modelling, we can achieve a similar value of $J_{SC}$ (13.5 mA/cm$^2$) as that in a 300 nm thick a-Si layer (13.8 mA/cm$^2$) with an only 20 nm thick a-Si layer. Then, we fabricate the hetero-structured lumpy nanoparticles by coating small Ag nanoparticles (~10 nm) on the outer surface of the closely-packed $SiO_2$ nanoparticles and imprint these nanoparticles half into the solar cell by the nano-imprinting method. By comparing the optical and electrical properties of the solar cell with lumpy nanoparticles and $SiO_2$ nanoparticles, we find that the photocurrent generated with lumpy nanoparticles can be further enhanced with respect to the solar cell with only the $SiO_2$ nanoparticles. Compared to the reference case, the $J_{SC}$ value is enhanced by 62.5%. This confirms that the small metallic nanoparticles in the hetero-structured nanoparticles play an important role in improving the solar cell performance due to the near field effect. The combination of the optimised lumpy nanoparticles, the embedding depth, and the conformal deposition show the enormous potential of producing high performance devices with ultra-thin solar cells.

## 6.2 Future work

### 6.2.1 Plasmonic nanoparticles and nanostructures for tandem thin film solar cells

There exists an efficiency limitation for single junction a-Si solar cells due to the bandgap of the material at around 1.7 eV, allowing only the wavelength lower than 800 nm to be absorbed by the solar cell. This limitation cannot be overcome by the light trapping methods. However, single junction a-Si solar cell is a useful example to investigate light management with nanoparticles and nanostructures, and the work in this Thesis show significantly higher absorbance using the novel nanoparticles and naturally formed a-Si nanostructures based on these nanoparticles.

To make the efficiency of the solar cell even higher, one method is to allow more light to be absorbed in solar cells, which can be achieved by attaching another lower bandgap solar cell material under the a-Si solar cell. Micro-crystalline Si (μ-Si) is a good choice for this purpose because of the bandgap near 1.1 eV. In fact, light trapping is much more important for μ-Si because the optical property of μ-Si is more similar to the c-Si, which is much weaker than the a-Si. Usually, the sharp textured TCO layers are not suitable for μ-Si deposition because the grain growth of μ-Si can result in cracking. The designed solar cell structures in this Thesis could be applied for a-Si/μ-Si tandem solar cells with proficient light trapping structures. Furthermore, in this thesis, the absorption enhancement in the a-Si layer is mainly achieved by engineering the top surface of the solar cell by integrating metallic or dielectric nanoparticles and embedding dielectric or lumpy nanoparticles half into the solar cells. It is thus promising to achieve much higher absorbance enhancement by adjusting both the top solar cell surface structures for the short wavelength response and the rear surface for the long wavelength response.

Plasmonic nanoparticles or nanostructures can be applied into the rear surface of the solar cell to boost the longer wavelength light absorbance after optimising the top surface morphology of the solar cell. Several geometry designs for plasmonic tandem solar cells are shown in Fig. 6.1 based on these ideas. The idea to design these solar cell structures is to trap more light in the short wavelength range in the top a-Si subcell and more light in the longer wavelength range in the bottom μ-Si subcell to maximise the total absorbance in the solar cells. In the first design, metallic nanoparticles are placed on both top and bottom of the tandem solar cell to scatter light of different wavelength with different angles. The top surface metallic nanoparticles can scatter blue light into the top subcell while the rear located metallic nanoparticles are able to redirect the red light into the bottom subcell, thereby increasing the whole wavelength range absorbance.

The second design is similar to the solar cell structure we discuss in Chapter 4. The difference is that here the solar cell is a-Si/μ-Si tandem geometry. Both the a-Si top cell and the μ-Si bottom cell will form the hemi nanoshell structures due to the embedded nanoparticles, which can enhance the absorbance in both active layers. Besides, the nanostructured Ag back reflector will further improve the absorbance in the μ-Si layer due to the high absorbance rate of the material at the plasmonic resonance wavelength range of nanostructured Ag back reflector.

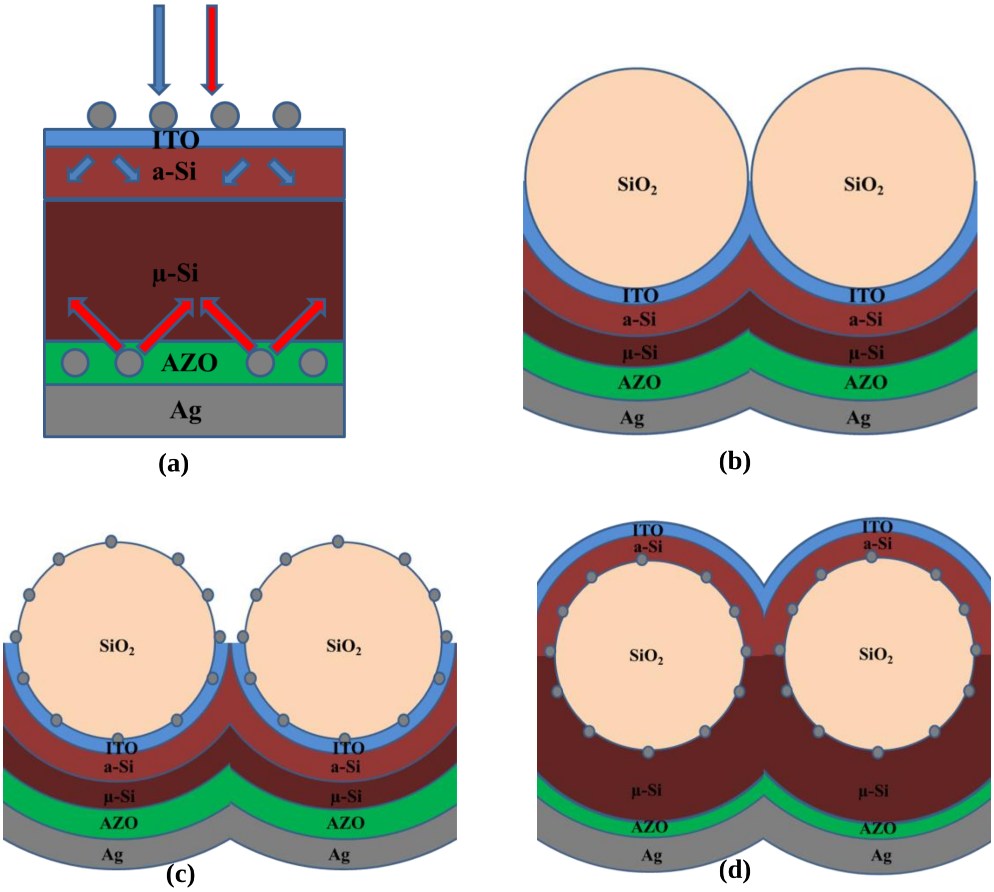

(a) (b) (c) (d)

Fig. 6.1 Concept of designed tandem solar cell structures based on the plasmonic nanoparticles and lumpy nanoparticles.

The third design as shown in Fig. 6.1 (c) is the tandem solar cell with conformal nanostructure formed by the hetero-structured lumpy nanoparticles. By replacing the $SiO_2$ nanoparticles with the lumpy nanoparticles, we can harness the near field light concentration from the small metallic nanoparticles to increase the absorbance of the top a-Si subcell.

The fourth solar cell structure is shown in Fig. 6.1. (d). A more complicated light trapping structure is presented, incorporating the closely-packed lumpy nanoparticles as an intermediate reflector between the top cell and the bottom cell.

A continuous transparent film (flat or random textured) such as ZnO:Al or $SiO_2$ has been widely applied as the interlayer to reflect more red light back into the top cell, thereby enhancing the red-side absorbance of the a-Si subcell. However, this interlayer could be potentially designed by using novel nanoparticles to enhance both red-side absorbance for the a-Si top cell and blue-side absorbance for the μ-Si bottom cell. Through applying the lumpy nanoparticles as the interlayer inside the tandem solar cell, a nanoshell structured solar cell can be made around the nanoparticles. The novel interlayer can couple incident light into the WGM modes and produce a profitable recirculation of light inside the shell shape absorbers, thereby increasing the light path length in the active material. Different from the normal single material nanoshell solar cell structure, in this nanoshell solar cell system, half of the shell is made from a-Si acting as the top subcell while another half of the shell is made from μ-Si acting as the bottom subcell. When light is recirculated inside the nanoshell tandem solar cell systems, both short wavelength light and long wavelength light absorbance can be strongly enhanced by tuning the sizes of the lumpy nanoparticles to excite different WGM modes.

Based on the solar cell structures designed above, higher efficiency solar cell with much more thinner thickness could be achieved by applying novel light trapping strategies.

### 6.2.2 Application to other active materials for solar cells

The photoactive materials investigated in this thesis are all amorphous silicon. In fact, our designed solar cell structure can be applied for many other thin film solar cell materials such as polymer solar cells, dye-sensitized solar cells and perovskite solar cells, which are hot topics in recent years. As discussed in Chapter 4, the hybrid plasmon modes excited by plasmonic Ag back reflector are not easy to be absorbed or coupled into the a-Si layer, especially with thin AZO thickness. And even though these modes are coupled into the a-Si layer with thicker AZO layer, the absorbance enhancement in a-Si at the plasmon resonance is still comparatively weak mainly because of the low absorption of the a-Si material. So the high degree of confinement in plasmon modes in the active material is attractive for high absorbance and severely collection-limited materials especially at the plasmon resonance wavelength range. For solar cells with plasmonic back reflector close to the rear surface of the semiconductor layer, a high absorption ratio close to the band-gap edge is desired. Since light of shorter wavelength is preferentially absorbed near the front surface, plasmonic reflectors at the back of the cell should be optimally designed to increase the absorption of long wavelength light near the bandgap edge. For low refractive index active material, plasmonic back reflector would excite the hybrid plasmon modes at short wavelength range. It is expected that those hybrid plasmon modes may strongly enhance the absorbance of the polymer solar cells or perovskite solar cells with high absorbance active material instead of causing parasitic loss in the metal.

### 6.2.3 Optimisation of the top electrode with Ag nanowires for higher efficiency thin film solar cells

In our experiments, the top electrode material we apply to solar cell is 80 nm thick indium tin oxide (ITO) which is a common option for top electrode. To fully manipulate light in solar cells with the nanoparticles as discussed in Chapter 4 and Chapter 5, the thickness of the ITO layer cannot be too thick otherwise the active layer would be too far away from the nanoparticles to fully appreciate the absorbance benefit. Due to the thin thickness of the ITO layer and the high Schottky barrier between the ITO layer and the p-type a-Si, the series resistance of the solar cell is comparatively high. This leads to the unexpected lower overall performance of the solar cell, especially for $FF$ and $J_{SC}$. To address this issue, a hybrid electrode, which is composed of thin ITO layer and Ag nanowires can fulfil this objective with high transparency (above 90%) and low resistivity (below 10 Ω/□) [124]. There is a strong possibility that our designed a-Si solar cells can achieve a further enhanced efficiency by utilising the hybrid ITO/Ag nanowire top electrode. The nanoparticles and nanostructures can provide a light manipulation method to improve the absorbance in optical way while the hybrid top electrode can offer a solution to enhance the solar cell performance in an electrical way.

# Bibliography

[1] 2012 central intelligence agency world factbook, (2012). (http://www.indexmundi.com/g/g.aspx?c=xx&v=81).

[2] $CO_2$ Emissions from Fuel Combustion, International Energy Agency (2012).

[3] N. S. Lewis. Powering the planet. MRS Bulletin **32**, 808-820 (2007).

[4] M.A. Green, “High Efficiency Silicon Solar Cells,” Proceedings of the International Conference, held at Sevilla, Spain, 27-31 October (1986).

[5] J. Zhao, A. Wang, M. A. Green and F. Ferrazza, “19.8% efficient “honeycomb” textured multicrystalline and 24.4% monocrystalline silicon solar cells,” Appl. Phys. Lett. **73**, 1991 (1998).

[6] M.A. Green, J. Zhao, A. Wang and S. R. Wenham, “Progress and outlook for high-efficiency crystalline silicon solar cells,” Sol. Energ. Mater. Sol. Cells **65**, 9-16 (2001).

[7] O.Schultz, S. W. Glunz and G. P. Willeke, “Multicrystalline silicon solar cells exceeding 20% efficiency,” Progress In Photovoltaics: Research and Applications **12**, 553-558 (2004).

[8] Rohatgi A and Narasimha S. “Design, fabrication, and analysis of greater than 18% efficient multicrystalline silicon solar cells,” Proceedings of the 9th International Photovoltaic Science and Engineering Conference, 187-197 (1996).

[9] P. Campbell and M. A. Green, “High performance light trapping textures for monocrystalline silicon solar cells,” Sol. Energ. Mater. Sol. Cells **65**, 369-375

(2001).

[10] T. M. Bruton, “General trends about photovoltaics based on crystalline silicon,” Sol. Energ. Mater. Sol. Cells **72**, 3-10 (2002).

[11] A. Morales, “Towards 19% Efficient CdTe Solar Cells,” 27th European Photovoltaic Solar Energy Conference and Exhibition, 2812-2814 (2013).

[12] N. Romeo, A. Bosio, V. Canevari, and A. Podesta, “Recent progress on CdTe/CdS thin film solar cells,” Sol. Energ. Mater. Sol. Cells **77**, 795-801 (2002).

[13] P. Jackson, D. Hariskos, E. Lotter, S. Paetel, R. Wuerz, R. Menner, W. Wischmann, M. Powalla, “New world record efficiency for $Cu(In,Ga)Se_2$ thin-film solar cells beyond 20%,” Progress In Photovoltaics: Research and Applications **19**, 894-897 (2011).

[14] S. Benagli, D. Borrello, E. Vallat-Sauvain, J. Meier, U. Kroll, J. Hötzel, J. Spitznagel, J. Steinhauser, L. Castens and Y. Djeridane, 24th European Photovoltaic Solar Energy Conference and Exhibition, “High-efficiency Amorphous Silicon Devices on LPCVD-ZnO TCO Prepared in Industrial KAI-M R&D Reactor,” 2293, Hamburg, Germany, September (2009).

[15] U. Kroll, J. Meier, L. Fesquet, J. Steinhauser, S. Benagli, J. B. Orhan, B. Wolf, D. Borrello, L. Castens, Y. Djeridane, X. Multone, G. Choong, D. Dominé, J.-F. Boucher, P.-A. Madliger, M. Marmelo, G. Monteduro, B. Dehbozorgi, D. Romang, E. Omnes, M. Chevalley, G. Charitat, A. Pomey, E. Vallat-Sauvain, S. Marjanovic, G. Kohnke, K. Koch, J. Liu, R. Modavis, D. Thelen, S. Vallon, A. Zakharian and D. Weidman, “Recent developments of high-efficiency micromorph tandem solar cells in KAI-M Plasmabox PECVD reactors,” 26th European Photovoltaic Solar

Energy Conference and Exhibition, 2340, Hamburg, Germany, September (2011).

[16] D. E. Carlson and C. R. wronski, “Amorphous silicon solar cell,” Appl. Phy. Lett. **28**, 671-673 (1976).

[17] A. Shah, P. Torres, R. Tscharner, N. Wyrsch and H. Keppner, “Photovoltaic Technology: The Case for Thin-Film Solar Cells,” Science **285**, 692-698 (1999).

[18] K. Yamamoto, M. Yoshimi, Y. Tawada, Y. Okamoto and A. Nakajima, “Thin film Si solar cell fabricated at low temperature,” Journal of Non-Crystalline Solids **266**, 1082-1087 (2000).

[19] J. Meier, S. Dubail, D. Fischer, J. A. Anna Selvan, N. Pellaton Vaucher, R. Platz, C. Hof, R. Fluckiger, U. Kroll, N. Wyrsch, P. Torres, H. Keppner, A. Shah and K.-D. Ufert, “The ‘Micromorph’ Solar Cells: a New Way to High Efficiency Thin Film Silicon Solar Cells,” Proceedings of the 13rd EC Photovoltaic Solar Energy Conference, 1445, Nice, France, October (1995).

[20] J. Yang, A. Banerjee and S. Guha, “Triple-junction amorphous silicon alloy solar cell with 14.6% initial and 13.0% stable conversion efficiencies,” Appl. Phy. Lett. **70**, 2975-2977 (1997).

[21] R. C. Chittick, Alexande.Jh, and H. F. Sterling, “The preparation and properties of amorphous silicon,” Journal of the Electrochemical Society **116**, 78-81 (1969).

[22] A. V. Shah, H. Schade, M. Vanecek, J. Meier, E. Vallat-Sauvain, N.Wyrsch, U. Kroll, C. Droz and J. Bailat, “Thin-film silicon solar cells technology,” Progress In Photovoltaics: Research and Applications **12**, 113-142 (2004).

[23] Tom Markvart and Luis. Practical Handbook of Photovoltaics Fundaments and Applications. Part II C, thin film technologies (2003).

[24] J. Carabe and J. J. Gandia, “Thin-film-silicon solar cells,” Opto-electronics review **12**, 1-6 (2004).

[25] G. Beaucarne, “Silicon Thin-Film Solar Cells,” Advances in OptoElectronics, **2007**, 1-12 (2007).

[26] M. Zeman, O.Isabella , S.Solntsev, K.Jäger, “Modelling of thin-film silicon solar cells,” Sol. Energ. Mater. Sol. Cells **119**, 94-111 (2013).

[27] R.E.I. Schropp, and J.K. Rath, “Novel profiled thin-film polycrystalline silicon solar cells on stainless steel substrates,” Electron Devices, IEEE Transactions **46,** 2069-2071 (1999).

[28] D.L. Staebler and C.R. Wronski, “Reversible conductivity changes in discharge-produced amorphous Si”, Appl. Phys. Lett. **31**, 292-294 (1977).

[29] A. Kolodziej. “Staebler-Wronski effect in amorphous silicon and its alloys,” Opto-Electronics Review **12**, 21-32 (2004).

[30] J. Meier, H. Keppner, S. Dubail, U. Kroll, P. Torres, P. Pernet, Y. Ziegler, J. A. Anna Selvan, J. Cuperus, D. Fischer, and A. Shah, “Microcrystalline Single-Junction and Micromorph Tandem Thin Film Silicon Solar Cells,” Mater. Res. Soc. Symp. Proc. **507**, 139-146 (1998).

[31] F. Meillaud et al., “Efficiency limits for single junction and tandem solar cells,” Sol. Energ. Mater. Sol. Cells **90**, 18-19 (2006).

[32] J. Yang, and S. Guha, “Status and future perspective of a-Si:H, a-SiGe:H, and

nc-Si:H thin film photovoltaic technology," Proc. of SPIE **7409**, 74090C (2009).

[33] K. Yamamoto, M. Yoahimi, Y. Tawada, S. Fukuda, T. Sawada, T. Meguro, H. Takata, T. Suezaki, Y. Koi, K. Hayashi, T. Suzuki, M. Ichikawa, A. Nakajima, "Large area thin film Si module," Sol. Energ. Mater. Sol. Cells **74**, 449-455 (2002).

[34] http://rredc.nrel.gov/solar/spectra/am1.5/.

[35] Green, M. A. "Solar Cells: Operating Principles, Technology and System Applications" (Univ. New South Wales, 1998).

[36] Yablonovitch, E. & Cody, G. D. "Intensity enhancement in textured optical sheets for solar cells," IEEE Trans. Electr. Dev. **29,** 300-305 (1982).

[37] Deckman, H. W., Roxlo, C. B. & Yablonovitch, E. "Maximum statistical increase of optical absorption in textured semiconductor films," Opt. Lett. **8,** 491-493 (1983).

[38] M. Gu, Z. Ouyang, B. Jia, N. Stokes, X. Chen, N. Fahim, X. Li, M. Ventura, and Z. Shi, "Nanoplasmonics: a frontier of photovoltaic solar cells," Nanophotonics **1**, 235-248 (2012).

[39] H. Atwater and A. Polman, "Plasmonics for improved photovoltaic devices," Nature Mater. **9**, 205-213 (2010).

[40] Y. A. Akimov, W. S. Koh, "Design of Plasmonic Nanoparticles for Efficient Subwavelength Light Trapping in Thin-Film Solar Cells," Plasmonics **6**, 155-161 (2011).

[41] A. Polman and H. A. Atwater, "Photonic design principles for ultrahigh

efficiency photovoltaics," Nature Mater. **11**,174-177 (2012).

[42] M. L. Brongersma, Y. Cui and S. Fan, "Light management for photovoltaics using high-index nanostructures," Nature Mater. **13**, 451-460 (2014).

[43] V. E. Ferry, M. A. Verschuuren, Hongbo B. T. Li, Ruud E. I. Schropp, H. A. Atwater, and A. Polman "Improved red-response in thin film a-Si:H solar cells with soft-imprinted plasmonic back reflectors. Appl. Phys. Lett. **95**, 183503 (2009).

[44] D. Derkacs, S. H. Lim, P. Matheu, W. Mar, and E. T. Yu, "Improved performance of amorphous silicon solar cells via scattering from surface plasmon polaritons in nearby metallic nanoparticles," Appl. Phys. Lett. **89**, 093103 (2006).

[45] K. Nakayama, K. Tanabe, and H. A. Atwater. "Plasmonic nanoparticle enhanced light absorption in GaAs solar cells," Appl. Phys. Lett. **93**, 121904 (2008).

[46] S. Pillai, K. R. Catchpole, T. Trupke, and M. A. Green. Surface plasmon enhanced silicon solar cells. Journal of Applied Physics **101**, 093105 (2007).

[47] F. J. Beck, A. Polman, and K. R. Catchpole, "Tunable light trapping for solar cells using localized surface plasmons," Journal of Applied Physics **105**, 114310 (2009).

[48] S. S. Kim, S. I. Na, J. Jo, D. Y. Kim, and Y. C. Nah, "Plasmon enhanced performance of organic solar cells using electrodeposited Ag nanoparticles," Appl. Phys. Lett. **93**, 073307 (2008).

[49] X. Chen, B. Jia, J. Saha, B. Cai, N. Stokes, Q. Qiao, Y. Wang, Z. Shi, and M.

Gu, “Broadband enhancement in thin-film amorphous silicon solar cells enabled by nucleated silver nanoparticles,” Nano Lett. **12**, 2187-2192 (2012).

[50] Y. A. Akimov and W. S. Koh, “Resonant and nonresonant plasmonic nanoparticle enhancement for thin-film silicon solar cells,” Nanotechnology **21**, 235201 (2010).

[51] H. Tan,R. Santbergen, A. H. M. Smets, and M. Zeman, “Plasmonic Light Trapping in Thin-film Silicon Solar Cells with Improved Self-Assembled Silver Nanoparticles,” Nano Lett. **12**, 4070-4076 (2012).

[52] Z. Sun, X. Zuo, and Y. Yang, “Role of surface metal nanoparticles on the absorption in solar cells,” Opt. Lett. **37**, 641-643 (2012).

[53] V. E. Ferry, L. A. Sweatlock, D. Pacifici and H. A. Atwater. “Plasmonic nanostructure design for efficient light coupling into solar cells,” Nano Lett. **8**, 4391-4397 (2008).

[54] P. Berini, “Plasmon–polariton waves guided by thin lossy metal films of finite width: bound modes of asymmetric structures,” Phys. Rev. B **63**,125417 (2001).

[55] V. Giannini, Y. Zhang, M. Forcales and J. Gómez Rivas, “Long-range surface plasmon polaritons in ultra-thin films of silicon,” Opt. Express **16**, 19674-19685 (2008).

[56] F. J. Haug, T. Söderström, O. Cubero, V. Terrazzoni-Daudrix and C. Ballif, “Plasmonic absorption in textured silver back reflectors of thin film solar cells,” J.Appl. Phys. **104**, 064509 (2008).

[57] R. B. Konda, R. Mundle, H. Mustafa, O. Bamiduro, A. K. Pradhana, U. N. Roy, Y. Cui, and A. Burger. “Surface plasmon excitation via Au nanoparticles in n-CdSe/p-Si heterojunction diodes,” Appl. Phys. Lett. **91**, 191111 (2007).

[58] J. Weickert, R. B. Dunbar, H. C. Hesse, W. Wiedemann, and L. Schmidt-Mende, “Nanostructured organic and hybrid solar cells,” Adv. Mater. **23**, 1810-1828 (2011).

[59] L. Lu , Z. Luo , T. Xu , and L. Yu, “Cooperative Plasmonic Effect of Ag and Au Nanoparticles on Enhancing Performance of Polymer Solar Cells,” Nano Lett. **13**, 59-64 (2013).

[60] D. M. Callahan, J. N. Munday, and H. A. Atwater. “Solar cell light trapping beyond the ray optic limit,” Nano. Lett. **12**, 214-218 (2011).

[61] J. N. Munday and H. A. Atwater, “Large Integrated Absorption Enhancement in Plasmonic Solar Cells by Combining Metallic Gratings and Antireflection Coatings,” Nano Lett. **11**, 2195-2201 (2011).

[62] M. G. Deceglie , V. E. Ferry , A. P. Alivisatos , and H. A. Atwater, “Design of Nanostructured Solar Cells Using Coupled Optical and Electrical Modeling,” Nano Lett. **12,** 2894-2900 (2012).

[63] M. Kirkengena, J. Bergli, and Y. M. Galperin, “Direct generation of charge carriers in c-Si solar cells due to embedded nanoparticles,” J. Appl. Phys.**102**, 093713 (2007).

[64] J. Yang, J. You, C. Chen, W. Hsu, H. Tan, X. Zhang, Z. Hong, and Y. Yang, “Plasmonic Polymer Tandem Solar Cell,” ACS Nano **5**, 6210-6217 (2011).

[65] C. Hägglund and S. Apell, “Plasmonic Near-Field Absorbers for Ultrathin Solar Cells,” J. Phys. Chem. Lett. **3**,1275-1285 (2012).

[66] J. Zhu, M. Xue, H. Shen, Z. Wu, S. Kim, J. Ho, A. Hassani-Afshar, B. Zeng, and K. L. Wang, “Plasmonic effects for light concentration in organic photovoltaic thin films induced by hexagonal periodic metallic nanospheres,” Appl. Phys. Lett. **98**, 151110 (2011).

[67] V. Gusak, B. Kasemo, and C. Hagglund, “Thickness Dependence of Plasmonic Charge Carrier Generation in Ultrathin a-Si:H Layers for Solar Cells,” ACS Nano **5**, 6218-6225 (2011).

[68] N. N. Lal, B. F. Soares, J. K. Sinha, F. Huang, S. Mahajan, P. N. Bartlett, N. C. Greenham, and J. J. Baumberg, “Enhancing solar cells with localized plasmons in nanovoids,” Opt. Express **19**, 11256-11263 (2011).

[69] R. B. Dunbar, H. C. Hesse, D. S. Lembke, and L. Schmidt-Mende, “Light-trapping plasmonic nanovoid arrays,” Phys. Rev. B **85**, 035301 (2012).

[70] H. Huang, L. Lu, J. Wang, J. Yang, S. Leung, Y.Q. Wang, D. Chen, X.Y. Chen, G. Shen, D. Li and Z. Fan, “Performance enhancement of thin-film amorphous silicon solar cells with low cost nanodent plasmonic substrates,” Energy Environ. Sci. **6**, 2965-2971 (2013).

[71] C. Eisele, C. E. Nebel and M. Stutzmann, “Periodic light coupler gratings in amorphous thin film solar cells,” J. Appl. Phys. **89**, 7722-7726 (2001).

[72] C. Min, J. Li, G. Veronis, J. Y. Lee, S. Fan and P. Peumans, “Enhancement of optical absorption in thin-film organic solar cells through the excitation of

plasmonic modes in metallic gratings," Appl. Phys. Lett. **96**, 133302 (2010).

[73] J. Zhu, C. M. Hsu, Z. F. Yu, S. H. Fan and Y. Cui, "Optical absorption enhancement in amorphous silicon nanowire and nanocone arrays," Nano Lett. **10**, 1979-1984 (2010).

[74] C. M. Hsu, C. Battaglia, C. Pahud, Z. C. Ruan, F. J. Haug, S. H. Fan, C. Ballif and Y. Cui, "High-efficiency amorphous silicon solar cell on a periodic nanocone back reflector," Adv. Energy Mater. **2**, 628-633 (2012).

[75] C. Battaglia, C. M. Hsu, K. Söderström, J. Escarré, F. Haug, M. Charrière, M. Boccard, M. Despeisse, D. T. L. Alexander, M. Cantoni, Y. Cui, and C. Ballif, "Light Trapping in Solar Cells: Can Periodic Beat Random," ACS Nano **6**, 2790-2797 (2012).

[76] P. Matheu, S. H. Lim, D. Derkacs, C. McPheeters, and E. T. Yu, "Metal and dielectric nanoparticle scattering for improved optical absorption in photovoltaic devices," Appl. Phys. Lett. **93**, 113108 (2008).

[77] D. Wan, H. Chen, T. Tseng, C. Fang, Y. Lai, and F. Yeh, "Antireflective Nanoparticle Arrays Enhance the Efficiency of Silicon Solar Cells," Adv. Funct. Mater. **20**, 3064-3075 (2010).

[78] J. Grandidier, D. Callahan, J. Munday, H. Atwater, "Light Absorption Enhancement in Thin-Film Solar Cells Using Whispering Gallery Modes in Dielectric Nanospheres," Adv. Mater. **23**, 1272-1276 (2011).

[79] J. Grandidier, R. Weitekamp, M. Deceglie, D. Callahan, C. Battaglia, C. Bukowsky, C. Ballif, R. Grubbs, and H. Atwater, "Solar cell efficiency

enhancement via light trapping in printable resonant dielectric nanosphere arrays," Phys. Status Solidi A **210**, 255-260 (2013).

[80] Y. A. Akimov, W. S. Koh, S. Y. Sian, and S. Ren, "Nanoparticle-enhanced thin film solar cells: Metallic or dielectric nanoparticles," Appl. Phys. Lett. **96**, 073111 (2010).

[81] Y. Yao, J. Yao, V. K. narasimhan, Z. Ruan, C. Xie, S. Fan and Y. Cui, "Broadband light management using low-Q whispering gallery modes in spherical nanoshells," Nat. Commun. **3**, 664-671 (2012).

[82] J. Yin, Y. Zang, C. Yue, X. He, J. Li, Z. Wu, Y. Fang, "Self-assembled hollow nanosphere arrays used as low Q whispering gallery mode resonators on thin film solar cells for light trapping," Phys Chem Chem Phys. **15**,16874-16882 (2013).

[83] Bohren, C. F. & Huffman, D. R. "Absorption and Scattering of Light by Small Particles," Wiley, (2008).

[84] Stefan Alexander Maier, "Plasmonics: Fundamentals and Applications," Springer, (2007).

[85] K.R. Catchpole, and A. Polman, "Plasmonic solar cells" Opt. Express **16**, 21793-21800 (2008).

[86] X. Chen, B. Jia, Y. Zhang and M. Gu, "Exceeding the limit of plasmonic light trapping in textured screen-printed solar cells using Al nanoparticles and wrinkle-like graphene sheets" Light Science & Applications, **2**, e92 (2013).

[87] F. J. Beck, S. Mokkapati, and K. R. Catchpole, "Light trapping with plasmonic particles: beyond the dipole model," Opt. Express **19**, 25230-25241

(2011).

[88] F. J. Beck, S. Mokkapati, A. Polman, and K. R. Catchpole, Asymmetry in photocurrent enhancement by plasmonic nanoparticle arrays located on the front or on the rear of solar cells, Appl. Phys. Lett. **96**, 033113 (2010).

[89] F.O. Lenzmann, M.C. van Lare, J. Salpakari, P. Spinelli, J.B. Notta, M. Dörenkämper, N.J. Bakker, A.W. Weeber, and A. Polman, "Plasmonic light-trapping in a-Si:H solar cells by front-side Ag nanoparticle arrays: A benchmarking study" Phys. Stat. Sol. A **210**, 1571-1574 (2013).

[90] M. van Lare, F. Lenzmann, M.A. Verschuuren, and A. Polman, "Mode coupling by plasmonic surface scatterers in thin-film silicon solar cells," Appl. Phys. Lett. **101**, 221110 (2012).

[91] V. E. Ferry, M. A. Verschuuren, H. B. T. Li, E. Verhagen, R. J. Walters, R. E. Schropp, H. A. Atwater, and A. Polman, "Light trapping in ultrathin plasmonic solar cells," Opt. Express **18**, A237-A245 (2010).

[92] V. E. Ferry, J. N. Munday and H. A. Atwater, "Design considerations for plasmonic photovoltaics," Adv. Mater. **22**, 4794-4808 (2010).

[93] V. E. Ferry, M. A. Verschuuren, M. C. Lare, R. E. Schropp, H. A. Atwater, and A. Polman, "Optimised spatial correlations for broadband light trapping nanopatterns in high efficiency ultrathin film a-Si: H solar cells," Nano. Lett. **10**, 4239-4245 (2011).

[94] M. D. Brown, T. Suteewong, R.S. Kumar, V. DInnocenzo, A. Petrozza, M. M. Lee, U. Wiesner, and H. J. Snaith, "Plasmonic Dye-Sensitized Solar Cells Using

CoreShell Metal-Insulator Nanoparticles,” Nano Lett. **11**, 438-445 (2011).

[95] M. Stavytska-Barba, M. Salvador, A. Kulkarni, D. S. Ginger, and A. M. Kelley, “Plasmonic Enhancement of Raman Scattering from the Organic Solar Cell Material P3HT/PCBM by Triangular Silver Nanoprisms,” J. Phys. Chem. C, **115**, 20788-20794 (2011).

[96] D. Derkacs, W. V. Chen, P. M. Matheu, S. H. Lim, P. K. L. Yu, and E. T. Yu, “Nanoparticle-induced light scattering for improved performance of quantum-well solar cells,” Appl. Phys. Lett. **93**, 091107 (2008).

[97] G. Kang, H. Park, D. Shin, S. Baek, M. Choi, D. Yu, K. Kim and W. Padilla, “Broadband Light-Trapping Enhancement in an Ultrathin Film a-Si Absorber Using Whispering Gallery Modes and Guided Wave Modes with Dielectric Surface-Textured Structures,” Adv. Mater. **25**, 2617-2623 (2013).

[98] J. R. Nagel and M. A. Scarpulla, “Enhanced absorption in optically thin solar cells by scattering from embedded dielectric nanoparticles,” Opt. Express **18**, A139-A146 (2010).

[99] S. Nunomura, A. Minowa, H. Sai and M. Kondo, “Mie scattering enhanced near-infrared light response of thin-film silicon solar cells,” Appl. Phys. Lett. **97**, 063507 (2010).

[100] J. R. Nageland and M. A. Scarpulla, “Enhanced light absorption in thin film solar cells with embedded dielectric nanoparticles: Induced texture dominates Mie scattering,” Appl. Phys. Lett. **102**, 151111 (2013).

[101] P. Buehlmann, J. Bailat, D. Domine, A. Billet, F. Meillaud, A. Feltrin, and C.

Ballif, “In situ silicon oxide based intermediate reflector for thin-film silicon micromorph solar cells,” Appl. Phys. Lett. **91**, 143505 (2007).

[102] T. Söderström, F. -J. Haug, X. Niquille, V. Terrazzoni, and C. Ballif, “Asymmetric intermediate reflector for tandem micromorph thin film,” Appl. Phys. Lett. **94**, 063501 (2009).

[103] Y. Hsiao, S. Charan, F. Wu, F. Chien, C. Chu, P. Chen, and F. Chen, “Improving the Light Trapping Efficiency of Plasmonic Polymer Solar Cells through Photon Management,” J. Phys. Chem. C **116**, 20731-20737 (2012).

[104] C. Hagglund, M. Zach, and B. Kasemo, “Enhanced charge carrier generation in dye sensitized solar cells by nanoparticle plasmons,” Appl. Phys. Lett. **92**, 013113 (2008).

[105] N. Fahim, Z. Ouyang, Y. Zhang, B. Jia, Z. Shi, and M. Gu, “Efficiency enhancement of screen-printed multicrystalline silicon solar cells by integrating gold nanoparticles via a dip coating process,” Opt. Mater. Express **2**, 190-204 (2012).

[106] Y. Zhang, Z. Ouyang, N. Stokes, B. Jia, Z. Shi, and M. Gu, “Low cost and high performance Al nanoparticles for broadband light trapping in Si wafer solar cells” Appl. Phys. Lett. **100**, 151101 (2012).

[107] M. J. Mendes, A. Luque, I. Tobias, and A. Marti, “Plasmonic light enhancement in the near-field of metallic nanospheroids for application in intermediate band solar cells,” Appl. Phys. Lett. **95**, 071105 (2009).

[108] N. Lagos, M. M. Sigalas, and E. Lidorikis, “Theory of plasmonic near-field

enhanced absorption in solar cells," Appl. Phys. Lett. **99**, 063304 (2011).

[109] P. Spinelli and A. Polman, "Prospects of near-field plasmonic absorption enhancement in semiconductor materials using embedded Ag nanoparticles,"Opt. Express **20**, A641-A654 (2012).

[110] R. M. Cole, J. J. Baumberg, F. J. Garcia de Abajo, S. Mahajan, M. Abdelsalam, and P. N. Bartlett, "Understanding Plasmons in Nanoscale Voids," Nano. Lett. **7**, 2094-2100 (2007).

[111] Y. Sugawara, T. A. Kelf, and J. J. Baumberg, "Strong Coupling between Localized Plasmons and Organic Excitons in Metal Nanovoids," Phys. Rev. Lett. **97**, 266808 (2006).

[112] T. A. Kelf, Y. Sugawara, R. M. Cole, and J. J. Baumberg, "Localized and delocalized plasmons in metallic nanovoids," Phys. Rev. B **74**, 245415 (2006).

[113] M. Yu, Y. Z. Long, B. Sun and Z. Y. Fan, "Recent advances in solar cells based on one-dimensional nanostructure arrays," Nanoscale **4**, 2783-2796 (2012).

[114] W. Ren, G. Zhang, Y. Wu, H. Ding, Q. Shen, K. Zhang, J. Li, N. Pan, and X. Wang, "Broadband absorption enhancement achieved by optical layer mediated plasmonic solar cell," Opt. Express **19**, 26536-26550 (2011).

[115] V. E. Ferry, A. Polman and H. A. Atwater, "Modeling light trapping in nanostructured solar cells," ACS Nano **5**, 10055-10064 (2011).

[116] R. F. Oulton, V. J. Sorger, D. A. Genov, D. F. P. Pile and X. Zhang, "A hybrid plasmonic waveguide for subwavelength confinement and long-range propagation," Nat. Photonics **2**, 496-500 (2008).

[117] X. Chen, B. Jia, Y. Zhang and M. Gu, “Exceeding the limit of plasmonic light trapping in textured screen-printed solar cells using Al nanoparticles and wrinkle-like graphene sheets,” Light Science & Applications **2**, e92 (2013).

[118] N. Fahim, B. Jia, Z. Shi, M. Gu, “Simultaneous broadband light trapping and fill factor enhancement in crystalline silicon solar cells induced by Ag nanoparticles and nanoshells,” Opt. Express **20**, A694-A705 (2012).

[119] N. Stokes, B. Jia, and M. Gu, “Design of lumpy metallic nanoparticles for broadband and wide-angle light scattering,” Appl. Phys. Lett. **101**, 141112 (2012).

[120] S. Zhou, X. Hunang, Q. Li, and Y. Xie, “Optimising two-level hierarchical particles for thin-film solar cells,” Opt. Express **21**, A285-A294 (2013).

[121] E. Palik, “Handbook of Optical Constants of Solids,” Academic Press, (1998).

[122] K. X. Wang, Z. Yu, V. Liu,Y. Cui and S. Fan, “Absorption enhancement in ultrathin crystalline silicon solar cells with antireflection and light-trapping nanocone gratings,” Nano Lett. **12**, 1616-1619 (2012).

[123] J. Wallentin, N. Anttu, D. Asoli, M. Huffman, I. Aberg, M. H. Magnusson, G. Siefer, P. F.Kailuweit, F. Dimroth, B. Witzigmann, H. Q. Xu, L. Samuelson, K. Deppert, M.T. Borgström, “InP nanowire array solar cells achieving 13.8% efficiency by exceeding the ray optics limit,” Science **339**, 1057-1060 (2013).

[124] S. Xie, Z.Ouyang, B. Jia and M. Gu, “Large-size, high-uniformity, random silver nanowire networks as transparent electrodes for crystalline silicon wafer solar cells,” Opt. Express **21**, A355- A362 (2013).

# Publications of the Author

## Journal Articles

B. Cai, B. Jia and M. Gu, "Hetero-structured lumpy nanoparticle conformal structure for high absorbance of ultrathin film amorphous silicon solar cells," Appl. Phys. Lett. **103**, 253106 (2013).

B. Cai, B. Jia, Z. Shi and M. Gu, "Near-field light concentration of ultra-small metallic nanoparticles for absorption enhancement in a-Si solar cells," Appl. Phys. Lett. **102**, 093107 (2013).

X. Chen, B. Jia, J. K. Saha, B. Cai, N. Stokes, Q. Qiao, Y. Wang, Z. Shi and M. Gu, "Broadband Enhancement in Thin-Film Amorphous Silicon Solar Cells Enabled by Nucleated Silver Nanoparticles," Nano Lett. **12**, 2187-2192 (2012).

X. Chen, B. Jia, B. Cai, J. Fang, Z. Chen, X. Zhang, Y. Zhao and M. Gu, "Graphenized Carbon Nanofiber: A Novel Light-Trapping and Conductive Material to Achieve an Efficiency Breakthrough in Silicon Solar Cells," **Adv. Mater. 27**, 849-855 (2015).

B. Cai, B. Jia, J. Fang, X. D. Zhang and M. Gu, "Entire band absorption enhancement in ultrathin amorphous silicon solar cell by nanoparticle imprinting", to be submitted.

## Conference paper

B. Cai, B. Jia, Z. Shi and M. Gu, "Design of hetero-structured lumpy nanoparticles conformal structures for improved absorbance of amorphous silicon thin film solar cells," Renewable Energy and the Environment Optics and Photonics Congress, Tucson, USA, November 03-06 (2013).

B. Cai, B. Jia, Z. Shi and M. Gu, "Metallic nanodots for enhanced a-Si solar cells," 20th Australia Institute of Physics congress, Sydney, Australia, December 09-13 (2012).